p38 MAPK AND THE C_2C_{12} CELL CYCLE:

In vitro and in silico investigations

by

Scott Robert Ellery Driscoll

BSc. (Hons)

Submitted in fulfillment of the academic requirements for the degree of

Master of Science

in the School of Biochemistry, Genetics, and Microbiology

University of KwaZulu-Natal

Pietermaritzburg

March 2011

As the candidate's supervisor, I have approved this dissertation for submission.

Signed: _____ Dr. C. U. Niesler Date: _____

As the candidate's co-supervisor, I have approved this dissertation for submission.

Signed: _____ Dr. C. S. Pillay Date: _____

Abstract

The mammalian cell cycle and its points-of-entry are well characterized pathways. These points-of-entry are normally regulated via mitogens and include, amongst others, the ERK, JNK and p38 mitogen-activated protein kinase (MAPK) pathways. However, while the restriction point(R-point), the temporal switch-point at which a cell becomes irrevocably committed to division irrespective of mitogenic stimulus, is known among other cell types, its position within the murine myoblast line C_2C_{12} is currently unknown. Similarly, while MAPK pathways, such as JNK and ERK, have been modeled computationally, no model yet exists of p38 MAPK as stimulated by mitogens. The aims of this dissertation, then, were to determine the R-point within the C_2C_{12} cell cycle and construct a computational mitogen-stimulated p38 MAPK model.

It was found that a synchronous C_2C_{12} population, when stimulated to divide, took 7 to 9 hours to reach S-phase from G_0, consistent with data from the literature. The R-point was determined to lie between 6 and 7 hours post G_1-re-entry stimulation,which was consistent with studies in other cell types. Core modeling of the p38 MAPK pathway revealed that ultrasensitivitywas inherent within the pathway structure. Further, a branching/re-converging structure within the pathway imparted greater responsiveness to signal upon the pathway. A realistic p38 MAPK model demonstrated good responsiveness to signal, its output matched that of several other MAPK models, and it was capable of replicating previous *in vitro* data. This model can be used as a tool for further investigation of the mammalian cell cycle by linking it to other cell cycle models. The predictions by an expanded model may be better suited for understanding the effects of mitogen stimulus on the cell cycle *in situ*.

Preface

The experimental work described in this dissertation was carried out in the Discipline of Biochemistry, School of Biochemistry, Genetics & Microbiology, University of KwaZulu-Natal, Pietermaritzburg, from January 2008 to December 2010, under the supervision of Drs. C. U. Niesler and C. S. Pillay.

.

These studies represent original work by the author and have not otherwise been submitted in any form for any degree or diploma to any tertiary institution. Where use has been made of the work of others it is duly acknowledged in the text.

Signed:

Date:

FACULTY OF SCIENCE AND AGRICULTURE

Declaration- Plagiarism

I, Scott Robert Ellery Driscoll, declare that:

1. The research reported in this thesis, except where otherwise indicated, is my original research.

2. This thesis has not been submitted for any degree or examination at any other university.

3. This thesis does not contain other persons' data, pictures, graphs or other information, unless specifically acknowledged as being sourced from other persons.

4. This thesis does not contain other persons' writing, unless specifically acknowledged as being sourced from other researchers. Where other written sources have been quoted, then:

    a. Their words have been re-written but the general information attributed to them has been referenced
    b. Where their exact words have been used, then their writing has been placed in italics and inside quotation marks, and referenced.

5. This thesis does not contain text, graphics or tables copied and pasted from the Internet, unless specifically acknowledged, and the source being detailed in the thesis and in the References sections.

Signed

……

Date:

……

Declaration Plagiarism 22/05/08 FHDR Approved

Foreword

This dissertation is the culmination of three years' worth of work and research. The going has been far from easy and there have been many setbacks in the production of this work. However, this dissertation now stands complete and not solely by my own hand. Throughout this time my friends and family have been there to support and encourage me. To my two supervisors, Drs. Carola Niesler and Ché Pillay, I am profoundly grateful for all of the technical and literary support they have provided me, as well as putting up with my nonsense all these years. In closing, two quotes seem pertinent to both the development of this thesis, and to the future:

"There are no mistakes. The events we bring upon ourselves, no matter how unpleasant, are necessary in order to learn what we need to learn; whatever steps we take, they're necessary to reach the places we've chosen to go."

— Richard Bach, *The Bridge across Forever* (1984)

"There is a special sadness in achievement, in the knowledge that a long desired goal has been attained at last, and that life must now be shaped toward new ends."

— Arthur C. Clarke, *The City and the Stars* (1956)

Table of Contents

List of Figures

List of Tables

List of Equations

Abbreviations

[v/v] – volume for volume
ATF2 – Activating transcription factor 2
ATP – Adenosine triphosphate
BRENDA – Braunschweig enzyme database
CDK – Cyclin-dependent kinase
CDKI – CDK inhibitor
CHX – cycloheximide
dH2O – deionised water
DMEM – Dulbecco's modified eagle's medium
DMSO – dimethyl sulfoxide
DNA – Deoxyribonucleic acid
DRG – Delayed-response genes
ERG – Early-response genes
ERK – Extracellular-signal regulated kinase
FACS – Fluorescence-activated cell sorting
FCS – foetal calf serum
G0 – Gap 0
G1 – Gap 1
G2 – Gap 2
GTP – Guanosine triphosphate
H2O – water
iHOP – Information hyperlinked over proteins
IL-2 – Interleukin 2
JNK – c-Jun N-terminal Kinase
M – Mitosis
MAP2K – MAPK kinase
MAP3K – MAP2K kinase
MAPK – Mitogen activated protein kinase
Mekk1 – MAPK/ERK kinase kinase
MK2 – MAPK-activated protein kinase 2

MKK – Mitogen activated protein kinase kinase

MLK3 – Mixed-lineage kinase 3

mRNA – messenger ribonucleic acid

ODE – Ordinary differential equation

PBS – phosphate-buffered saline

Pi – Inorganic phosphate

PI – propidium iodide

PRAK – p38 regulated/activated kinase

PySCeS – Python simulator for cellular systems

Rb – Retinoblastoma

R-point – Restriction point

RPN – Rapidly proliferating nuclei

S – Synthesis

SBML – Systems biology markup language

STAT3 – Signal transducer and activator of transcription 3

STHC – spermine tetrahydrochloride

TAB – Transforming growth factor 1 binding protein

TAO – Thousand and one

Chapter One – Literature review

1.1 Introduction

Stem cell biology has proved itself in the past century as a potential 'holy grail' for the treatment of the pathologies of aging and disease. The idea of a stem cell, a cell capable of producing daughter cells of numerous lineages, was proposed early in the 20th century to describe the progenitor of the haematopoetic lineage but eventually came to be associated with all cells capable of producing cells of differing lineages (Petersen and Terada, 2001). While stem cells were seen as a potential font of information about biological processes, it would be another eighty years after their discovery before the establishment of a murine *in vitro* embryonic stem cell population was successfully accomplished (Petersen and Terada, 2001). These cells were derived from the inner cell mass of a developing embryo (Evans and Kaufman, 1981) and were capable of indefinite proliferation in an undifferentiated state while maintaining pluripotent characteristics (Martin, 1981).

The development of an expansive pluripotent cell line was seen as a method of treatment for many diseases, most especially after the development of human embryonic cell lines (Thomson et al., 1998). This discovery brought with it, however, the moral problem of utilizing tissue derived from the destruction of human embryos. The increasing prevalence and utility of adult-derived stem cells provided a solution (Goodell et al., 1996; Siminovitch et al., 1963). These stem cells were derived from post-natal organs and, as no embryos are destroyed in their isolation, the stigma associated with embryonic stem cells was absent in these lines. Moreover, as these cells were donor derived, they were also donor autologous and provided a more viable alternative to embryonic stem cells for therapy due to the lack of a requirement of immunosuppressive drugs after transplantation (Preston et al., 2003; Petersen and Terada, 2001)

With an aging world population, the pool of organs available for transplantation are on a steady decline (Hipp and Atala, 2004) and the benefits of donor-derived autologous adult

stem cells become manifold and impressive. Many advances have been achieved in the field of regenerative medicine, such as the development of *ex vivo* derived bladders (Oottamasathien et al., 2007) and trachea (Beyene et al., 2009). However, a major obstacle remains within the field of regenerative medicine as most adult-derived stem cells have a tendency either to differentiate *in vitro* or fail to establish themselves into viable expansive cell lines (Petersen and Terada, 2001).

There are many signals and mechanisms controlling cell fate and survival that remain to be elucidated. Investigations into the workings of these mechanisms, such as signal transduction pathways and the cell cycle, are therefore necessary for the further development of the fields of stem cell research and regenerative medicine. This project was undertaken to examine, both experimentally and computationally, the nature of signalling cascades and their relation to the cell cycle of murine adult muscle stem cells.

1.2 The Cell Cycle

The cell cycle is a critical process that occurs in all prokaryotic and eukaryotic organisms and is the mechanism through which a cell divides. It is constructed around four main phases, each with its own associated function, markers and checkpoints, and consists of: gap-1 (G_1), synthesis (S), gap-2 (G_2) and mitosis/meiosis (M) phases (Fig. 1.1). In the G_1 phase, the cell prepares for S-phase through replication of cytosolic machinery and synthesis of DNA replication proteins (Snustad et al., 1997). While having a sufficient supply of deoxyribonucleotides is important for entry into S-phase, their *de novo* synthesis is maintained independently of the cell cycle through the activity of ribonucleotide reductase (Herrick and Sclavi, 2007). Once S-phase preparation has been concluded, the cell moves through the G_1/S checkpoint and into S-phase. In S-phase, all nuclear DNA is replicated before moving through the S/G_2 checkpoint. Once in G_2, the DNA is checked to ensure that it has been replicated properly. If errors are detected, the cell will either attempt to correct the errors or, if these errors are irrevocable, apoptose. Once error checking is complete, and the cell has sufficient cellular mass for division into two daughter cells, the G_2/M checkpoint is crossed. M-phase sees the chromosomal and cytosolic content halved and upon mitotic exit, the cell will either re-commit to further division and re-enter G_1, or will be directed into a state of reversible or irreversible growth

arrest known as G_0 (van den Heuvel, 2005; Nurse, 1990). G_0 is divided into several different and distinct states, namely quiescence (reversible growth arrest), senescence (irreversible growth arrest), terminal differentiation (irreversible growth arrest), and apoptosis (programmed cell death) (Snustad et al., 1997).

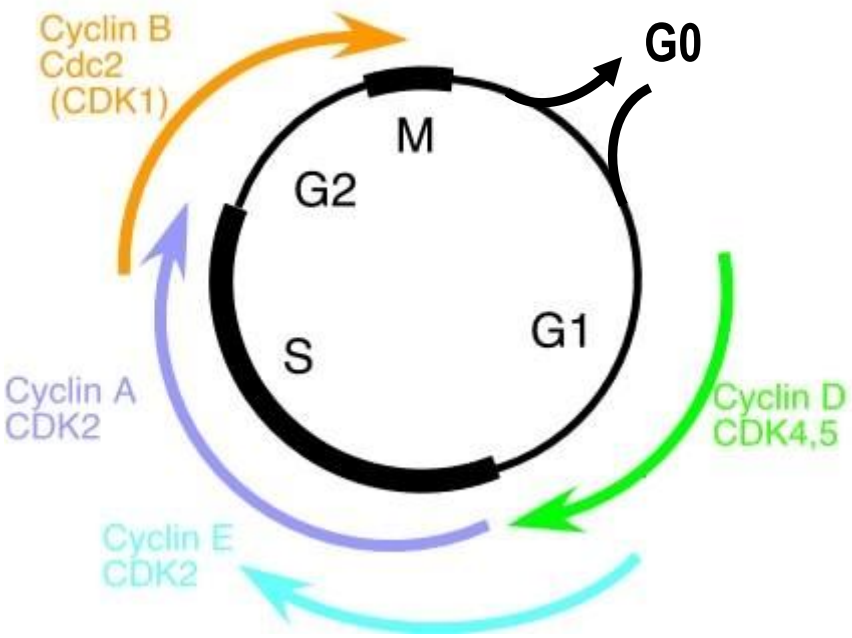

Figure 1.1: The 4 phases of the cell cycle. In G_1 the cell is receiving stimuli and is preparing for DNA synthesis. During S-phase the cell replicates its DNA. In G_2 the cell checks the DNA for errors and prepares for the division in M-phase. After division, the cell will either recommit to division and enter G_1, or enter into a growth-arrested G_0 state. Each arrow represents the time of activity of the various cyclins. (van den Heuvel, 2005)

On a molecular level, each phase of the cell cycle is co-ordinated primarily through the activities and associations of kinases, cyclins, and inhibitors. Principal amongst these kinases are the cyclin-dependent kinases (CDKs) which are constitutively expressed and are regulated through direct association with their counterparts: cyclins A, B, D and E (Koepp et al., 1999). The cyclins are rapidly synthesized and degraded at various points in the cell cycle in order to regulate progression through it. While the CDKs are the catalytic agents, the cyclins, due to their ubiquitous nature and timing within the cell cycle, largely direct progression by binding the CDKs (van den Heuvel, 2005). While the cell cycle is remarkably well-conserved amongst the eukaryotes (Nurse, 1990), certain differences,

such as the number and function of cyclins and their associated cyclin-dependent kinases, are present between the multicellular and unicellular eukaryotic cell cycles (van den Heuvel, 2005).

1.2.1 Entry into the cell cycle

A number of signalling pathways from the cell surface converge upon the cell cycle and, in most mammalian cells, the dominant family regulating entry into the cell cycle are the mitogen-activated protein kinases (MAPK) (Roux and Blenis, 2004). The basic MAPK signalling pathway is a modular cascade that starts with a surface receptor complex and leads to a target kinase that begins effector signalling. Upon stimulation by mitogens, the receptors activate their intrinsic tyrosine kinase activity via phosphorylation of their cytoplasmic tails, leading to the release of key sequestered regulators, such as the guanidine-nucleotide exchange factor (GEF) SOS, and the concomitant activation of the small GTPases Ras or Raf (Fig. 1.2) (Denhardt, 1996). Ras and/or Raf activates the initial signal transduction proteins of the MAPKs, the small GTPases Rac and Ral (Cano and Mahadevan, 1995). Rac and Ral may be viewed as pseudo-MAP4Ks as they activate their downstream targets, the MAP3Ks, through indirect phosphorylation (Teramoto et al., 1996). These MAP3Ks in turn activate the MAP2Ks, which finally activate the principle MAPK of the pathway (Pimienta and Pascual, 2007; Mor and Philips, 2006). This structural organization of the MAPK cascades (Fig 1.2) is conserved amongst the eukaryotes. Differences may arise due to different effector molecules having differing targets and/or effectors (Ferrell, 1996).

The three major MAPK pathways are the extracellular-signal regulated kinase (ERK), c-Jun N-terminal kinase (JNK) and p38 kinase pathways (Roux and Blenis, 2004). Each of the MAPKs comprises several splicoforms, which are active in different tissue types. All the MAPKs are fully activated only upon dual phosphorylation of both conserved residues of a T-x-Y motif, with the variable amino acid being defining of the family of origin: T-E-Y for ERKs, T-P-Y for JNKs and T-G-Y for p38 (Pimienta and Pascual, 2007).

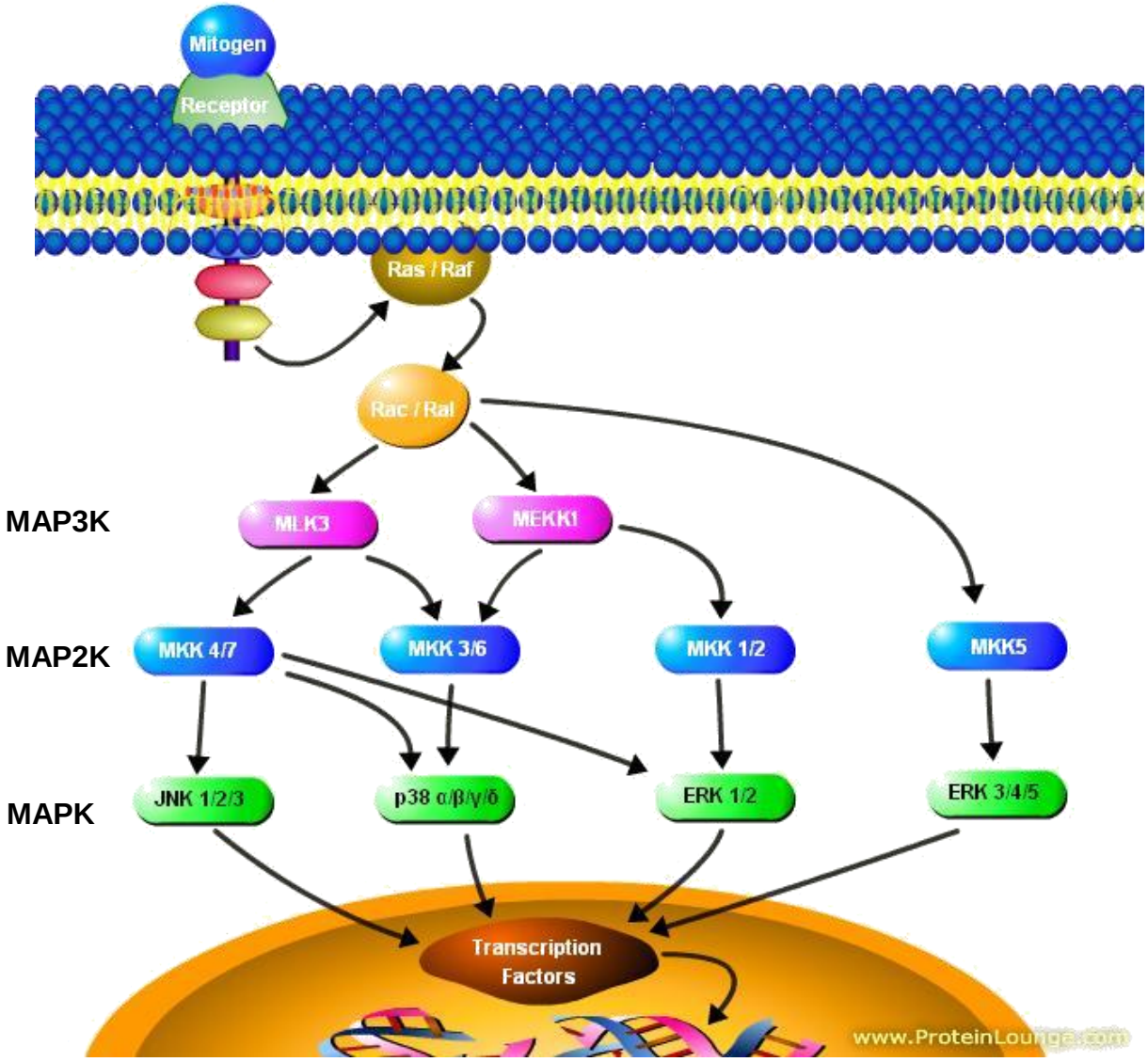

Figure 1.2: The hierarchical structure of the MAP kinase pathways. Once Ras/Raf (gold) and Rac/Ral (orange) have been activated by GEFs, each subsequent level of the cascade is activated though sequential phosphorylation events. The MAP3Ks (pink) activate the MAP2Ks (blue) through dual phosphorylation, which in turn activate the MAPKs (green) through dual phosphorylation. The active MAPKs then phosphorylate transcription factors in the nucleus, thereby promoting various outcomes such as differentiation or division. At each level of the pathway there is a noteworthy amount of crosstalk between the pathways. (Pimienta and Pascual, 2007; Zhang and Liu, 2002)

1.2.1.1 The ERK cascade

The ERKs were the first of the MAPKs to be discovered, and transduce a large variety of signals. Like the JNK and p38 pathways, the ERK pathway is activated through Ras

signalling. However, following Ras activation, and in contrast to the JNK and p38 pathways, the ERK pathway activity is promoted by the GTPase Raf. Raf is the indirect upstream activator of MEKK1 and, subsequently, MKK1/2/5. (Galabova-Kovacs et al., 2006). The ERK1 and ERK2 splicoforms are highly similar and share functionality in signal transduction (Lloyd, 2006). However, while $ERK1^{-/-}$ murine embryos develop normally, $ERK2^{-/-}$ embryos are aborted (Hatano et al., 2003), suggesting that ERK2 is more crucial during development. The other ERK splicoforms are still in the process of being characterised, but are activated in a similar manner to the original members of the ERK family (Nishimoto and Nishida, 2006; Kant et al., 2006).

The ERK pathway displays two activation patterns: transient and sustained, both of which may yield differing responses. Transiently activated ERK induces COS cells to migrate (Klemke et al., 1997), while prolonged activation is required for stimulation of the cell cycle in hamster fibroblasts (Cook and McCormick, 1996; Meloche et al., 1992a; Meloche et al., 1992b). In other cell types, like the 3T3 fibroblasts and MCF7 epithelial cells, excessive activation of the ERK pathway causes apoptosis (Calcabrini et al., 2006; Tang et al., 2002).

The ERK pathway is widely implicated in the regulation of cellular proliferation. The ERK pathway promotes the cell cycle through activation of transcription factors, such as c-Myc and Elk-1, (Murphy et al., 2002; Yang et al., 1998a; Yang et al., 1998b) and the subsequent down regulation of a plethora of anti-proliferative genes (Yamamoto et al., 2006). The ERK pathway has also been implicated in the regulation of pro-survival/anti-apoptotic pathways as it is activated via pro-survival sphingolipid signalling (Monick et al., 2004) and in turn activates via phosphorylation the anti-apoptotic protein BCL-2, favouring cell survival even during times of stress (Subramanian and Shaha, 2007). Their repression therefore attenuates proliferation (Squires et al., 2002; Dudley et al., 1995) due to the inhibition of several important cell cycle events such as pyrimidine synthesis (Graves et al., 2000), ribosome synthesis (Stefanovsky et al., 2006), protein translation (Waskiewicz et al., 1999) and cyclin D transcription (Lavoie et al., 1996).

1.2.1.2 The JNK cascade

The JNK pathway is activated via the Ras, Rac, Mekk1, MKK4/7 cascade (Davis, 2000) and regulates several pathways in the cell, including apoptotic and proliferative pathways (Kyriakis and Avruch, 1990). The two most commonly expressed JNK genes are JNK1 and JNK2, which can both undergo alternate splicing to produce several splicoforms of the kinase in a tissue-dependent manner (Gupta et al., 1996). The JNK2 splice variant binds more strongly to the c-Jun transcription factor than the JNK1 splice variant, and inhibits proliferation. JNK1, however, phosphorylates c-Jun more efficiently than JNK2 and actively promotes proliferation (Sabapathy et al., 2004; Sabapathy and Wagner, 2004; Gupta et al., 1996; Kallunki et al., 1994). Despite this antagonistic effect, it has also been shown that both genes are required for effective proliferation. $JNK1^{-/-}$ and $JNK2^{-/-}$ cells fail to proliferate upon mitogenic stimulation (Sabapathy et al., 2004; Sabapathy and Wagner, 2004; Tournier et al., 2000; Schreiber et al., 1999; Wisdom et al., 1999). This inhibition of the cell cycle occurs at the G_1/S transition as certain key regulatory elements, such as the transcription factor E2F and the CDKs, are not properly activated to allow for continuation to S-phase (Schreiber et al., 1999). JNK1 and JNK2 have also been shown to be necessary for differentiation in certain cell lines, such as T-cells, which cannot undergo maturation if these JNKs have been downregulated (Constant et al., 2000; Dong et al., 2000).

Similar to the ERK pathway, the JNK pathway also exhibits transient and prolonged activation patterns. Transient activation of the JNK pathway promotes mRNA stability of several targets, such as c-Jun itself and IL-2 of the immune response, while prolonged activation triggers the apoptotic pathways via p53 (Chen and Tan, 2000; Yang et al., 1997). However, unphosphorylated JNKs also play a regulatory role in the cell cycle by inhibiting transcription factors, such as STAT3, by destabilizing their mRNAs (Fuchs et al., 1998; Musti et al., 1997; Bray, 1995). The cell survival ERK pathways mitigate this anti-proliferative, pro-apoptotic behaviour almost completely (Xia et al., 1995).

1.2.1.3 The p38 cascade

The p38 cascade is a complex signalling system that can result in many outcomes for the cell depending on the source of activation. This cascade is activated by a variety of stimuli such as UV radiation, heat and mitogens. With many different functions, p38 has a large number of mitogen-independent upstream activators, such as the stress transduction kinases TAO and TAB, to transduce the various input stimuli (Sundaramurthy et al., 2009; Raman et al., 2007; Ichijo et al., 1997; Takekawa et al., 1997; Moriguchi et al., 1996). The specifics of p38 MAPK activation are dependent not only on signal input, but also on cell type, with different lineages responding distinctly to p38 stimulation (Shalom-Barak et al., 1998; Shapiro et al., 1998; Raingeaud et al., 1995; Freshney et al., 1994; Rouse et al., 1994). In terms of mitogenic stimulation, MAP3Ks, such as MLK3 and MEKK1, will activate p38's primary MAP2Ks (MKK3 and MKK6) as well as non-canonical MAP2Ks such as MKK4. While highly homologous in structure, the MAP2Ks activate the p38 isoforms differently and do not share all upstream activators (Hansen et al., 2008; Jiang et al., 1997a; Jiang et al., 1997b).

There are four main splice variants of p38: α, β, γ and δ. While the α/β splicoforms are found ubiquitously throughout various tissues, γ is found almost exclusively in muscle tissue and δ is predominantly expressed in endodermal tissues (Jiang et al., 1997a; Jiang et al., 1996; Lechner et al., 1996; Li et al., 1996). Of importance to the cell cycle are the α/β splice variants which are upregulated upon mitogenic stimuli and regulate proliferation and differentiation (Jones et al., 2005; Weston et al., 2003). Once their activity is no longer required, the splice variants of p38 are dephosphorylated and inactivated by phosphatases, with the α/β splice variants being more susceptible to dephosphorylation than the γ/δ splice variants (Camps et al., 1998; Muda et al., 1996a; Muda et al., 1996b; Sun et al., 1993). The γ splicoform, although not well understood, has also been implicated in both the proliferation and differentiation of satellite cells (Gillespie et al., 2009), while the δ splicoform is important in the transduction of external stress signals (Knebel et al., 2001).

Depending on the source of activation, p38 may potentially activate many targets both directly and indirectly. These include the transcription factors ATF2 and c-Myc, when

mitogenically stimulated (Zhao et al., 1999; Tan et al., 1996) and heat-shock and mRNA interacting proteins when activated via stressors (Mahtani et al., 2001; Stokoe et al., 1992). During mitogenic stimulation, the p38 cascade acts as an antagonist to the JNK cascade. This arises due to the inhibition of Ras via p38's downstream targets, p38 regulated/activated protein kinase (PRAK) and MAPK-activated protein kinase 2 (MK2) (Chen et al., 2000; Nemoto et al., 1998). Once activated, p38 is capable of inducing several physiological responses; promoting inflammation through induction of pro-inflammatory cytokines (Guan et al., 1998), apoptosis upstream and downstream of caspases (Cardone et al., 1997; Huang et al., 1997), proliferation through cyclin D induction, and myogenesis through MEF2, causing G_1 withdrawal (Wu et al., 2000a; Zetser et al., 1999).

The pyrinidile imidazole SB203580 is a highly specific inhibitor of the p38α/β splice variants, which neither inhibits the other MAPK pathways, nor the γ/δ splice variants of p38 (Cuenda et al., 1995). SB203580 is a structural analogue of ATP (Fig 1.3 A and B) and binds within the ATP-binding pocket of p38α/β (Fig 1.3 C) (Gum et al., 1998; Tong et al., 1997; Fry et al., 1994). SB203580 is capable of binding both the active and inactive forms of p38α/β (Tong et al., 1997; Wilson et al., 1996), and when bound to the inactive form of p38 it has been suggested that the p38/SB203580 complex is activated less efficaciously (Frantz et al., 1998). When p38 has been activated, the inhibition of SB203580 becomes competitive with respect to ATP (Tong et al., 1997; Fry et al., 1994). In either state, SB203580 does not affect the binding efficiency of the downstream targets of p38, but rather inhibits its ability to phosphorylate them (Lisnock et al., 1998).

It has been elucidated through p38 point mutagenesis that threonine 106 (isoleucine and methionine for ERK (Her et al., 1991) and JNK (Derijard et al., 1994) respectively) is particularly important for the high specificity of SB203580 (Lisnock et al., 1998). When threonine is substituted for glutamine, the *p*-fluorophenyl ring of SB203580 is sterically hindered from docking with the p38 molecule and hence the molecule is subsequently made SB203580-insensitive (Lisnock et al., 1998; Tong et al., 1997). Against wild-type p38, SB203580 is capable of partial inhibition at remarkably low concentrations in the nano-molar range, while at 10 μM *in vitro* p38 activity is nearly completely inhibited (Davies et al., 2000) as its IC_{50} ranges from 0.1 μM to 1 μM (Badger et al., 1998). When inhibition

is induced at concentrations several hundred fold higher, SB203580 begins to aggregate and non-specifically disrupt other molecules (McGovern et al., 2002; Davies et al., 2000).

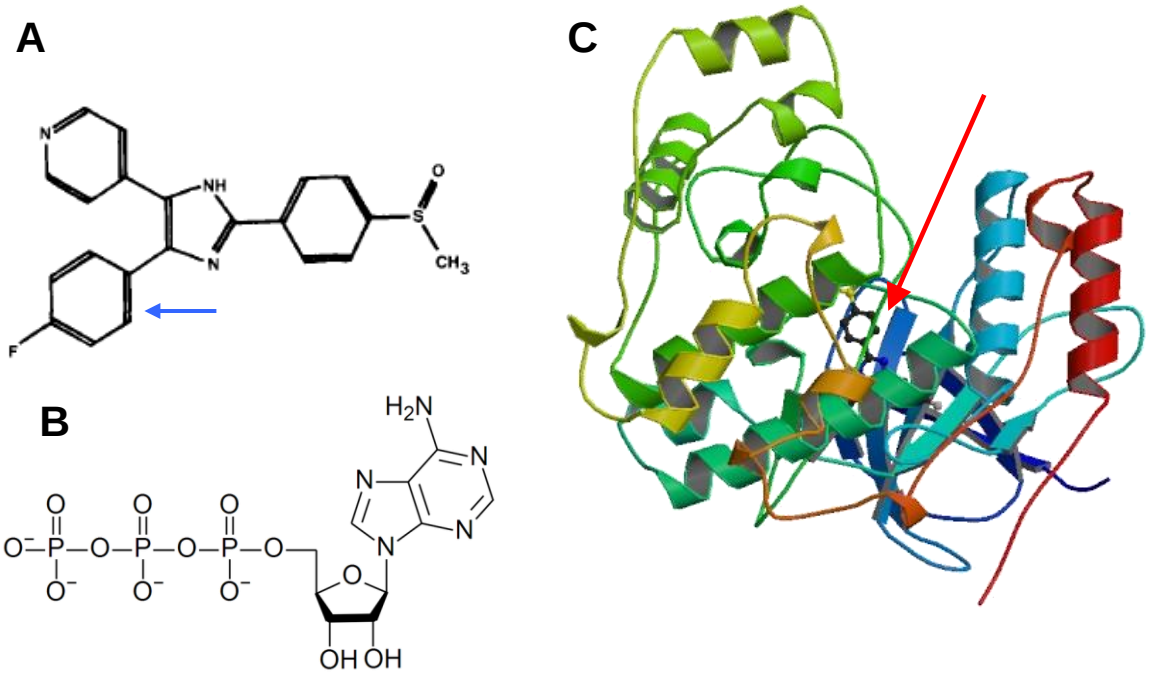

Figure 1.3: The structures of SB203580 (**A**), ATP (**B**) and p38 complexed with SB203580 (**C**, red arrow). Of importance in the SB203580 molecule is the ρ-flurophenyl ring on the lower left (blue arrow) which interacts directly with the p38 molecule and is the cause of SB203580's high specificity towards the enzyme. In C, SB203580 is shown docked within the ATP binding pocket near threonine 106 (red arrow). Structure of p38 with SB203580 from the Protein Database (Accession code 1A9U)

With a high specificity for p38 α/β and a low effective inhibitory concentration, SB203580 is therefore a useful tool for studying the effect of the p38 cascade on cell cycle entry and exit. The experimental inhibition of p38 has been implicated as the cause of several types of G_0 arrest. Kang *et al*.(2005) demonstrated that the addition of SB203580 to primary cultures of rabbit articular chondrocytes extended their life spans *in vitro*, inhibited the onset of senescence, and promoted proliferation. Jones *et al*. (2005), however, found that SB203580 addition to primary culture mouse satellite cells promoted a reversible quiescent state and New *et al*. (2001) found that SB203580 promoted differentiation in mouse neuronal PC12 cells.

1.2.2 Progression through the cell cycle

The MAPKs are an important point of entry into the cell cycle, transducing a number of extracellular mitogenic signals to the effectors of the cell cycle (Roux and Blenis, 2004). Activated p38 is specifically capable of phosphorylating ATF2 (Waas et al., 2001), which in turn is capable of transcriptionally activating the initial cyclin of G_1 (cyclin D), thereby promoting progression of the cell cycle (Beier et al., 1999).

1.2.2.1 G_1 to the Restriction-point

At the onset of G_1 cyclin D has yet to be expressed and is absent, whereas the A- and E-cyclins are present in very low concentrations due to constant turnover (Fig. 1.1). Prior to the transcription of the D-type cyclins, the repressor phosphoprotein retinoblastoma (Rb) exists in a hypo-phosphorylated state and is bound to the transcription factor E2F, thereby inhibiting E2F's activity (Neganova and Lako, 2008; van den Heuvel, 2005) (Fig. 1.4). When stimulated by mitogens, signal transduction pathways, such as the MAPK pathways, activate and induce the transcription of cyclin D (Recio and Merlino, 2002; Sherr, 1995a; Sherr, 1995b). As cyclin D levels elevate it promotes Rb phosphorylation, causing Rb to dissociate from the Rb-E2F complex (Sherr and Roberts, 1999). Free E2F is then able to promote the transcription of cyclins A and E (its downstream targets) allowing cyclin A and E concentrations and activity to elevate (Sherr, 1995b). Cyclin E is itself capable of phosphorylating Rb, releasing more sequestered E2F (hence facilitating further cyclin synthesis), and catalysing the degradation of the CDKI $p27^{KIP1}$(Planas-Silva and Weinberg, 1997; Vlach et al., 1997).

Cyclin E is required for the progression into S-phase (Stacey, 2003; Sherr and Roberts, 1999) and its activity is regulated through sequestration by $p27^{KIP1}$, inhibiting its ability to promote phosphorylation (Sherr, 1995b). Once cyclin D levels begin elevating the cyclin D/CDK complex is able to sequester $p27^{KIP1}$, forming a trimer of cyclin/CDK/CDKI. This complex is still catalytically active and facilitates cyclin D's translocation to the nucleus, promoting the hyper-phosphorylation of nuclear Rb (Stacey, 2003; Sherr and Roberts, 1999; Blain et al., 1997). In conjunction with the rise of free E2F, this results in a sudden and significant change from a highly repressed state to a highly catalytic state

promoting S-phase entry. Once this change has occurred, the cell is now irrevocably committed to completing the cell cycle (Zetterberg and Larsson, 1985).

1.2.2.2 The Restriction Point

The build-up of cyclins A and E allows the cell to progress from G_1 to S-phase. The critical juncture between these two states has been under scrutiny for some time and the term “restriction point” (or R-point) was coined to describe it (Pardee, 1974). The discovery of the R-point was necessary to clarify the distinction between the G_0 and G_1 states, which was poorly defined at the time. Although the specific mechanisms of the R-point were described later, Pardee’s work did manage to pinpoint a single critical point between proliferation and growth arrest in late G_1. Zetterberg and Larsson (1985) further clarified the R-point by demonstrating that there is a distinction between a pre-R cell and a post-R cell describing these two phases as G_1-post mitosis (G_1pm) for cells pre-R and G_1-pre synthesis (G_1ps) for cells post-R. While the length of the phases of the cell cycle, from S-phase through mitosis to the start of G_1ps, is relatively invariant irrespective of cell type, the variation in lengths of cell cycle division times arises almost exclusively from the G_1ps phase. Cells may spend a proportionately longer time within this phase than other neighbouring cells, or may skip G_1ps entirely and enter S-phase immediately (Zetterberg et al., 1995; Zetterberg and Larsson, 1985).

The R-point marks the point of irreversible commitment to cell division and lies directly between G_1pm and G_1ps. If division stimuli are inhibited after the R-point, such as through the removal of growth factors or the addition of cycloheximide (CHX) to inhibit protein synthesis, then the cell will continue through its current round of replication unabated. However, if these stimuli are removed prior to this point, then the cell can still enter a reversible growth-arrested state (Novák and Tyson, 2004; Zetterberg et al., 1995; Zetterberg and Larsson, 1985; Pardee, 1974). Once the mitogenic stimuli are reapplied, the cell will then re-enter G_1. (Novák et al., 2007).

In the G_1ps state several events occur that lead up to the S-phase. The rise of active cyclin E causes a subsequent rise in cyclin A levels and activation of the histone transcription promoter p220 through phosphorylation (Neganova and Lako, 2008). This

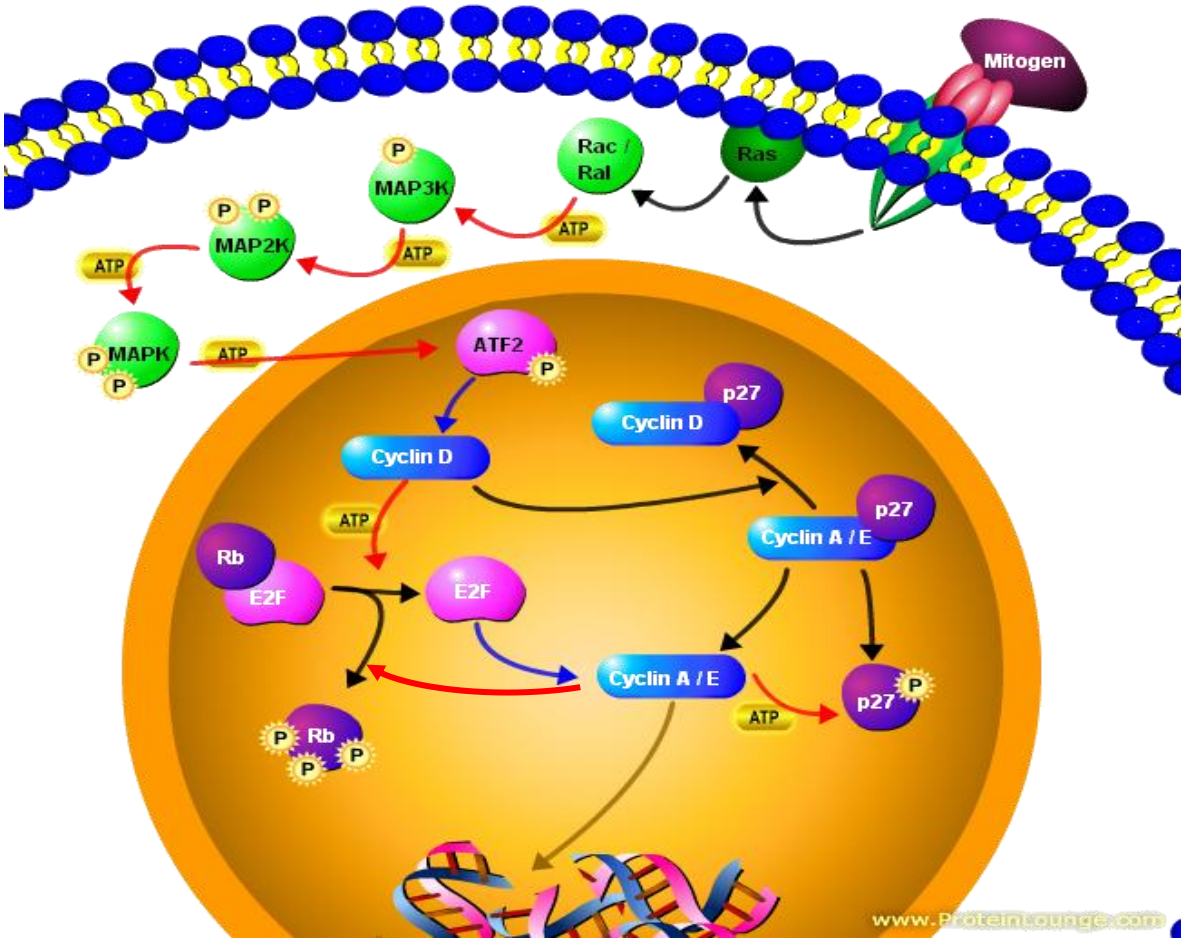

Figure 1.4: Cyclin autocatalysis and the entry into S-phase. During G_0, the cell exists in a state wherein cyclins A and E are being inhibited through sequestration by $p27^{KIP1}$ and are not being effectively transcribed by E2F, E2F itself being inhibited through sequestration by Rb. Upon mitogenic stimulation, the signal transduction pathways (such as the p38 MAPK cascade) activate and stimulate transcription factors, such as ATF2, to transcribe cyclin D, increasing its concentration. After binding CDK2, cyclin D is capable of sequestrating free $p27^{KIP1}$ while maintaining its ability to phosphorylate its targets. Rb is subsequently phosphorylated by the cyclin D complex releasing E2F. Cyclin E levels begin to elevate, due to transcription by E2F, and also begins to phosphorylate Rb as well as targeting $p27^{KIP1}$ for degradation though phosphorylation. These combined actions ultimately allow for an exponential rise of free cyclins, culminating in the synthesis of cyclin A and movement from G_1 to S (Brown arrow). Black arrows – binding / release. →: Phosphorylation. → Transcription. → Binding/releasing. → Promotion of DNA synthesis. Blue – cyclins. Green – MAPKs. Pink – Transcription factors. Purple – inhibitors.

increases histone production, a prerequisite for the further synthesis of DNA nucleosomes. Unlike the other cyclins, at this stage cyclin D is exported out of the nucleus and into the cytoplasm, preventing its degradation. This reservoir of cyclin D assists in the shortening of subsequent cell cycle G_1/S transitions under the influence of constant mitogenic

stimulation (Alt et al., 2000). With increasing levels of cyclin A, maximal activity of cyclin E, and nuclear export of cyclin D, the cell transits the G_1/S boundary.

1.2.2.3 S/G_2/M

Once critical levels of cyclin E have been reached in G_1ps, the cell undergoes an irrevocable commitment to division (Zetterberg and Larsson, 1985; Campisi et al., 1982a) where even if the mitogenic stimulation that promoted division ceases, the cell will continue the process of division (Zetterberg et al., 1995). In late G_1, CDK2 is bound to cyclin E and promotes cyclin A transcription (Ekholm and Reed, 2000). However, once in S-phase, cyclin A replaces cyclin E as the CDK2 regulator (Fung and Poon, 2005), which then subsequently promotes S-phase progression and degradation of cyclin E (Ekholm and Reed, 2000).

Cyclin B synthesis begins during the S-phase, promoted indirectly by E2F (Zhu et al., 2004) and continues through G_2, but it is localized in the cytoplasm, preventing its activity (Pines and Hunter, 1991). The nuclear import of cyclin B occurs constitutively, but it is actively exported from the nucleus when its activity is not required (Molinari, 2000; Hagting et al., 1998). The phosphorylation of cytoplasmic cyclin B by MAPKs (Walsh et al., 2003) promotes its translocation into the nucleus while simultaneously inhibiting its export (Molinari, 2000; Hagting et al., 1998). As nuclear cyclin B levels begin elevating, the cell continues through M and divides to produce two daughter cells (Geley et al., 2001; Sigrist et al., 1995).

1.2.2.4 Mitotic exit

Upon completion of M-phase, the cell must commit itself to one of several states: resumption of G_1 and the continuation of the cell cycle, temporary withdrawal from the cell cycle and entry into quiescence, permanent withdrawal due to replicative senescence or apoptosis, or permanent withdrawal to begin differentiation. Terminal differentiation, quiescence and senescence are similar as they are all growth arrested states with higher CDKI activities and elevated levels of hypo-phosphorylated Rb (Pajalunga et al., 2007;

Lowe and Sherr, 2003). In addition, several levels of redundancy exist in the mechanisms that promote M-phase exit (Buttitta and Edgar, 2007).

Several reversible events keep the cell in a state of quiescence if it is required. The presence of a functioning APC with the cdh1 adaptor is capable of binding hypophosphorylated Rb, inhibiting its ability to be phosphorylated, and promoting the destruction of p21- and p27-specific ubiquitin transferases (Binne et al., 2007). With p21 and p27 levels elevated, the cell will be unable to enter G_1. Rb is also capable of inducing chromosomal rearrangements through histone transferases that repress targets of the E2F transcription factor (Frolov and Dyson, 2004). It has also been mooted that in mammalian cells there are certain repressor complexes that actively promote the quiescent phenotype (Litovchick et al., 2007; Korenjak et al., 2004). While similar events take place in senescent cells, the DNA damage pathways are also activated, which promotes the formation of heterochromatic foci and senescent gene expression, such as the DNA damage protein p53 binding protein 1 (53BP1) (Pazolli and Stewart, 2008; Bartkova et al., 2006; Campisi, 2005a; Campisi, 2005b; Narita and Lowe, 2005).

1.3 The satellite cell cycle

In vivo, skeletal muscle myoblast cells fuse together to form long fibers of multinucleated myotubes; aggregating into the structures known as myofibrils. The cells that maintain the myoblast levels for growth and repair of the muscle tissue are known as satellite cells, due to their physiological location between the basal lamina and the sarcolemma of the myofibril (Collins, 2006; Mauro, 1961), i.e. they are ‘satellites’ to the main muscle fiber. In comparison to myoblasts, satellite cells are myogenic-lineage negative, displaying few myogenic markers, and are comprised mainly of a nucleus with very little cytoplasm (Dhawan and Rando, 2005; Charge and Rudnicki, 2004).

In vivo, satellite cells exist in a quiescent growth-arrested state awaiting proliferative signals to resume the cell cycle, or inductive signals to begin differentiation. Once proliferative mitogens are detected by the cell, it resumes proliferation. Withdrawal of such agents will cause the cell to cease proliferating, so long as the cell has not reached the

restriction point which, as mentioned earlier, is located at some point before the entry of the cell into S-phase (Zetterberg and Larsson, 1985).

When a myoblast has committed itself to myogenic differentiation, a different paradigm of exit is employed. The inhibitor of differentiation (Id) negatively regulates the muscle-specific transcription factors MyoD and myogenin through sequestration (Benezra et al., 1990a; Benezra et al., 1990b). Its levels are promoted by mitogenic stimulation, but are also inhibited by their withdrawal (Walsh and Perlman, 1997). Thus, the presence of Id maintains a division-ready phenotype and its downregulation is required for differentiation as it is well known that differentiation and proliferation are mutually exclusive cell states (Müller et al., 1999; Olsen, 1992). This promotes elevation of the levels of MyoD, followed by myogenin (Walsh and Perlman, 1997). An increase in MyoD activity in part promotes the elevation of p21 and p27 activity (Liu et al., 2004; Walsh and Perlman, 1997). These levels are kept elevated even in mitogen-plenty environs as both p21 and p27 exhibit positive feedback as they stabilize their own transcription factors (Walsh and Perlman, 1997). With the cell cycle machinery highly repressed and muscle-specific transcription factors highly active, the cell will then commit itself to myogenic differentiation.

The C_2C_{12} mouse satellite cell line has regularly been used in the experimentation of the muscle stem cell cycle, including its entry and exit (Jones et al., 2005; Dhawan and Rando, 2005; Koh et al., 1993). C_2C_{12} cells are therefore commonly used as an *in vitro*satellite cell model although they were initially derived for the study of muscular dystrophy. The line ultimately, however, became a model for many other studies of muscle and satellite cell behaviour (Yaffe and Saxel, 1977), as well as stem cell behaviour. The C_2C_{12} line is an immortalized satellite cell line where cells are continuously proliferative, given the correct mitogenic stimulus (Blau et al., 1985) and upon subjection to mitogen withdrawal or contact inhibition, myoblasts terminally differentiate and fuse into contractile myotubes. (Buttitta and Edgar, 2007)

1.4 Systems Biology

The cell cycle is an exceedingly complex and intricate system, consisting of hundreds of effectors working in concert to drive the cell cycle forward (Kaizu et al., 2010; Kohn,

1999). Due to this intense level of interactivity, the system is intrinsically complex and can produce situations or outputs that may seem counter-intuitive when looking at superficial structure. Top-down systemic analyses, such as large-scale network analysis or whole-genome expression profiles for this system, have been unattainable until relatively recently due to the lack of appropriate technology (Gilbert et al., 2006).

Large-scale networks are, however, generally considered to approximate a "sum-of-parts" system where simple interactions are successively modelled mathematically and combined to obtain a final, complex system (Tyson et al., 2003; Kohn, 1999). When derived in this way, these models may be analysed both singly and in concert. Models are thus constructed using equations and "viewed" using mathematical modelling software. The equations most often used for modelling of biological systems are ordinary differential equations (ODEs) with each equation representing the rate of change of a particular species. Parameters, constants, variables and kinetics, derived both empirically and from the literature, may be utilized to construct ODEs. Such ODEs are derived in the form:

$$\frac{dx}{dt} = f(x, p, t) \qquad 1$$

indicating that the change in substrate (or x) over time is a function dependent on the initial values of substrate, the parameters (p) of the reaction kinetics, and the point in time (t) the measurement was made (Klipp et al., 2009). The parameters of a given reaction, for example, may include the k_{cat} and the K_M values of the given reaction. Creating a set of ODEs for a network of reactions provides a means for solving the system numerically using computational solvers.

Following model construction, the calculation of the responsiveness of a cascade to input signal is a useful measure in the elucidation of the cascade's behaviour in response to a stimulus. Kholodenko *et al*. (1997) provided a means of mathematically modeling the effects of signal upon a target to investigate pathway response. This "response co-efficient" was defined as the change in target concentration due to a 1% change in signal concentration:

$$R_S^T = \frac{d\ln[T]}{d\ln[S]} \qquad 2$$

Thus, the change in the concentration of *S* will result in amplification (or dampening) in the concentration of *T* by a factor of *R*. This particular value describes the total responsiveness of an entire pathway. However, this global responsiveness arises as a nett response of all the local responses at each level of the pathway (Kholodenko et al., 1997). The local responsiveness for any level *i*, if the concentrations of effectors of prior levels remain constant, is given by:

$$r_{i-1}^{i} = \frac{d\ln[E_i]}{d\ln[E_{i-1}]} \qquad 3$$

As the global response co-efficient, the overall response from the original signal to final target over a linear pathway, arises as a result of its constituent local response co-efficients (Kholodenko et al., 1997), equation 2 may then be rewritten as the combined products of the local responses at each cascade level and may be calculated as follows:

$$R_S^T = r_s^1 r_1^2 r_2^3 \ldots r_{n-1}^T = \prod_{i=1}^{T} r_{i-1}^{i} \qquad 4$$

The response co-efficient of a branched pathway is simply the sum of the response co-efficients of all the independent linear branches of that pathway (Kholodenko et al., 1997). *i.e*:

$$R_S^T = \sum_{i=1}^{T} \prod (r_{i-1}^{i}) \qquad 5$$

where s_i and t_i are the signal and target respectively for the independent branches.

A response co-efficient greater than one implies that the target is being amplified at a rate greater than signal increase. A response co-efficient equal to one implies that the target is being amplified at an equivalent rate to signal, and a response co-efficient less than one, but greater than zero, implies that the target is being amplified at a slower rate than signal. When the response co-efficient is 0, the target is unaffected by any change in

signal and any response co-efficient less than 0 implies that the target is being dampened by an increase in signal (Kholodenko et al., 1997). The response co-efficient of a pathway may then be used as a tool to investigate further mechanisms within the pathway. For instance, highly responsive pathways are more likely to be ultrasensitive and display switch-like behaviour (Kholodenko, 2000).

1.4.1 Models

Computational models may be very generally divided into two categories: core models, and realistic models. Core models represent a system with simplified kinetics, rate equations, and parameters (Klipp et al., 2009). The usefulness of such models lies in their ability to elucidate underlying patterns of behaviour that are present within the structure of a system. For example, initial *in silico* core modelling predicted the presence of ultrasensitivity within the MAPK cascade (Huang and Ferrell, 1996). This observation was then verified *in situ* through experimentation on *Xenopus laevis* oocyte extracts. In these experiments, the activity of p42 MAPK *in vitro* was shown to be ultrasensitive to its upstream activator Mos (Huang and Ferrell, 1996).

The models generated for the cell cycle and MAPK pathways have ranged from the quite simple (Goldbeter, 1991) to the very intricate (Novák and Tyson, 2004) and may use equations for changes in metabolite concentrations that are generic across species (Csikász-Nagy et al., 2006) (Table 1.1). However, as more metabolites or effectors are added to a pathway, the more complex such models become. Greater pathway complexity tends to lead to increasingly difficult interpretations and predictions. As networks become increasingly larger, there is also a correspondingly larger amount of cross-talk between the components of the network; where the output of one pathway is the input of another, or where one pathway regulates the activity of another (Bray, 1995). Although models may be constructed modularly through component pathways models (Novák et al., 2007), due to cross-talk the output of such models may demonstrate emergent, rather than linear hierarchical, behaviour. This indicates that a network may be more than merely the sum of its parts (Bhalla and Iyengar, 1999).

Table 1.1: Mathematical models of the cell cycle and MAPK cascades in chronological order

Reference	Year	Purpose	Type	Number of Reactions
Goldbeter	1991	Cyclin activity	Core	6
Tyson	1991	Cyclin activity	Realistic	9
Huang and Ferrell	1996	ERK ultrasensitivity	Core / Realistic	11
Aguda and Tang	1999	Restriction point	Core	28
Kholodenko	2000	ERK cascade	Realistic	10
Tyson and Novák	2001	Cell cycle	Realistic	8
Heinrich *et al*.	2002	Signal transduction	Core	8
Novák and Tyson	2004	Cell cycle	Realistic	18
Hornberg *et al*.	2005	MAPK cascade	Core	8
Srividhya and Gopinathan	2006	Cell cycle	Core	8
Csikász-Nagy *et al*.	2006	Cell cycle	Core	13
Sundaramurthy *et al*.	2009	MAPK network	Realistic	20
Lim *et al*.	2009	ERK feedback	Realistic	20
Kaizu *et al*.	2010	Cell cycle	Realistic	732

1.4.1.1 Cell cycle models

The cell cycle is frequently studied, both in vitro and in silico, as a number of physiological disorders, such as cancer, arise from its dysfunction (Schubbert et al., 2007). Initially it was thought that cellular growth and division (i.e: DNA replication) were coordinated via a common mechanism (Harvey, 1940). However, cells were shown to attempt division even when their nuclei were removed (Hara et al., 1980). With this observation, studies into the cell cycle focused on how anuclear components, such as cyclins and CDKs, were able to co-ordinate division.

Tyson (1991) modelled cyclin synthesis, CDK pairing and CDK phosphorylation in an attempt to develop a mathematical model to describe the aforementioned observed behaviours. The model was highly simplified given what was known at the time. Parameters for the major metabolites, the catalytic rate constants and Michaelis-Menten constants, were unknown. Values for these unknowns were, however, tailored to produce outputs that matched *in vitro* data. For instance, the cycling of M-phase promoting factor (MPF, the factor believed to have the most significant impact on the cell cycle at the time), between active and inactive forms was assigned a period of 35 minutes. Although the model mainly focused on MPF autocatalysis and degradation, it revealed that the rate of

cyclin synthesis, rather than the activity of MPF, had a greater impact on the period of the cell cycle.

Numerous models of the cell cycle describing various particulars of cell growth and division, such as the link between cell size and division (Yang et al., 2006) or the restriction point (Aguda and Tang, 1999), have subsequently been developed (Table 1.1). Common to many of these models, however, is that they do not include MAPK entry into the cell cycle. Similarly, many models of MAPK pathways do not extend into the cell cycle (Sundaramurthy et al., 2009; Hornberg et al., 2005; Heinrich et al., 2002) In order to develop a more detailed understanding of how extracellular signalling is able to control the cell cycle, expanded models that link growth factors through signalling cascades to the cell cycle itself need to be developed.

1.4.1.2 MAPK models

MAPK cascades have been extensively modeled to more fully understand the mechanisms through which extracellular signal may be transduced to downstream targets. A common theme among the MAPK cascades is the capacity to promote switch-like (or ultrasensitive) behaviour from a graded signal (Huang and Ferrell, 1996). Michaelis-Menten enzymes require an 81-fold increase in stimulus to go from 10% to 90% V_{max}, while an ultrasensitive enzyme requires less, and a subsensitive enzyme more (Goldbeter and Koshland, 1981). Enzyme co-operativity normally imparts an ultrasensitive response, but the effect may also arise due to inter-converting enzyme cycles operating at near saturation. Ultrasensitivity generated under such conditions is denoted as being “zero-order” (Goldbeter and Koshland, 1982). Huang *et al*. (1996) investigated such zero-order ultrasensitivity within the ERK MAPK cascade; both *in silico* and *in vitro*. The *in silico* model was comprised of a cascade in which each level is modeled as a two-step dual-phosphorylation of the MAP kinases (Fig. 1.5).

The model was very robust and produced similar ultrasensitive responses over a large range of assumed kinetic values. Of importance, the entire cascade behaved like a single co-operative enzyme. As with the initial subunit of a co-operative enzyme, the initial kinase

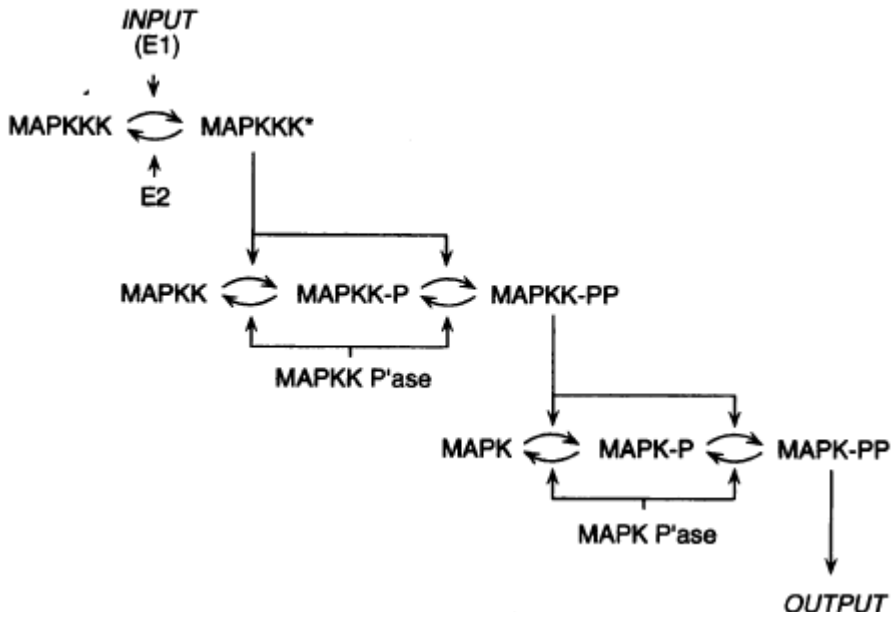

Figure 1.5: The Huang *et al*.(1996) model of ERK ultrasensitivity. Mitogens, through E1, activate MAPKKK, which in turn phosphorylates MAPKK sequentially to MAPKK-P and MAPKK-PP. Similarly, MAPK-PP then sequentially phosphorylates MAPK to MAPK-P and MAPK-PP. MAPK-PP, as the final MAPK cascade kinase then elicits an output. All the kinases are dephosphorylated at each step by specific phosphatases.

(MAPKKK) displayed a hyperbolic activation profile under the influence of input. Each subsequent kinase, however, like subsequent subunits of a co-operative enzyme, displayed the sigmoidal activation profiles indicative of an ultrasensitive mechanism. This ultrasensitive behaviour was found to be extremely sensitive to the total concentrations of the effectors, indicating that zero-order conditions were vital to overall pathway responsiveness (Huang and Ferrell, 1996).

The model similarly demonstrated that a two-step, rather than a single-step, dual-phosphorylation was important. To elicit a zero-order ultrasensitive response from a single-step phosphorylation cascade required biologically implausible kinase concentrations. A comparison of kinase substrate concentrations and kinase K_M values found that the substrate concentrations, of necessity, must be relatively higher than the K_M values, as would be expected of zero-order systems. All the predictions of the model were validated *in vitro* through observation of the equivalent of the ERK cascade, p42 MAPK, in *Xenopus laevis* egg extracts (Huang and Ferrell, 1996).

Kholodenko (2000) found several problems with the Huang and Ferrell(1996) model. During the *in vitro* validation of the model, Huang and Ferrell (1996) showed that amplification diminished down the cascade chain with p42 MAPK being amplified by signal input far less than the amplification of its effector kinase MEK (Fig. 1.5, MAPKK) over the same stimulus range, contrary to the known responsiveness of MAPK cascades to signal. Kholodenko (2000) intimated that embedded feedback within this pathway was capable of increasing pathway responsiveness by approximately seven-fold. Notably, feedback is present only in whole *Xenopus* egg cells, not egg extracts (Ferrell and Machleder, 1998), and therefore no feedback was present in the original Huang and Ferrell (1996) model. Kholodenko (2000) then constructed a model that was similar to the Huang and Ferrell (1996) model, which included feedback from the output of the model to the input (Fig. 1.6).

When the Kholodenko (2000) pathway was modeled without feedback, it quickly resulted in an effectively inactive state after removal of stimuli. However, with positive feedback, transient signal reduction over the switch-point between the active and inactive stable steady states did not immediately affect the pathway. Negative feedback, however, promoted oscillatory behaviour in the model under constant signaling conditions. With either the presence or absence of positive or negative feedback, the model maintained its ultrasensitive characteristic. However, with both feedback and ultrasensitivity, a small change in feedback strength was capable of destabilizing a static activated or inactivated steady state. While Kholodenko (2000) did not validate the model *in vitro*, subsequent experimentation has provided evidence for the presence of embedded feedback loops in the MAPK cascade (Vera et al., 2010).

Hornberg *et al*. (2005) constructed a core model of the MAPK pathway to investigate interplay between the kinases and phosphatases within the pathway. The model was based on the ERK MAPK cascade of a slowly-cycling receptor and three single-step dual-phosphorylation cycles. This model (Fig. 1.7) was used to generate predictions about signaling behaviour, which were then verified *in vitro*. The Hornberg *et al*. (2005) model demonstrated several important characteristics. Firstly, although the kinases were modeled as starting with low levels of active kinases, once the model reached a steady state under minimal mitogenic stimulation, the levels of active kinases were higher than their initial values. Secondly, while these steady-state levels were very low, their basal

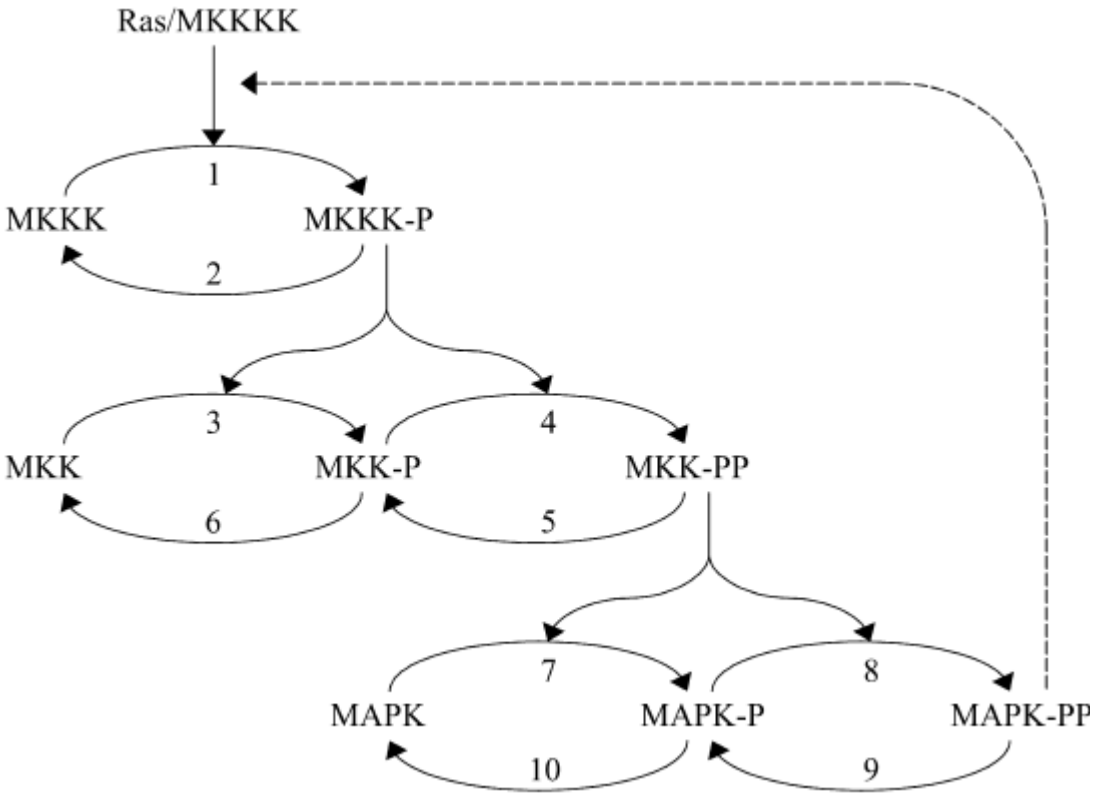

Figure 1.6: The Kholodenko (2000) model of negative feedback. Akin to the Huang *et al*. model (1996) model, each cascade is phosphorylated by the preceding active kinase and dephosphorylated by specific phosphatases. However, the activation of MAPK-PP in turn leads to the downregulation of the first reaction, causing MKKK to be phosphorylated with less efficacy.

activation suggested that, even under negligible signaling conditions, there was a low but constant presence of active effector kinases capable of responding faster to stimuli than a completely inactive cascade (Hornberg et al., 2005).

It was originally predicted that phosphatases and kinases operate with equivalent efficacy, but with an opposite sign (Kahn and Westerhoff, 1991). Indeed, the Hornberg *et al*. (2005) model demonstrated through metabolic control analysis that, as expected, the kinases impart positive control on enzyme activation, while the phosphatases impart negative control. However, the absolute overall control on activation was not equivalent. To investigate this control, the model was modulated through the use of inhibitors. Phosphatase and kinase activity was modulated by lowering the V_{max} of the kinases and increasing concentrations of a simulated competitive inhibitor of the phosphatases. Under

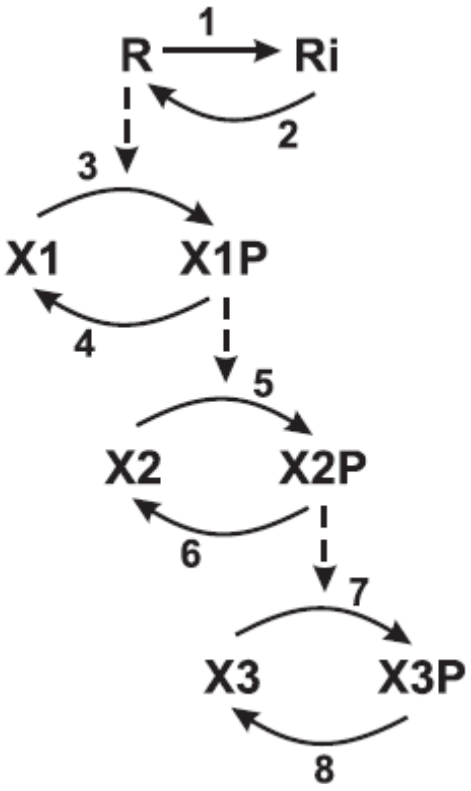

Figure 1.7: The Hornberg *et al*.(2005) model of signal transduction. A receptor complex slowly cycles between inactive (Ri) and active (R) forms under the influence of mitogens. The active complex then triggers the activation of a MAP4K (X1 → X1P). Each level of the cascade triggers the activation of the subsequent downstream kinase, culminating in the formation of X3P. Each active kinase is also inactivated by specific phosphatases (X1P → X1).

these conditions, the model demonstrated that the kinases controlled downstream signal amplitude, as inhibition thereof only lowered X3P levels, while the phosphatases controlled both signal amplitude and duration, as their inhibition affected both the level of X3P and the length of its activation (Hornberg et al., 2005). A long-standing assumption was that kinases were the most important effectors of a cascade and the primary finding of the Hornberg *et al*. (2005) model and experimentation was that the sum of the signal amplitude control coefficients tended towards 1, while the sum of the duration control coefficients tended towards -1. This finding demonstrated that while phosphatases control signal duration more than the kinases the kinases and phosphatases were of equal import in a signaling cascade. The predictions of the model were then verified *in vitro* through the investigation and inhibition of the ERK pathway in mouse renal fibroblasts, which showed similar effects (Hornberg et al., 2005).

Originally, p38 MAPK was isolated and characterized as a stress-activated protein kinase (Zarubin and Han, 2005). Modeling of the p38 MAPK pathway has recently been performed, but with emphasis on p38's activation via stressors, utilizing stress-transducing molecules, such as TAB, as activators of p38 (Sundaramurthy et al., 2009). The Sundaramurthy *et al*. (2009) model was constructed to mimic the MAPK network and the cross-talk present between the MAPK families (Fig. 1.8). While the ERK pathway was modeled as being activated solely by mitogen signal transducers, the p38 and JNK pathways were modeled as being activated primarily by stress signal transducers. The primary findings of the model were that transient activation of ERK5, JNK1 and p38β became sustained due to the two-way cross-talk between the pathways while the sustained activation of JNK2/3 and p38δ were unaffected by the presence of cross-talk within the network. Similarly, ERK5 activation was unaffected by the activation or inactivation of the other cascades due to their being no cross-talk to ERK from their activators. The main hypothesis of Sundaramurthy *et al*. (2009) was that systems were better represented if adjacent pathways and their potential cross-talk interactions are present within a network. While p38's activation via stressors and its interaction with other pathways has been investigated, a gap currently remains in the computational modeling literature on the mechanism through which p38 is activated via growth factor stimulation.

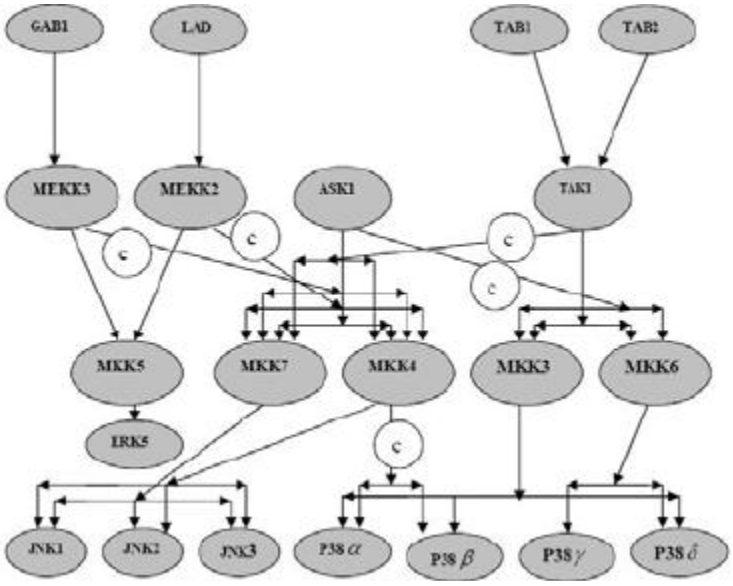

Figure 1.8: The Sundaramurthy *et al*. (2009) model of MAPK cross-talk. The ERK5, p38 and JNK pathways are represented as a network with crosstalk (C) between the pathways. In this model ERK5 is activated solely by mitogenic stimuli while the p38 and JNK cascades are activated primarily by stress signal transducers.

1.5 Aims

This project was initially undertaken with two distinct yet interconnected goals. The first was to elucidate events within the mouse C_2C_{12} cell cycle in a traditional 'wet-lab' approach, and the second was to model computationally these findings in a 'dry-lab' approach. The wet-lab experimentation included

1.) *Clarification of the C_2C_{12} cell cycle*

This element of the thesis involved the clarification of the lengths of the G_0 and G_1 phases in the C_2C_{12} cell cycle. After induction of growth-arrest through serum deprivation treatment the following was determined:

a.) The length of time for a cell to re-enter the cell cycle from a growth-arrested state

b.) The location of the R-point through addition of cycloheximide to C_2C_{12} cells at different time points in G_1, followed by FACS analysis several hours later, to determine if the cells re-entered G_0

2.) *Assaying the effect of the inhibition of p38 on the C_2C_{12} cell cycle*

This part of the thesis entailed the use of SB203580 as a potential agent to induce growth arrest. To clarify if the growth arrest induced was one of quiescence a panel of quiescence-specific markers were tested upon the arrested populations.

The dry-lab experimentation included:

3.) *Modelling the p38 MAPK pathway via mitogenic stimulation*

Many models have been developed for the inner-workings of the cell cycle but none have fully realised the method through which this mechanism becomes activated. Therefore, the third aim of this thesis was to construct a model of the p38 MAPK

pathway that could, in future, be used as a front-end regulatory mechanism for the cell cycle. The p38 MAPK pathway had not yet been specifically modelled mathematically under the effects of mitogenic stimulation. Therefore, a *de novo* formulation of a model of the p38 MAPK pathway was necessary and included:

a.) The effect of SB203580 on the activity of p38

b.) Exploration of the model to describe pathway behaviour due to the structure of the pathway

c.) Attempts to validate the model with *in vitro* data

Chapter Two – Investigation of the C_2C_{12} cell cycle

2.1 Introduction

Previous studies have shown that asynchronous C_2C_{12} populations require approximately 12 hours to undergo one population doubling (Rossi et al., 1997) and a growth-arrested population requires approximately 8 hours to enter the S-phase (Tintignac et al., 2000). However, no information on the position of the R-point within the C_2C_{12} cell cycle has yet been published. In the 3T3 primary culture murine embryonic fibroblast line, it was determined that the restriction point lies most likely 2 to 3 hours prior to the inception of DNA synthesis in S-phase (Campisi et al., 1982b).

In order to elucidate the R-point position, a synchronous population of C_2C_{12} cells is required and there are many methods, both *in vivo* and *in vitro*, capable of promoting cell cycle exit (Collins et al., 2009; Gillespie et al., 2009; Donati et al., 2005; Gredinger et al., 1998; Lassar et al., 1994). A relatively inexpensive method involves culturing the cells for several hours in serum-depleted media, thereby limiting mitogenic stimuli (Fujita et al., 2010), while another method exposes cells for 30 – 36 hours to a 1% (v/v) foetal calf serum growth medium that has been methionine-depleted to limit protein synthesis (Kitzmann et al., 1998). Serum deprivation allows cells to both exit G_1 and return to G_0 as well as allowing cells past the R-point to complete division and reversibly enter G_0(Hlaing et al., 2002). However, if exposed to serum-free media for too long, this method is capable of inducing two other irreversible states of G_0, namely differentiation through autocrine/paracrine signaling (Mercer et al., 2005; Wu et al., 2000b) and apoptosis (Kummer et al., 1997). While the relative low cost of this method will allow a good approximation of the location of the R-point to be determined, a more effective method of growth-arrest should ideally be employed to ensure the cells exit into G_0 quiescence and not apoptosis or differentiation.

Cycloheximide (CHX) is a bacterially derived protein that inhibits protein synthesis by binding directly to the ribosome and preventing polypeptide elongation (Stöcklein and

Piepersberg, 1980; Trakatellis et al., 1965; Siegel and Sisler, 1964). It has been shown to arrest proliferating cellular populations if applied to the cells before the R-point has been reached (Zetterberg and Larsson, 1985). Those cells beyond the R-point will continue through the cell cycle. The molecule SB203580 is also capable of inducing growth arrest through the specific inhibition of p38 as it is known to regulate both the proliferative (Jones et al., 2005) and differentiation (Gredinger et al., 1998) pathways. Using the MM14 satellite cell analogue line Jones *et al*. (2005) demonstrated that the inhibition of p38 α/β by SB203580 was sufficient to cause cells under mitogenic stimulus to cease proliferation and differentiation. Additionally, the presence of an SB203580-resistant mutant of p38 caused cells to proliferate during mitogenic stimulation even in the presence of SB203580. An important aspect of the action of SB203580 was that cells treated by it are capable of re-entering the cell cycle upon its removal (Jones et al., 2005; Kang et al., 2005).

As cells adopt the different states of the cell cycle, a number of molecules are expressed that may be used as markers to identify these states. In order to determine whether a cellular population has entered into a quiescence-specific growth-arrested state, a several markers were employed to determine the specific cell cycle state. Pertinent to the C_2C_{12} cell line, MyoD, sphingomyelin, and the monoclonal antibody SM/C-2.6 were used to determine if a population exists in a quiescent state.

MyoD is a very well characterized myogenesis-commitment transcription factor that controls the expression of many muscle-specific genes and its induction is sufficient to cause other cells, such as fibroblasts, to transdifferentiate into the myogenic lineage (Tapscott, 2005). Myoblast progenitors are induced to commit to myogenesis through the activities of various signals such as the wingless and sonic hedgehog proteins (Münsterberg et al., 1995) which upregulate the activities of several myogenic proteins including, amongst others, the MyoD family of transcription factors (Lassar and Münsterberg, 1996). Upon exposure to differentiation stimuli MyoD is specifically directed into the nucleus (Vandromme et al., 1994) where it coordinates the expression of muscle-specific transcripts such as myogenin and MRF-4 (Tapscott, 2005). When there are no explicit differentiation signals, MyoD is then actively exported out of the nucleus (Sun et al., 2008). The nuclear activity of MyoD is coordinated, in part, through phosphorylation by p38. This phosphorylation both promotes the nuclear import of MyoD (Vandromme et al.,

1994) and the capacity of MyoD to bind to its DNA promoter region (Gillespie et al., 2009). Therefore, a quiescent cell will display cytoplasmic MyoD, while an activated cell will display nuclear MyoD.

Lipids have been implicated as being important molecules for signaling in various cellular pathways, such as myoblast fusion and cytokinesis (Donati et al., 2005) and it has been demonstrated that sphingomyelinis an integral molecule for signaling during quiescence (Nagata et al., 2005). In C_2C_{12} cells, sphingomyelin forms compact micro-domains, known as rafts,on the cell surface of quiescent cells to assist in molecular signal aggregation. These rafts are themselves bioactive as sphingomyelin metabolic products, such as ceramide, are involved in proliferation, apoptosis, and differentiation signaling processes (Donati et al., 2005; Nagata et al., 2005). Sphingomyelin is metabolized by phospholipase A2, which is itself activated by p38. Hence, upon p38 activation, the levels of sphingomyelin will drop (Jones et al., 2005). It is normally difficult to detect lipids directly *in situ* and they are normally detected through homogenization of cellular material (Yamaji *et al*., 1998). However, lysenin, a lipid binding protein from the earthworm *Eisenia foetida*,is capable of specifically binding sphingomyelin, allowing its presence to be determined through immunocytochemical methods (Yamaji et al., 1998).

The monoclonal antibody, SM/C-2.6, recognizes an epitope present solely on quiescent satellite cells. The antibody does not non-specifically bind other common myoblast quiescence protein markers, such as CD34 and M-cadherin (Fukada et al., 2004). Cells isolated through fluorescence-activated cell sorting (FACS) using SM/C-2.6 from homogenized tissue samples *ex vivo* were capable of division and formation of new myofibrils both *in vivo* and *in vitro*. Furthermore, cells expressing SM/C-2.6 concurrently express the truncated CD34 isoform, itself a marker of quiescence(Cossu and Molinaro, 1987; Campion, 1984).

A proper understanding of the cell cycle is necessary for the development of a model that accurately reflects the behaviour of the dividing cell. The fine details of the C_2C_{12} cell cycle, such as the position of the R-point, remain undetermined. To facilitate further understanding of the cell cycle, experiments were undertaken to determine the position of

the R-point, and the efficacy of using the p38 inhibitor SB203580 to modulate the entry into the cell cycle.

2.2 Materials and Methods

2.2.1 Cells and culture

C_2C_{12} cells were donated by the CapeHeartCenter of the University of Cape Town. The C_2C_{12} cell line (Blau et al., 1985) is a post-replicative crisis diploid sub-clone of the C2 line originally developed by Yaffe and Saxel (1977) from isolated myogenic satellite cells (Mauro, 1961). All cells were cultured under sterile conditions from passages 10 to 25 and were kept at 37.5^{o}C under 5% CO_2 in a humidified incubator during experimentation or, for long-term storage, were kept under liquid nitrogen at -196^{o}C.

2.2.2 General Reagents

2.2.2.1 Dulbecco's Modified Eagle's Medium (DMEM): (pH 7.3)

The contents of 1 vial of DMEM (Sigma-Aldrich, D5648) was added to deionized water (dH_2O) (900 ml) and stirred until dissolved. Sodium hydrogen carbonate (3.7 g) was then added and stirred until dissolved. The pH was then lowered to 7.3 with dilute hydrochloric acid and the solution brought to a final volume of 1 L with dH_2O.

2.2.2.2 Dulbecco's Phosphate-Buffered Saline (PBS): (8 mM Na_2HPO_4, 2 mM KH_2PO_4, 140 mM NaCl, 2.7 mM KCl, 0.5 mM $MgCl_2$, 0.9 mM $CaCl_2$, pH 7.2)

Sodium chloride (16 g), potassium chloride (0.4 g), disodium hydrogen orthophosphate (2.3 g) and potassium hydrogen phosphate (0.4 g) were dissolved in dH_2O (1600 ml). Calcium chloride dihydrate (0.264 g) was dissolved in dH_2O (200 ml) and magnesium chloride hexahydrate (0.2 g) was dissolved in dH_2O (200 ml). All three solutions were autoclaved separately and then combined when cooled under sterile conditions.

2.2.2.3 Growth media: (10% [v/v] Foetal calf serum (FCS), 2% [v/v] penstrep, pH 7.4)
FCS (100ml) and a penicillin (10000 $U.ml^{-1}$)/streptomycin (10 $mg.ml^{-1}$) mixture (20 ml) were thoroughly mixed with 1 L DMEM before sterilization via UV light for 30 minutes and ultra-filtration through a 0.22 µm filter.

2.2.2.4 Serum-free media: (2% [v/v] penstrep, 4 mM L-glutamine, pH 7.4)
A penicillin (10'000 $U.ml^{-1}$)/streptomycin (10 $mg.ml^{-1}$) mixture (1 ml) was thoroughly mixed with filter-sterilized DMEM (48 ml).

2.2.2.5 Cycloheximide (CHX): (196.8 $mg.ml^{-1}$ primary stock, 10 $mg.ml^{-1}$ secondary stock)
CHX (49.2 mg) was diluted in DMSO (250 µl) and vortexed vigorously to prepare the 196.8 $mg.ml^{-1}$ primary stock. The 10 $mg.ml^{-1}$ secondary stock was made by diluting the primary stock (2.5 µl) in dH_2O (50 µl). A working concentration of 10 $\mu g.ml^{-1}$ was used for all experiments.

2.2.2.6 Vindeløv Nuclei Extraction Buffer Solution: (250 mM sucrose, 40 mM trisodium citrate, 5% [v/v] DMSO)
Sucrose (1.71 g), trisodium citrate (0.235 g) and DMSO (1 ml) were dissolved in dH_2O (16 ml) and the solution titrated to pH 7.6 before being made up to a final volume of 20 ml.

2.2.2.7 Spermine Tetrahydrochloride (STHC) solution: (10 $mg.ml^{-1}$ spermine tetrahydrochloride)
Spermine tetrahydrochloride (0.5 g) was dissolved in dH_2O (50 ml).

2.2.2.8 Diluent: (3.4 mM trisodium citrate, 0.1% [v/v] Triton X-100, 1.5 mM spermine tetrahydrochloride, 0.5 mM Tris, pH 7.6)
Trisodium citrate (0.2 g), Triton X-100 (200 µl), Tris (0.012 g) and STHC (10.44 ml) solution were dissolved in dH_2O (175 ml). The solution was titrated to pH 7.6 and then made up to a final volume of 200 ml.

2.2.2.9 Trypsin extraction solution:
A 0.25% trypsin solution (500 µl) was diluted with Diluent (42 ml) and titrated to pH 7.6.

2.2.2.10 Inhibitor solution:

FCS (500 µl) and 1 $mg.ml^{-1}$ RNase A solution (500 µl) was diluted with Diluent (4 ml) and titrated to pH 7.6.

2.2.2.11 Propidium Iodide (PI) solution: (pH 7.6)

A 1 $mg.ml^{-1}$ propidium iodide solution (1040 µl) and STHC solution (290 µl) were mixed with Diluent (1170 µl) before being titrated to pH 7.6.

2.2.2.12 Hoechst solution:

10 $mg.ml^{-1}$ Hoechst 33342 (Invitrogen) nuclear counterstain (2 µl) was diluted in PBS (400 µl).

2.2.2.13 Antibody/detector preparation

All antibodies and secondary detectors were supplied in solution and were diluted with PBS to the values given parentheses. Lysenin ($^1/_{1000}$) was purchased from Sigma-Aldrich. Rabbit anti-lysenin ($^1/_{200}$) was purchased from the Peptide Institute. FITC-conjugated donkey anti-rabbit-IgG ($^1/_{4000}$), FITC-conjugated donkey anti-mouse-IgG ($^1/_{4000}$) and FITC-conjugated streptavidin ($^1/_{2000}$) were purchased from Jackson ImmunoResearch. Mouse anti-MyoD ($^1/_{50}$) was purchased from BD Biosciences. Biotinylated SM/C-2.6 was a gift from Dr. Hiroshi Yamamoto of the University of Osaka.

2.2.3 Flow cytometry

A Beckman-Coulter Epics XL-MCL flow cytometer with a 488 nm argon ion excitation laser was employed for the generation of all flow cytometry data. The specific protocols employed in the generation of data from prepared samples are detailed in Appendix A. Two methods were employed to determine the chromosomal content of the C_2C_{12} cells viz. whole cell (Crissman and Steinkamp, 1982) and nuclear extract (Vindeløv et al., 1983b; Vindeløv et al., 1983a) cytometry. In both cases, a final concentration of propidium iodide of 2.5 $\mu g.ml^{-1}$ were used for the analyses (Schutte et al., 1985).

2.2.3.1 Whole-cell and nuclear extraction flow cytometry

Whole-cell flow cytometry

Cells were prepared according to a modified version of the method of Crissman and Steinkamp (1982). Following harvesting via trypsinization, the cells were pelleted in a 15 ml falcon tube in a desktop centrifuge for 5 minutes and excess supernatant discarded. The cells were then resuspended PBS (1 ml) and the solution centrifuged. The supernatant was discarded and the cells resuspended in PBS (1 ml) whereupon ice-cold absolute ethanol (2.5 ml) was gently added down the side of the tube while vortexing and the tube incubated for 10 minutes on ice. The cells were then centrifuged for 5 minutes and the supernatant discarded. The cells were then resuspended in PBS (1 ml) and centrifuged again and the supernatant discarded to remove traces of ethanol. The cells were resuspended in PI solution (1 ml), incubated at 4^{o}C for 15 minutes and were then run through the flow cytometer on the whole-cell settings outlined in Appendix A.

Nuclear extraction flow cytometry

Cellular nuclei were isolated and prepared for cytometric analysis according to the method of Vindeløv *et al.*(1983b). Following harvesting via trypsinization, cells were pelleted in a desktop centrifuge for 5 minutes and the supernatant discarded. The pellet was then resuspended in Vindeløv nuclei extraction buffer (200 µl) and Trypsin extraction solution (450 µl) was added before incubating at room temperature for 10 minutes. Inhibitor solution (375 µl) was then added and the mixture incubated at room temperature for 10 minutes. PI solution (375 µl) and STHC solution (40 µl) were then added and the solution incubated at 4^{o}C for 15 minutes in the dark. Following staining, the nuclei were sheared from their cytoplasmic coats through filtration through a cell strainer. The prepared nuclei were then run through a flow cytometer according to the settings for extracted nuclei detailed in Appendix A.

2.2.3.2 Induction of growth arrest

Cells were subjected to three different treatments known to induce growth-arrest: serum deprivation, CHX treatment, and SB203580 treatment. Cells for serum-deprivation were plated with serum-free media for 16 hours before being harvested for flow cytometric analysis. The cells for CHX treatment were treated with 10 $\mu g.ml^{-1}$CHX in growth media for 20 hours before being harvested for flow cytometry (Zetterberg and Larsson, 1985). The cells for SB203580 treatment were initially exposed to 40 μM SB203580 in growth media, followed by a second dose 16 hours later. Four hours after the second dose, the cells were harvested for flow cytometry. The 40 μM double dose of SB203580 was chosen as a method of growth arrest as prior work had shown that this was required to inhibit an asynchronous population from undergoing DNA synthesis (Van den Heever, 2006).

2.2.3.3 Length of G_0/G_1 to S

The length of G_0/G_1 to S-phase was determined using both whole C_2C_{12} cells and isolated nuclei of C_2C_{12} cells as mentioned in 2.2.3.1. While whole-cell preparation for flow cytometry is cheap, fast and relatively easy, isolation of cellular nuclei removes extraneous cytoplasm and may lower non-specific binding of fluorophores (Vindeløv et al., 1983a). Cells were plated in growth media and allowed to reach a confluency of 70%. The media was then discarded and the cells washed with PBS before being treated with serum-free media for 16 hours to induce growth arrest. A control group was harvested at hour 0 that represented a population synchronized in a growth-arrested state. All other flasks then had growth media reapplied to stimulate proliferation. Cells were harvested every hour from hour 5 to hour 14. This procedure was performed for both whole-cell and nuclear-extraction experiments.

2.2.3.4 R-point position determination

C_2C_{12} cells were synchronized by serum starvation for 16 hours before serum-containing media was re-applied. This point was called hour 0. Each flask was then treated

with a single dose of CHX to a final concentration of 10 µg.ml^{-1} at hours 6 through 10 and all populations were harvested at hour 14 for analysis for flow cytometry as described in 2.2.3.1 as this was a sufficient length of time for synchronized C_2C_{12} cells to reach S-phase (Tintignac et al., 2000). Each hour had one replicate, and the experiment was performed in triplicate. The experimental scheme is outlined in Table 2.1.

Table 2.1: Experimental scheme for the R-point determination

Hour	Flask					
	A	B	C	D	E	F
-16	Add serum-free media					
0	Harvest	Change to growth media				
6		Add CHX				
7			Add CHX			
8				Add CHX		
9					Add CHX	
10						Add CHX
14		Harvest 5 remaining flasks				

2.2.4 Immunocytochemistry

C_2C_{12} cells were allowed to proliferate to approximately 70% confluency in either 12-well or 24-well plates before being treated twice with 40 µM SB203580 as a final concentration. Control plates that did not receive SB203580 treatment were also prepared. Cells were prepared for confocal microscopy as mentioned below 20 hours after final SB203580 addition and were analysed on a Zeiss LSM 710 ConfoCor 3 confocal microscope. All steps after culturing were conducted at 4^{o}C, including each 5 minute PBS wash. Cells were rinsed of excess media with PBS, followed by a 15 minute fixation with a 4% paraformaldehyde solution (50 µl). Post fixation, cells were washed three times before being blocked with 2% donkey serum for 20 minutes. Following blocking, the cells were washed three times.

For lysenin staining, the coverslips were incubated for 30 minutes in lysenin solution (1:1000, Sigma-Aldrich) before being washed three times. Rabbit anti-lysenin solution (1:200, Peptide Institute) was added as primary antibody and incubated for 90 minutes,

followed by washing four times. Coverslips were then incubated with FITC-conjugated donkey anti-rabbit-IgG solution (1:4000, Jackson ImmunoResearch) as a secondary detector before being washed five times. In the last wash, Hoechst solution (100 µl) was added and incubated with the solution for 5 minutes. After Hoechst staining, a further five washes were performed before the coverslips were mounted on slides with fluorescent mounting media.

For MyoD staining, mouse anti-MyoD solution (1:50, BD Biosciences) was added as primary antibody and incubated for 90 minutes, followed by washing four times. Coverslips were then incubated with FITC-conjugated donkey anti-mouse-IgG solution (1:4000, Jackson ImmunoResearch) as a secondary detector before being washed five times. In the last wash, Hoechst solution (100 µl) was added and incubated with the solution for 5 minutes. After Hoechst staining, a further five washes were performed before the coverslips were mounted on slides with fluorescent mounting media.

For SM/C-2.6 staining, biotinylated SM/C-2.6 solution (1:500, a gift from Dr. Hiroshi Yamamoto of the University of Osaka) was added as primary antibody and incubated for 90 minutes, followed by washing four times. Coverslips were then incubated with FITC-conjugated streptavidin solution (1:2000, Jackson ImmunoResearch) as a secondary detector before being washed five times. In the last wash, Hoechst solution (100 µl) was added and incubated with the solution. After Hoechst staining, a further five washes were performed before the coverslips were mounted on slides with fluorescent mounting media.

2.2.5 Statistical Analysis

Sample distributions were tested for normality using the Shapiro-Wilk test. Those samples that were normally distributed were tested for significance using the parametric one-tailed unpaired Student's T-test. The samples that were not normally distributed were tested for significance using the nonparametric Mann-Whitney U test. All data represented graphically will be of the sample mean ± the standard error of the mean (SEM).

2.3 Results

2.3.1 Serum deprivation and SB203580 induced C_2C_{12} cells into growth arrest

To synchronize cells, several methods of growth arrest induction were analyzed, namely serum deprivation, CHX treatment and SB203580 treatment (Fig. 2.1). Flow cytometric analysis revealed that control cells from a normal, untreated population (Fig. 2.1A) showed 67 ± 1% of the population in G_0/G_1, the lowest of all the samples, and approximately 33 ± 1% of the population in $S/G_2/M$, the highest of all the samples. The serum-deprived cells exhibited 78 ± 8% of the cells in G_0/G_1 and 20 ± 9% of the populations in $S/G_2/M$. The CHX-treated cells showed the least tendency towards growth arrest with 71 ± 3% of the populations in G_0/G_1 and 29 ± 3% in $S/G_2/M$.. The SB203580-treated populations showed the greatest tendency towards growth arrest with 81 ± 0.5% of the populations in G_0/G_1 and 18 ± 0.1% in $S/G_2/M$. As SB203580 treatment is considerably more expensive and time consuming to implement, serum-deprivation treatment was initially used as the method of growth arrest induction.

2.3.2 C_2C_{12} cells take 7 to 9 hours to enter S-phase

As the R-point marks the junction between G_1 and irreversible commitment to S, it was necessary to first determine how long it takes a synchronized population to reach S. The length of time of re-entry into S-phase from a growth-arrested state was therefore investigated using whole-cell flow cytometry as per 2.2.3.1.

Once cells were subjected to serum-containing media, levels of G_0/G_1 and S chromatin content of the population remained roughly unchanged for 7 hours post serum re-addition at 68 ± 2% and 24 ± 1% respectively (Fig. 2.2). After hour 7, however, a significant increase in S-phase was noticeable, and by hour 10 there was 47 ± 1% of the population was in G_0/G_1 and 46 ± 1% in S. These results suggest that the population had undergone a significant switch from a G_0/G_1 state and had entered into S-phase 7 hours after the re-addition of serum.

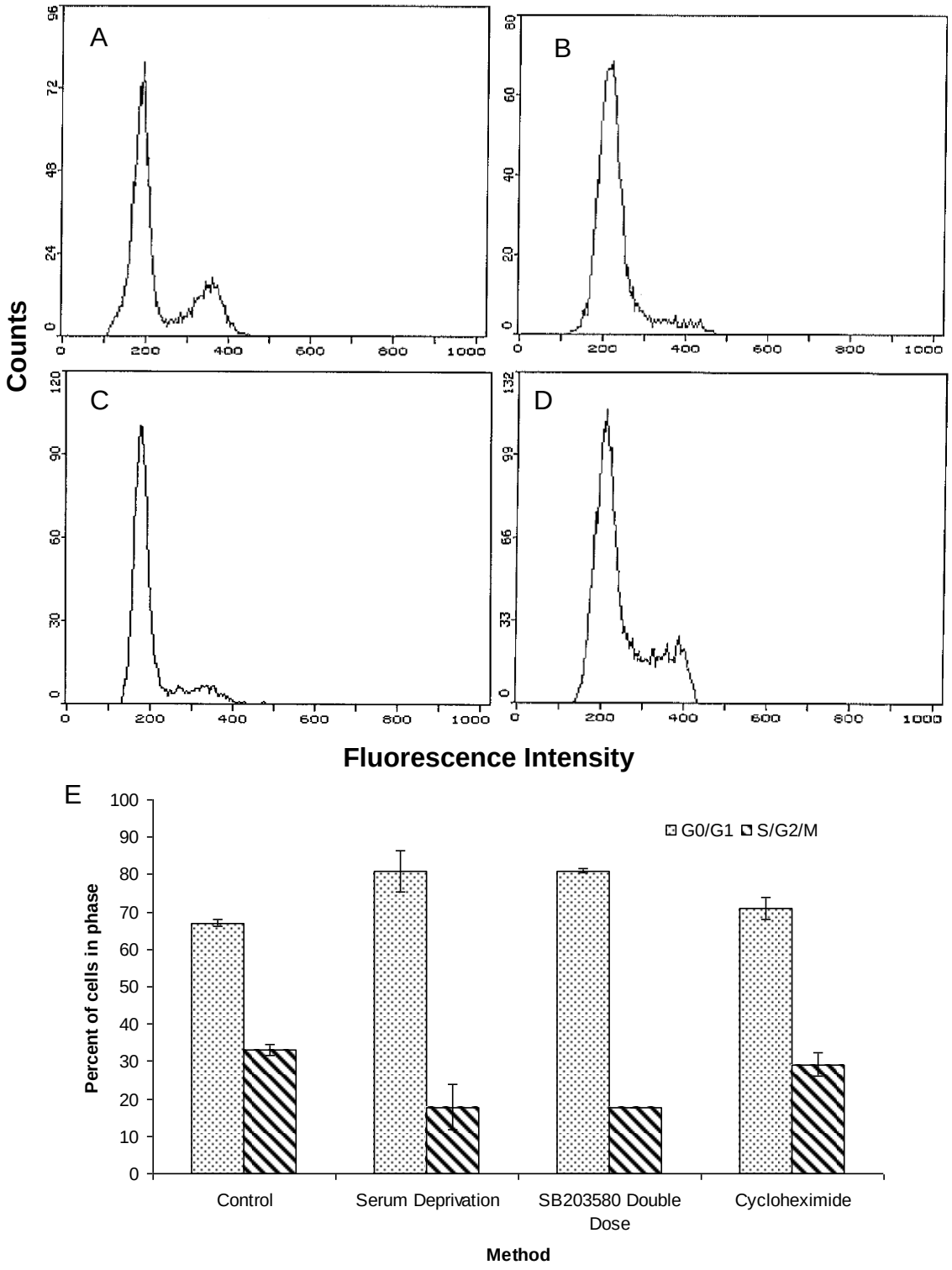

Figure 2.1:C_2C_{12} growth arrest induction. Several treatments were used to induce growth arrest and their efficacies compared. Control cells (A) were allowed to proliferate until 70% confluency before harvesting. Serum-deprived cells (B) were subjected to mitogen withdrawal for 16 hours before being harvested. SB203580-treated cells (C) were SB203580-treated twice in growth media prior to harvesting. 10 $\mu g.ml^{-1}$ cycloheximide was added to growth media and cells were harvested 20 hours later (D).E: graph of harvest data. Data presented as mean ± SEM. n=2.

Following serum deprivation, cells were induced into a growth-arrested state and a substantial proportion of the population were seen to be in S-phase (Fig. 2.2). By hour 5, S-phase percentage was lowest at 20%, indicating that most of the population was in G_0/G_1.

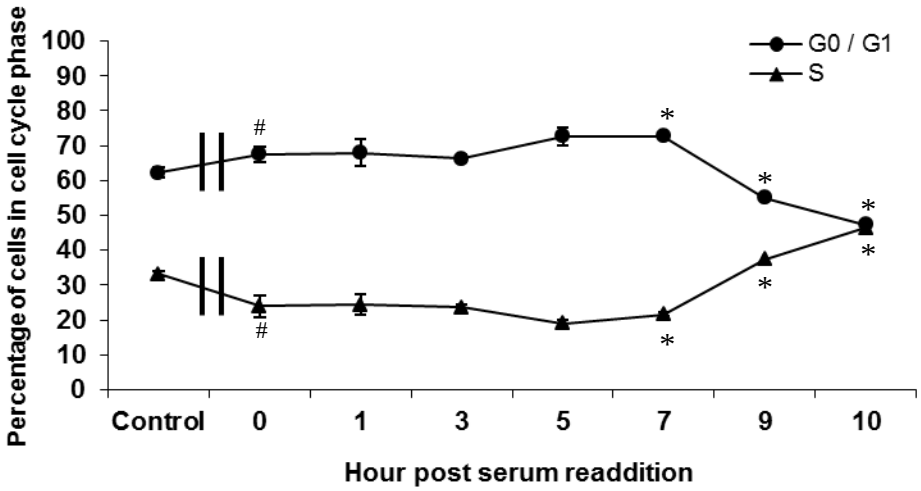

Figure 2.2: Length of S-phase re-entry of growth-arrested whole-cells. Cells were serum starved for 16 hours. Growth media was then added and the cells were allowed to proliferate. The percentage in G_0/G_1 and $S/G_2/M$ was monitored over the next 10 hours. Control cells were of an untreated normally proliferative population. Data presented as mean ± SEM. n=3. $^{\#}$: $p < 0.05$ as compared to Control. *: $p < 0.05$ as compared to hour 0.

The S-phase values found were more elevated than was to be expected of a growth-arrested population. However, it is also known that ploidy analysis of whole cells imparts a high level of background fluorescence (Vindeløv et al., 1983a; Vindeløv et al., 1983b). This caused difficulty in the accurate determination of the point of S-phase commitment as there appeared to be more cells in S-phase than would be expected of a growth-arrested population. To mitigate such background fluorescence the nuclei of the C_2C_{12} cells were extracted and their chromatin content re-confirmed as per 2.2.3.1. Cells were growth-arrested via serum deprivation and re-entry to S-phase upon mitogen stimulation analyzed every hour for 10 hours (Fig. 2.3). When compared to an unsynchronized, rapidly proliferating population (RPN), synchronized cells (hour 0) were found to have a significantly higher G_0/G_1 content of 88.5 ± 1% and a concomitant significantly lower $S/G_2/M$ content of 12 ± 1%. These populations were therefore considered growth-arrested.

Hours 5 through 14 were then compared against hour 0 to see when the first significant difference was found in G_0/G_1 and $S/G_2/M$. The first significant difference was seen at hour 8 with 84.7 ± 1% of the populations in G_0/G_1 and 15.6 ± 1% in $S/G_2/M$. Hour 14 culminated with G_0/G_1 levels of 56.2 ± 1% and $S/G_2/M$ levels of 44.8 ± 1%. These results confirmed that most C_2C_{12} cells had entered S-phase between hours 7 and 8 post serum re-addition.

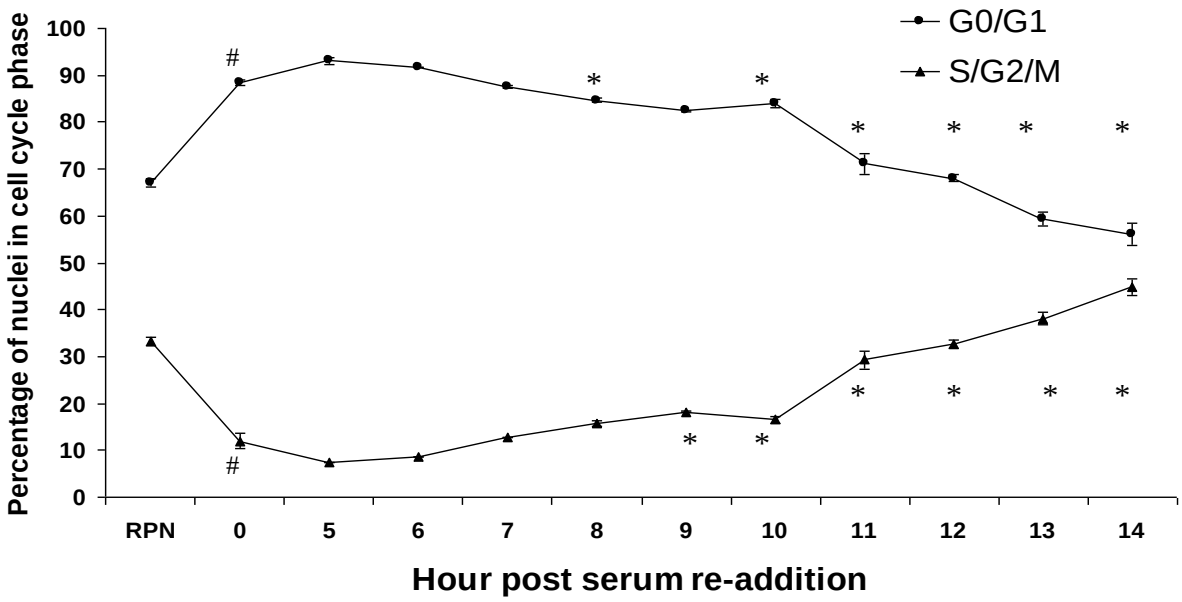

Figure 2.3: Length of S-phase re-entry of growth-arrested nuclei. Cells were serum-starved for 16 hours before being changed to growth media. Every hour for 14 hours the cells were harvested and their nuclei extracted as described previously to monitor theirG_0/G_1 and $S/G_2/M$ chromatin content. RPN: Rapidly proliferating nuclei (Control). Data presented as means ± SEM. n = 3. #: $p < 0.05$ compared to RPN. *: $p < 0.05$ compared to hour 0.

2.3.3 The Restriction-point in C_2C_{12} cells lies between hours 6 and 7

To determine the position of the R-point C_2C_{12} cells were growth-arrested via serum deprivation for 16 hours. After 16 hours, a control flask was harvested (hour 0) and CHX was added once to each flask consecutively over a 10-hour period (Table 2.1). Four hours after the last addition of CHX, the remaining flasks were harvested for flow cytometric analysis (at hour 14). If the R-point were yet to be crossed, the addition of CHX would cause the cells to exit once again into G_0, while those cells beyond the R-point would continue through S-phase. When hour 0 (G_0/G_1: 88.1 ± 1%, $S/G_2/M$: 9 ± 1%) was

compared with the unsynchronized rapidly proliferating nuclei (RPN) population (G_0/G_1: 67 ± 1%, S/G_2.M: 33.2 ± 1%), significance was obtained, indicating that the nuclei of hour 0 were growth-arrested (Fig 2.4).

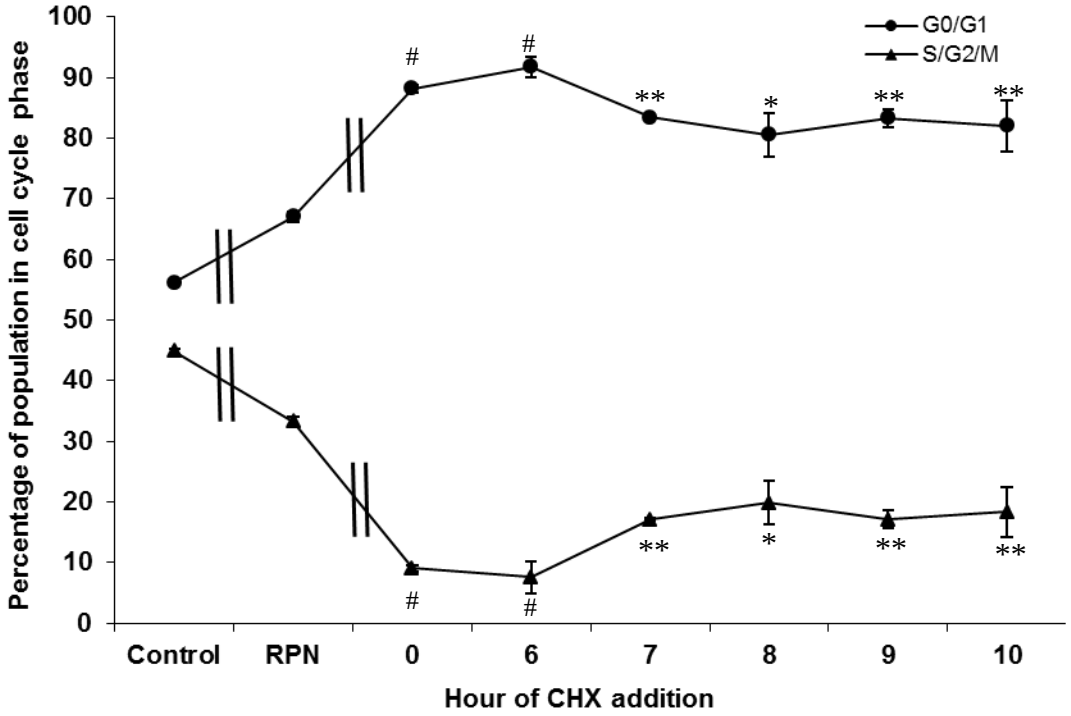

Figure 2.4: Determination of the position of the Restriction point. Cells were synchronized via serum starvation for 16 hours. The cells were then exposed to growth media and CHX added to each consecutive flask at the hours indicated, while the RPN population remained in growth media. All flasks were then harvested at hour 14 and their nuclei analyzed by flow cytometry. Data presented as mean ± SEM. n = 3. Control population representative of a synchronous population 14 hours post-synchrony.$^{\#}$: $p < 0.05$ compared to RPN. *: $p < 0.05$ compared to hour 0. **: $p < 0.005$ compared to hour 0. RPN: rapidly proliferating nuclei. Double bars represent discontinuity in the data.

As expected from the data of Figure 2.2, there was no significant difference between hours 0 and 6 (G_0/G_1: 91.7 ± 2%, S/G_2/M: 7.54 ± 3%), indicating that the addition of CHX was sufficient to induce the proliferating population back into the G_0 state. While this may seem to contradict Figure 2.1, the CHX in this experiment was used to maintain a state of growth-arrest, rather than induce growth-arrest, as was the case in Figure 2.1. At hours 7 (G_0/G_1: 83.4 ± 1%, S/G_2/M: 17.1 ± 1%) through 10 (G_0/G_1: 82 ± 4%, S/G_2/M: 18.3 ± 4%)

there was a significant difference when compared to hour 0 (Fig. 2.4), indicating that these populations were no longer in a growth-arrested state.

2.3.4 SB203580 inducts cells into a quiescent state

Although SB203580 was shown to induce growth-arrest (Fig. 2.1), it was not clear from the data generated if SB203580 induced the cells specifically into a state of quiescence. MyoD localization, and the presence of sphingomyelin rafts and the SM/C-2.6 epitope were assessed to confirm quiescence.

Control cells were seen to express MyoD in both the cytoplasm (Fig. 2.5A) and the nucleus (Fig. 2.5B). However, following treatment with SB203580, MyoD was localized to the cytoplasm (Fig. 2.5C, D). Sphingomyelin was absent in rapidly proliferating cells (Fig. 2.6A). Clearly, the sphingomyelin raft micro-domains had not formed on the outer cellular membrane. The SB203580-treated cells, however, do display the capacity to retain lysenin (Fig. 2.6B). As the cells were not permeabilized, the cells were retaining lysenin on the outer cellular membrane. Finally, C_2C_{12} cells did not display the SM/C-2.6 epitope while undergoing proliferation (Fig. 2.7A). When treated with SB203580, the cells cease division and begin displaying the SM/C-2.6 epitope (Fig. 2.7B). These results, therefore, indicate that SB203580 has inducted the population into a quiescent growth-arrested G_0 state.

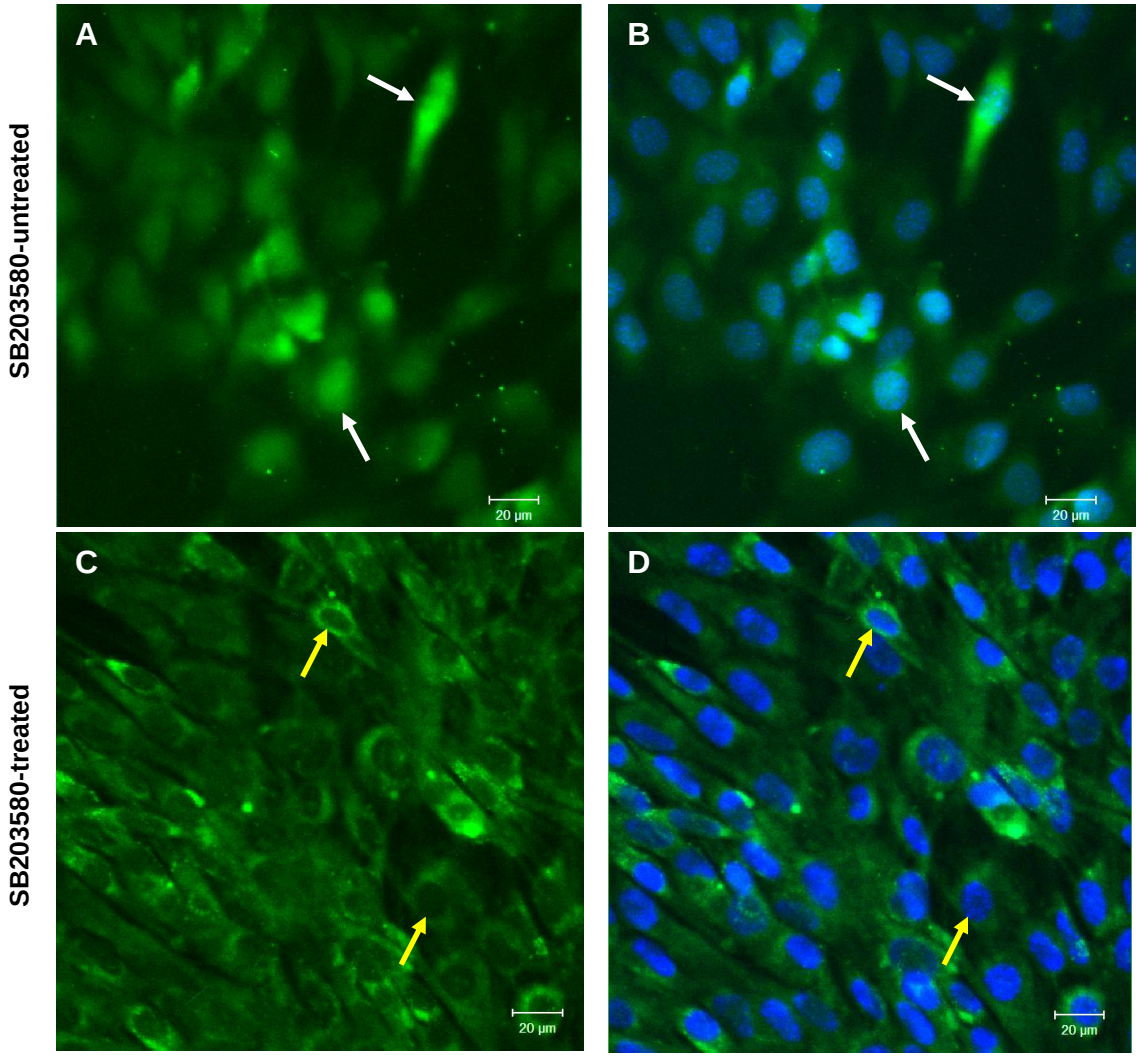

Figure 2.5: Change in localization of MyoD under the effects of SB203580. Proliferating cells (A, B)were cultured in growth media and harvested after 3 days. SB203580-treated cells (C, D) were cultured in growth media and treated with 40 µM SB203580 on days 1 and 2 before being harvested on day 3. A, B: SB203580-untreated cells. C, D: SB203580-treated cells. Green: MyoD. Blue: Hoechst. White arrows: MyoD nuclear localization. Yellow arrows: MyoD cytoplasmic localization. Scale bar = 20µm.

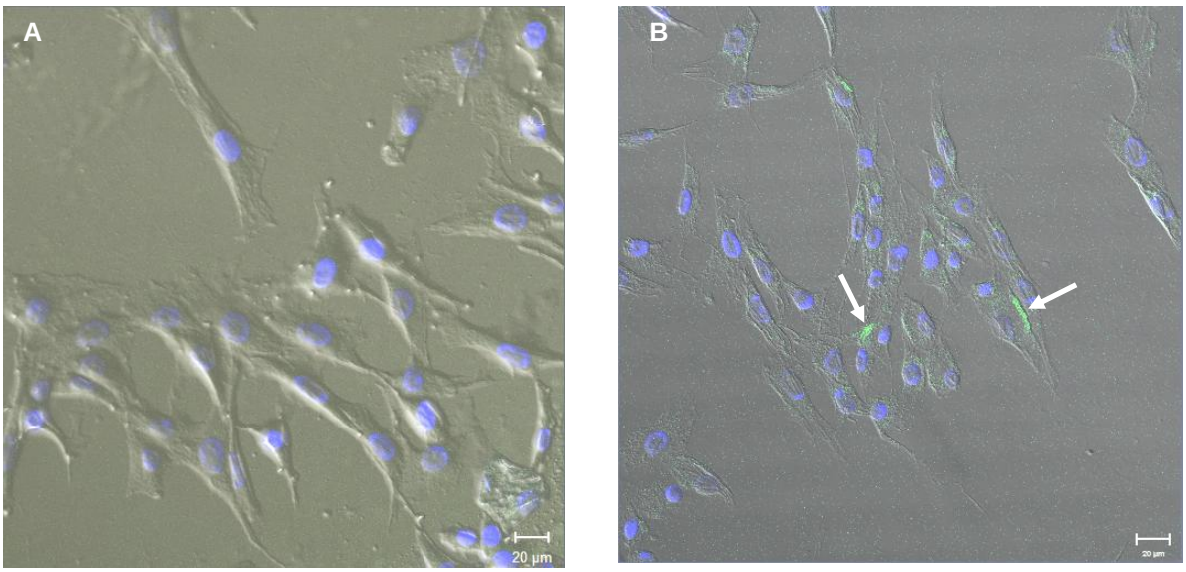

Figure 2.6: Phase-contrast of sphingomyelin on the surface of quiescent C_2C_{12} cells. Proliferating cells (A) were cultured in growth media and harvested after 3 days. SB203580-treated cells (B) were cultured in growth media and treated with 40 µM SB203580 on days 1 and 2 before being harvested on day 3.Blue: Hoechst.Green (Arrows):Sphingomyelin rafts. Scale bar = 20µm.

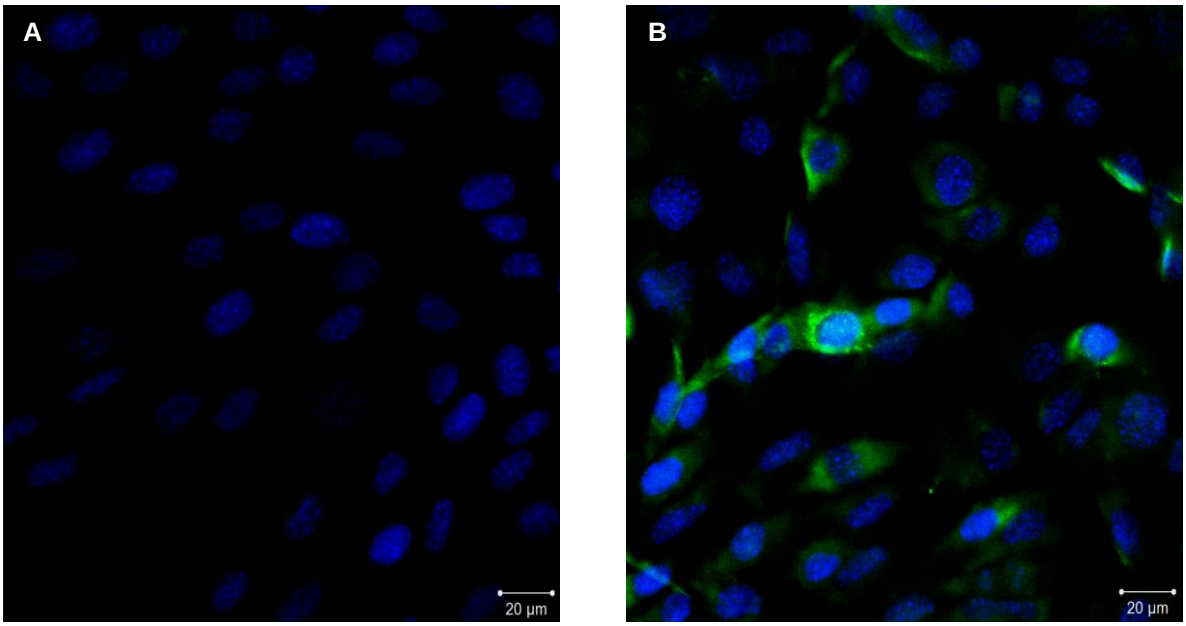

Figure 2.7: SB203580-treated C_2C_{12} cells display the SM/C-2.6 epitope. Proliferating cells (A) were cultured in growth media and harvested after 3 days. SB203580-treated cells (B) were cultured in growth media and treated with 40 µM SB203580 on days 1 and 2 before being harvested on day 3. Blue: Hoechst nuclear stain. Green:SM/C-2.6. Scale bar = 20µm.

2.4 Discussion

The main aim of the wet-lab experimentation was to describe the C_2C_{12} cell cycle more fully. While the doubling time of an asynchronous population is known to be approximately 12 hours (Rossi et al., 1997), the length of re-entry time of a synchronous population into S-phase as reported earlier (Tintignac et al., 2000) needed to be clarified with more accuracy and the position of the R-point determined. These events were therefore investigated using both whole-cell and nuclear-isolation flow cytometry on serum-deprived growth-arrested synchronized populations.

A normal proliferative population of C_2C_{12} cells will be asynchronous, with the population as a whole being present in all stages of the cell cycle (Evangelisti et al., 2007). In order to reproducibly study many events surrounding the cell cycle, a synchronous population was required wherein all the cells were at the same point within the cell cycle. The activities of SB203580 and CHX, as mentioned earlier, provided a means through which this synchronization was achieved. The synchronized cell line provided a platform from which further experimentation into the workings of the cell cycle were attempted.

While the methionine-depletion growth arrest method of Kitzmann *et al*. (1998) was sufficient to induce growth-arrest of myoblast cells, it required a much longer time frame and a more complex medium than the serum-free medium utilized in the experiments of this chapter. The generated data demonstrated that complete serum deprivation, when used over a short (16 hour) period, was sufficient to induce cells into a growth-arrested state. Although serum deprivation removed mitogens that were present in serum, cells themselves are capable of secreting their own mitogens and may have stimulated each other in an autocrine and/or paracrine manner to proliferate. In spite of this drawback, and given the sufficiently short experimental period, serum deprivation proved to be a capable inducer of growth-arrest, if not with the same efficiency that SB203580 has proven to do so (Jones et al., 2005; Kang et al., 2005; Gum et al., 1998).

Monitoring of G_0/G_1 levels in whole cells was hampered by consistently elevated levels of cells in $S/G_2/M$ even in growth-arrested populations. Intact cells contain mitochondrial

DNA and double-stranded RNAs, which will allow PI to intercalate with them. This may yield erroneously higher levels of chromatin content being detected in whole cells (Vindeløv et al., 1983a; Vindeløv et al., 1983b). The specific cell cycle phase, however, may also be determined solely by nuclear chromatin content. With no cytoplasm, potential false-positives are discarded, and the nuclear DNA content may be more accurately determined. Each nucleus is also less likely to adhere to its neighbours, therefore significantly lowering the ability of nuclei to form large clumps that may be detected as being an erroneously larger, more complex, single cell (Vindeløv et al., 1983a).

In spite of the S-phase background levels of whole cells (Fig. 2.2), both the whole cell data and the extracted nuclei data were in agreement that the onset of S-phase was between the 7^{th} and 9^{th} hour post activation in a synchronous C_2C_{12} population. This data is in agreement with previously generated data on S-phase entry of C_2C_{12} cells (Tintignac et al., 2000) and the growth-arrest induced was one of reversible growth arrest, as the cells resumed their division when mitogenic stimuli were reapplied to them.

In knowing more accurately the length of S-phase re-entry of synchronized nuclei, it is possible to estimate the position of the restriction point. It has been shown that synchronized cells in other cell lines take several hours to reach the R-point (Zetterberg and Larsson, 1985; Campisi et al., 1982c) and that cells may bypass G_1ps and enter S-phase immediately after passing the R-point. Prior work demonstrated that the R-point in most lines is likely approximately 2 to 3 hours prior to the initiation of DNA replication (Campisi et al., 1982c). As DNA replication does not start immediately upon entry into S-phase (Takeda and Dutta, 2005), the data generated in this chapter (Figs. 2.2, 2.3) is indicative of an R-point lying between hours 6 and 7 in a synchronous C_2C_{12} population.

While the data of Figures 2.2, 2.3 and 2.4 look similar, it need be noted that the experiments were conducted differently and that the hours mentioned in the graphs represent either the hour harvested (for Figures 2.2 and 2.3) or the hour at which CHX was added (Figure 2.4). It was assumed that if the populations used in the generation of Figure 2.4 were beyond the restriction point, then the population phase composition should be similar to hour 14 of Figure 2.3, while if they were not beyond the restriction point then they would be of a similar phase composition to hour 0 of Figure 2.3. While this was not the

case, a significant difference is nonetheless seen after hour 6 of Figure 2.4. This indicates jointly that the populations were beyond the restriction point and that the addition of CHX was capable of slowing down the cell cycle, even if it was unable to stop it.

As expected, cells synchronized by serum free media (hour 0) were significantly different from their proliferating controls (Fig. 2.4). After hour 0, regardless of time of CHX treatment, the cells were kept in culture until hour 14. Therefore, without any treatments, by the 14^{th} hour, levels of $S/G_2/M$ should be similar to hour 14 from Figure 2.3. While this was not explicitly seen in Figure 2.4, the populations before hour 6 were similar to hour 0 and were therefore deduced to be growth-arrested. The populations after hour 7, however, were all similar to one another, but statistically significantly different from hour 0, suggesting that they have committed to S-phase. This data therefore indicates that the R-point in a synchronous C_2C_{12} population must lie at some point after hour 6 but before hour 7.

The 6 – 7 hour position of the R-point determined in this chapter is in accordance with other papers published on the position of the R-point in other lines. Murine fibroblast 3T3 cells, renal BHK21/C13 cells, renal J1 PyBHK and Nil8 fibroblast cells take approximately 8 hours to reach S-phase from synchronous growth-arrest (Zetterberg and Larsson, 1985; Pardee, 1974) and data from asynchronous populations places the R-point at 2 -3 hours prior to S-phase induction (Campisi et al., 1982a). This yields an approximate position of the R-point of 6 hours post synchronicity, 2 hours longer than asynchronous post-mitotic 3T3 cells (Ekholm et al., 2001) and human diploid fibroblasts (Martinsson et al., 2005). The R-protein, the hypothetical protein whose increasing concentration or activity throughout G_1pm is hypothesized to be responsible for the procession past the R-point (Zetterberg et al., 1995), is presumed to be labile (Ekholm et al., 2001; Aguda and Tang, 1999; Zetterberg et al., 1995). Thus, the increased time required for a synchronous population to reach the R-point may be due to the fact that this R-protein has been completely degraded during the growth-arrest period and requires this extra time to become concentrated to, or as active as, the levels of R-protein in asynchronous cells (Blagosklonny and Pardee, 2002).

The results obtained in Figure 2.4 for the position of the R-point were both expected and surprising. Given that all the populations were allowed to proliferate for a total of 14 hours, if the populations were untreated it would be expected that they would all be similar to the percentage of cells in G_0/G_1 and $S/G_2/M$ of hour 14 of Figure 2.3. However, hour 6 of Figure 2.2 had similar G_0/G_1 and $S/G_2/M$ percentages to that of hour 0, as would be expected of a population that had not yet crossed the R-point and had returned to a G_0 growth-arrested state. Although hours 7 through 10 were not growth-arrested, neither were they of a composition similar to an untreated population at hour 14. This data indicates that CHX addition at these hours was insufficient to induce growth-arrest, though it was sufficient to prolong the cell cycle phases post-R.

Cycloheximide is a powerful protein synthesis inhibitor that blocks synthesis at the ribosome itself (Siegel and Sisler, 1964). This means, however, that potentially allpathways within the cell will be inhibited to some extent, likely yielding artefactual results through unforeseen consequences. A more viable alternative to synchronize cells would therefore be a method that is capable of inhibiting as few pathways as possible, without promoting differentiation or apoptosis. Since the p38 MAPK pathway has been shown to be pivotal in the proliferation of satellite cells and other myoblast progenitor lines (Jones et al., 2005), it was necessary to investigate whether the inhibition of p38 in the C_2C_{12} line was capable of inducing growth-arrest. SB203580 presented itself as a tool for this induction to growth-arrest as it is known to be highly specific to the p38α/β isoforms (Davies et al., 2000; Eyers et al., 1999). With SB203580 being highly specific towards its target there should be minimal alteration of activity of other pathways within the cell. Nonetheless, the high concentration of SB203580 utilized in the experiments of this chapter may cause the non-specific inhibition of other targets, such as the TGF-β receptor and JNK (Eyers et al., 1999). The IC_{50} for these are, however, orders of magnitude higher than that of p38 at 40 μM each (Eyers et al., 1999). While the high concentration of SB203580 may have caused unforeseen effects, the high specificity towards p38 and the relatively higher IC_{50} of its non-canonical targets implies that the data generated is likely due to the inhibition of p38 alone.

G_0 is a group of several related states, and entry into G_0 does not imply which specific state is induced. The data generated demonstrated that SB203580 treatment inhibits

proliferation and that the cells were not committed to begin differentiation as nuclear localization of MyoD, a requirement of C_2C_{12} cells to begin differentiation (Lassar et al., 1994; Vandromme et al., 1994), was not observed. The induced state is unlikely to be one of senescence as the C_2C_{12} cell line is immortalized and, as such, is more robust to senescence (Blau et al., 1985). In addition, no apoptotic nuclei were observed in any confocal image frames. This data, in conjunction with the presence of the known quiescence markers sphingomyelin and the SM/C-2.6 epitope (Fukada et al., 2004; Yamaji et al., 1998) on the surface of SB203580-treated cells, indicated that SB203580 induced C_2C_{12} cells specifically into a reversible quiescent state. As a method of quiescence induction, SB203580 presents itself as a more efficacious method for long-term induction of quiescence than does serum-deprivation. While in the short-term serum-free media promotes quiescence, in the medium- and long-term it is known to induce differentiation (Fujita et al., 2010).

Future experimentation could be attempted to narrow further down the position of the R-point further. Using 40 μM of SB203580 as opposed to CHX may yield more easily interpretable data as only a very specific enzyme would be inhibited. In order to overcome the problems of non-specificity at these high concentrations, utilizing much lower SB203580 concentrations of around 10 μM (Eyers et al., 1999) in primary myoblast culture should be able to confirm the observations seen in the C_2C_{12} cell line. In knowing that the R-point lies somewhere between hours 6 and 7, ten minute intervals could be investigated to more precisely determine its locality.

The efficacy of SB203580 in the induction of synchronicity and the more-detailed position of the R-point could then allow for a more-complete understanding of the mechanics of the C_2C_{12} cell cycle. The data thus generated could therefore be used in the creation of computational models to accurately model behaviour under various conditions. This tool would then provide a means of preliminary testing of hypotheses before experimental work is conducted.

Chapter Three – *In silico* modeling of the p38 MAPK pathway

3.1 Introduction

Traditional biochemistry is the study of biomolecules, usually in isolation from the milieu of normal cellular activities. Systems biology differs in this approach as it emphasizes the interactions between biomolecules and seeks to construct complete systems using kinetic models (Snoep et al., 2006). While the field of kinetic modeling is not new (Chance et al., 1960; Turing, 1952), the implementation and manipulation of mathematical models in the 50's was tedious and difficult. The advent of personal computing and cellular simulation software has greatly expedited exploration of such models, both simple and complex.

Biological systems tend to be both large, and organizationally complex (Table 1.1), but there is a tendency within biological systems to have a hierarchical structure as well as modularity amongst its components (Voit et al., 2006). This modularity allows smaller systems, such as independent MAPK pathways and limited cell cycle models, to be linked together, yielding larger systems, from mitogen stimulus to cytokinesis, that are more complete (Snoep et al., 2006; Voit et al., 2006). The utility of such larger models lies in their ability to be mathematically perturbed by modulating specific reactants at any point in time. Thus key components within a larger network may be identified that have the greatest effect on the network and significantly reduces the number of *in vitro* or *in vivo* experiments required to understand a biological system (Kolch et al., 2005).

As small modules are prone to errors within themselves, networks as modular constructs are likely to be more error-prone due to the fact that inconsistencies within and between the various constituent modules may become amplified upon their interconnection. It thus becomes crucial that all models are validated against *in vitro* data sets to ensure that their outputs are not spurious (Snoep et al., 2006; Gilbert et al., 2006). While such differences between *in silico* generated data and *in vitro* derived data may be

due to incorrect parameterization of the model, care must be taken to not overly optimize parameters to fit the *in vitro* data. Discrepancies between *in silico* data and *in vitro* data may be due to unknown effectors or unseen connections not present within the model which need to be described and included therein (Snoep, 2005). When validating against biological data it is imperative that the model does not dramatically contradict known *in vitro*/*in vivo* observations. A model may, however, be incomplete in that it does not describe all known observations, or that it makes predictions that have not yet been verified (Gilbert et al., 2006).

Models of the MAPK cascade have traditionally been of the ERK pathway, and tended to be strictly linear (Table 1.1). This method of modeling largely overlooks the interconnections between the various pathways (Kolch et al., 2005). Taking this into account, a p38 MAPK model was constructed in an attempt to replicate *in silico* the data generated *in vitro,* both in Chapter 2 and derived data and behaviours of the literature.

3.2 Methods

Data mining: Model parameters, where available, were obtained from the online BRENDA comprehensive enzyme database (www.brenda-enzymes.org). If the required data was unavailable from BRENDA, further searches were conducted using Information Hyperlinked Over Proteins database (www.ihop-net.org), or the HarvardUniversity's Bionumbers database (http://bionumbers.hms.harvard.edu). Those parameters that could not be found though BRENDA, IHOP or Bionumbers were co-opted from already published models that used either similar or identical molecules to the p38 MAPK pathway. Such models were found either through searching the PubMed database of the AmericanNationalCenter for Biotechnology Information (www.ncbi.nlm.nih.gov/pubmed) or downloading deposited models from systems biology databases JWS Online (http://jjj.biochem.sun.ac.za) and the European Bioinformatics Institute's Biomodels repository (http://www.ebi.ac.uk/biomodels-main). Care was taken during the data mining procedures to ensure that all obtained models and parameters were properly curated or accurately reflected the data presented in the original papers.

Software: All graphical data presented in this chapter was generated using the programming language Python 2.6 (http://www.python.org) with PySCeS (Python Simulator for Cellular Systems) 0.7.4 (http://pysces.sourceforge.net) (Olivier et al., 2005), matplotlib 0.99.3 (http://matplotlib.sourceforge.net), numpy 1.5.0b (http://numpy.scipy.org), and scipy 0.8.0 (http://www.scipy.org) as installed modules. Models obtained from internet sources were converted from SBML to the PySCeS format using the PySCeS Core2 module.

Model construction: The computational model was constructed according to the input format required of PySCeS (Olivier et al., 2005). Reaction kinetics were modelled using Michaelis-Menten kinetics. Dual phosphorylation reactions were modelled as a two-step mechanism where an unphosphorylated molecule is first mono-phosphorylated, whereby it may be dephosphorylated or be phosphorylated again to the active dual-phosphorylated form. The dual-phosphorylated molecule may then in turn be dephosphorylated to a mono-phosphorylated form (Kholodenko, 2000; Huang and Ferrell, 1996). None of the reactants

were fixed or made static in the models generated. Concentrations of miscellaneous reactants (such as H_2O and P_i) were assumed to be constant at all times and were therefore included in the rate constants (Huang and Ferrell, 1996). The constants and concentrations used in the experimental model are referenced in Table 3.1 while the models and Python scripts used in the generation of data are included both on the accompanying disk and in Appendix B and are based on the cascade structure presented in Figure 3.3A.

Table 3.1: Parameters used in the construction of the p38 MAPK model. Concentration of reactants, the k_{cat} and K_M values were all standardized to μM, s^{-1} and μM respectively. **+** implies activation (phosphorylation), **-** implies inactivation (dephosphorylation).

Reaction	Effector	Concentration (μM)	Target	Activity	k_{cat} (s^{-1})	k_M (μM)	References	Note
1	Mitogens	Varied	Ras	+	0.038	1.9	Das et al., 2009	1
2	Ras GAP	Constant	Ras	-	0.1	0.11		2
3	Ras	0.1	Rac1	+	0.151	1.98	Hatakeyama et al., 2003; Sasagawa et al., 2005	
5	Rac1	0.5	Mekk1	+	2.025	10	Tan et al., 2002; Hatakeyama et al., 2003	
7			MLK3	+	2.025	29.7		
4	Rac1 GAP	Constant	Rac1	-	0.39	18.7	Zhang et al., 1998	2
10, 13	Mekk1	2.01	MKK4	+	0.025	15	Brightman & Fell, 2000; Kholodenko 2000; Hatakeyama et al., 2003; Sundaramurthy et al., 2009	3
9, 12	MLK3	1.01	MKK4	+	0.005	0.31	Kholodenko, 2000; Jia et al., 2005; Sundaramurthy et al., 2009	3, 4
19, 21			MKK6	+				
23, 27	MKK4	0.3	p38β	+	0.0883	0.4	Kholodenko, 2000; Lisnock et al., 2000; Sundaramurthy et al., 2009	
25, 29	MKK6	0.3	p38β	+	0.0022	0.6	Kholodenko, 2000; Sundaramurthy et al., 2009	
31	p38β	0.27	ATF2	+	0.18	1.6	Stein et al., 1997; Kholodenko, 2000; Sundaramurthy et al., 2009	5
6	PP2A	0.168	Mekk1	-	6	7.82	Denu & Dixon, 1995; Hatakeyama et al., 2003; Caunt et al., 2008	4
8			MLK3	-				
32			ATF2	-				
11, 14	PP2C	0.01	MKK4	-	0.23	15	Denu & Dixon, 1995; Fjeld & Denu, 1999; Legewie et al., 2005; Caunt et al., 2008	4
20, 22			MKK6	-				
26, 30	MKP-1	0.0032	p38β	-	0.0238	0.067	Denu & Dixon, 1995; Hatakeyama et al., 2003	

1 – This parameter was used in the study of pathway behaviour and as such was varied considerably.
2 – The effectors, as well as ATP and water, were assumed to be at constant levels and were therefore included in the k_{cat} constants.
3 – The values used for the k_{cat} and K_M differ from their reported literature values in an attempt to match the experimental pathway behaviour with expected behaviour from the literature. The experiments to determine these values are included in Appendix B.
4 – Due to a lack of published evidence of the k_{cat} and K_M values for the effector on their specific targets, it was assumed that the effector interacts with and catalyses all its targets with equal efficacy.
5 – To model the competitive inhibition pattern of SB203580, the concentration of ATP was not included in the rate constant. A K_i of 0.021 μM and an ATP concentration of 3 μM were used in the modelling of this reaction (Young *et al*., 1997).

3.3 Results

3.3.1 Core Modelling

Core modelling serves several functions in the process of building realistic models. Errors in the construction of a pathway are more readily apparent in a core model, and core models provide a means to understand the dynamics of the structure of a system. To investigate whether ultrasensitivity is intrinsic within the basic structure of a tiered cascade, two core models were constructed and their outputs examined. These models consisted of a single-step dual-phosphorylation ("monocore", Fig. 3.1A) model and a two-step dual-phosphorylation model ("dualcore", Fig. 3.2A). All core models included simplified parameters with all k_{cat} values being set to 1.0, all K_M values being set to 0.01, and the total concentration of each reactant being set to 1.0. These values were similar to other core models (Klipp et al., 2009; Novák and Tyson, 2004; Huang and Ferrell, 1996).

Due to their similar constructions, the "monocore" model was compared to the Hornberg *et al*.(2005) model (Fig. 3.1A, Table 1.1). The "monocore" model differed slightly from the Hornberg model in terms of input and output, though the basic structure was similar. The "monocore" model was activated by a single input I, representing mitogenic stimulus, and terminated at the monophosphorylated target Op. The Hornberg model began with a receptor cycling slowly between active and inactive forms (R and Ri respectively) and terminated at the final MAPK effector x3p. To examine output due to stimulus, the "monocore" model was scanned with varying mitogen concentrations (I) and the Hornberg model was scanned by varying the V_{max} of the receptor activation reaction ($R_i \rightarrow R$, v2_Vm2). Data was generated as the ratio of phosphorylated to unphosphorylated enzyme at each level.

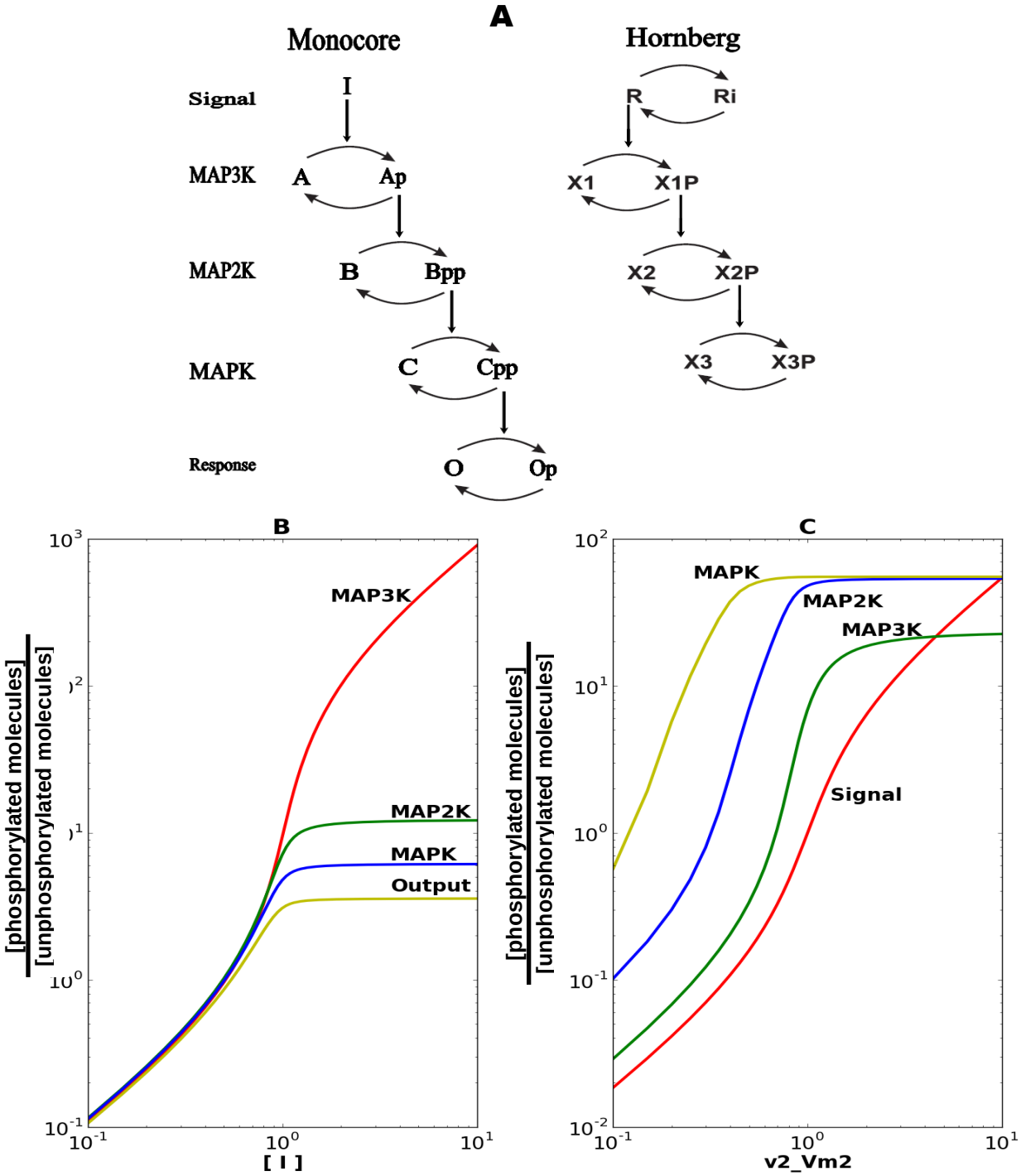

Figure 3.1: Comparison between a single-step dual phosphorylation model and the Hornberg (2004) model. Both models share similar medial structure for the MAPKs, but differ in input signals and output responses. **A**: Basic structures of the p38 MAPK model ("Monocore") and the Hornberg *et al*., 2004 model (Hornberg). **B**: Change in relative activated steady states (Δ Relative [Steady State]) of the members of the "Monocore" model as a function of input signal strength (I). **C**: Change in relative activated steady states of the members of the Hornberg model as a function of the reaction efficacy of the activation of receptor (Ri → R). Both B and C are displayed as ratios of phosphorylated to unphosphorylated molecules at each level ([phosphorylated molecules] / [unphosphorylated molecules]).

When comparing the first two moiety conserved cycles of both the “monocore” and Hornberg model (A and R respectively), the change in relative steady states matched one another, while each subsequent level of the “monocore” model was activated to lower levels over the same stimulation range than that of the preceding level. This was in contrast to the Hornberg model which predicted that each subsequent level of the cascade would be activated to higher levels over a smaller stimulation range. In both models, however, the ultrasensitive response becomes less apparent at each subsequent level.

The decrease in activation efficiency displayed by the “monocore” model may be expected if each prior level of the pathway was not activated fully. Each subsequent level will then have a maximum level of activation being lower than the preceding level and the capacity for zero-order switch-like behaviour will become increasingly attenuated. The differences between the two models are likely due to the differences in parameter values. There was a ten-fold increase in parameter values from the “monocore” model to the Hornberg model and the total concentration of receptor in the Hornberg model was half of all other concentrations of that model. The smaller initial pool and higher catalytic values were then likely able to promote zero-order conditions in the initial level of the cascade that would propagate through the model (Goldbeter and Koshland, 1984; Goldbeter and Koshland, 1982).

As has been noted before (Kholodenko, 2000; Huang and Ferrell, 1996), there was a significant increase in ultrasensitivity when the MAPK cascade was modelled as a two-step dual-phosphorylation. The “monocore” model was altered into the “dualcore” model wherein the MAPK analogues *B* and *C* were modelled as being activated via two-step dual-phosphorylation (Fig 3.2A) without changing the overall parameter sets. The scanning range of input signal was kept equivalent to the range of the “monocore” input signal (Fig 3.1B) for comparative purposes.

An interesting observation of the “dualcore” model was that, while the second level MAP2K (B) reached a maximum level of activation lower than that of MAP3K (A), the downstream target of the MAP2K, MAPK (C) eventually reached an equivalent level of relative phosphorylation to MAP3K (A) over the same scanning range. The increased relative concentrations of phosphorylated MAPK also fostered an increase in the ratio of

phosphorylated to unphosphorylated response (O) in that the "dualcore" output levelled-off at 1.42, while the "monocore" output levelled-off at 1.27 (Fig. 3.1B). The "dualcore" model was thus able to promote higher maximal levels of activation at all levels of the cascade including the response (O).

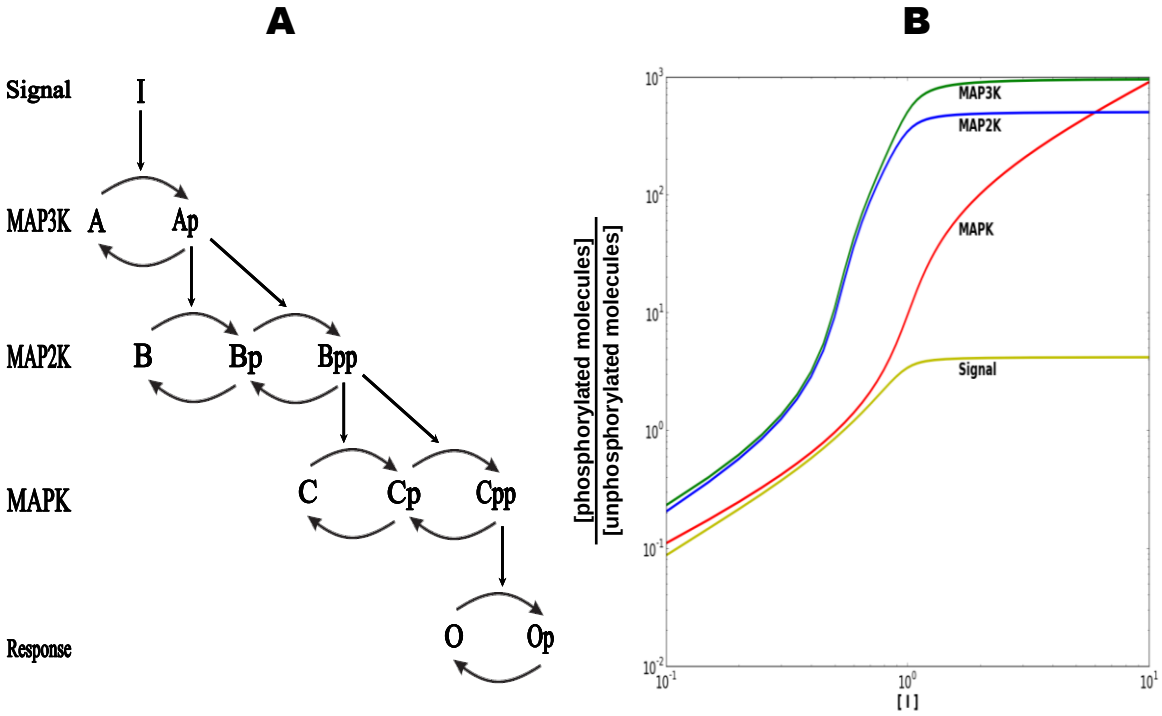

Figure 3.2: Two-step dual phosphorylation model. **A** – "Dualcore" model structure. **B** – "Dualcore" model output as a function of the change in relative active steady state concentration ([phosphorylated molecules] / [unphosphorylated molecules]) and input signal ([I]). The change in steady state values were calculated as a ratio of phosphorylated to unphosphorylated molecules.

With ultrasensitivity presenting itself as an inherent structural property of a multi-tiered two-step dual-activation, a core model was constructed of the p38 MAPK pathway as it is encountered *in situ*. The p38 MAPK core model ("realcore") differs significantly from the original core models in its construction (Fig. 3.3). Two single-step activation cycles representing Ras and Rac1 are the uppermost steps in the model. Rac1 is a joint activator of the MAP3Ks, which in turn activate the MAP2Ks in a two-step dual-phosphorylation. Both then activate p38 MAPK in a similar. Finally the activated p38 MAPK mono-phosphorylates the output molecule ATF2, a canonical p38 target that is capable of promoting the synthesis of cyclin D (Recio and Merlino, 2002). Each

phosphorylation step is mirrored by a dephosphorylation step (Table 3.1)

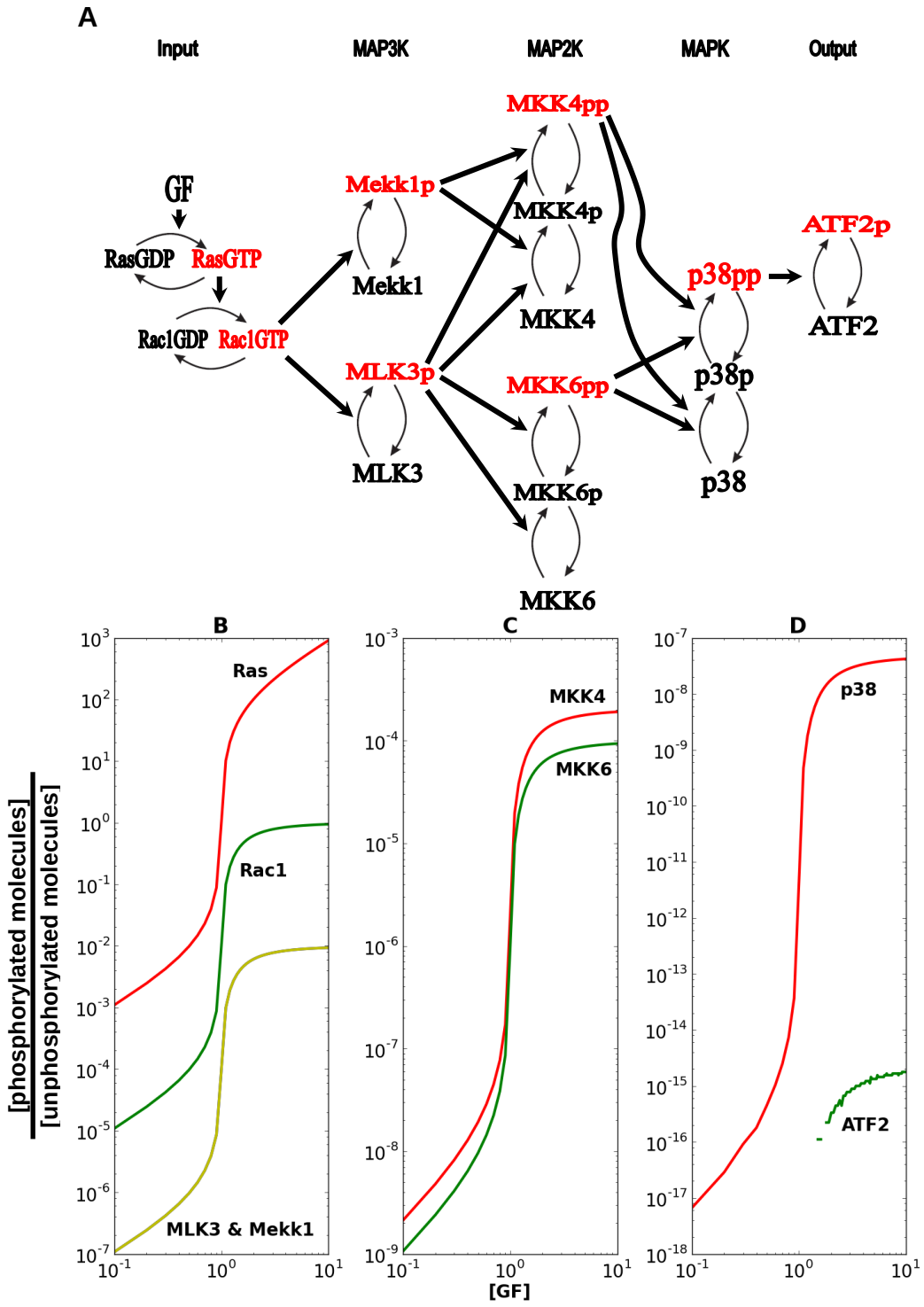

Figure 3.3: p38 MAPK *in situ* analogue core model ("realcore") layout and output. **A**: "Realcore" structure. Red: active molecules. **B – D**: "Realcore" model output as a function of relative active steady state concentration ([phosphorylated molecules] / [unphosphorylated molecules]) and growth factor input ([GF]). Steady state values were calculated as a ratio of phosphorylated to unphosphorylated molecules.

(Sundaramurthy et al., 2009; Caunt et al., 2008; Jia et al., 2005; Tan et al., 2002; Brightman and Fell, 2000; Lisnock et al., 2000; Camps et al., 2000; Fjeld and Denu, 1999; Zhang et al., 1998; Stein et al., 1997).

The “realcore” model, with its two-step dual-phosphorylation as well as branching within the pathway produces a striking ultrasensitive response over the same input stimulus range as the “monocore”, “dualcore” and Hornberg models. Although input was scanned over the same range as the other core models, all kinases undergo a rapid conversion from an inactive state to a maximally activated state in a much narrower range than the prior models (Fig. 3.3B – D). While this sharp reaction to stimulus is expected of a MAPK cascade (Kholodenko, 2000; Huang *et al*., 1996), although the ratio of phosphorylated to unphosphorylated molecules dropped considerably down the cascade. Maximum Ras ratios reached 10^{3} (Fig. 3.3B), while p38 ratios reached below 10^{-7}. ATF2 fails to activate properly and most of the data remains mathematically undefined (Fig. 3.3C). This may be due to the fact that the activation levels reached by ATF2 were sufficiently close to the numerical lower limit of most computers whereby the computer is unable to distinguish the number from 0. This behaviour was expected to be resolved with the implementation of *in situ* parameterization of the experimental model.

While all the core models share similar properties with one another and the Hornberg model, the efficacy of information transfer through the various pathways is difficult to estimate or compare graphically. However, the responsiveness (represented by the response co-efficients mentioned in chapter 1.4) of each pathway provides a measure with which to compare pathways even across widely differing inputs and concentration ranges (Kholodenko, 2000; Kholodenko et al., 1997). The methods through which the response coefficients were calculated are described in section 1.4 andthe response coefficients for each of the core models are summarized in Table 3.2. While the responsiveness of each model (and level therein) varies according to the level of input, the response coefficients described below were calculated according to the initial level of input specified by the model files. These levels are described in the corresponding model file included in Appendix C.

The responsiveness of the Hornberg model stays relatively constant down the MAPK cascade with a response co-efficient of just over 1 (Table 3.2) The “monocore” and “dualcore” models decrease in responsiveness down the cascade, culminating at 0.235 and 0.283 respectively at the MAPK level. The “dualcore” model, however, displays a higher responsiveness than the “monocore” at most levels and this is most likely due to the two-step dual-phosphorylation mechanism used. While the “realcore” model initially displays a lower responsiveness, it also displays an increasing response down the cascade in contrast to the “monocore” and “dualcore” models with the terminal MAPK having a response co-efficient of 0.246. The elevating response is most likely due to the branched structure evident within the “realcore” pathway (Fig. 3.3A). On a biochemical level, having several upstream activators provides multiple paths for a signal to transduce through, and is capable of potentially sustaining a signal since multiple effectors must be simultaneously deactivated for the target itself to become deactivated. This is in agreement with equation 5, which demonstrates that the more convergent the branches within a pathway, the greater the overall responsiveness of that pathway is likely to be.

Table 3.2: The response coefficients of the various core models. Input represents the non-MAPK cycle that is directly stimulated by mitogens. This is R and Ras for the Hornberg and “realcore” models respectively. Note that the response coefficients are unitless.

Substrate	Hornberg	Monocore	Dualcore	Realcore
Input	1.008			$1.22x10^{-3}$
MAP4K		0.525	0.525	0.032
MAP3K	1.01	0.335	0.39	0.062
MAP2K	1.018	0.263	0.323	0.123
MAPK	1.04	0.235	0.283	0.246

4.3.2 Realistic modelling

A core model can provide information about patterns of behaviour of a pathway based solely on its structure. Any other information generated by such models is, however, at best, qualitative. In order to computationally generate quantitative data from a model, the model must be populated with parameters which mimic *in vitro* and *in vivo* kinetics and rate equations. The more accurate these kinetics and rate equations are, the more realistic the model. This approach is known as the silicon cell approach (Snoep et al., 2006). The main feature of this approach is that parameters and independent data

sets are used to both construct and validate models. To this end, the “realcore” model was populated with the parameters presented in Table 3.1.

Due to the stiffness of the model and the resultant solver limitations, simulation of the model resulted in undefined regions where PySCeS was unable to generate applicable data. They were generated by PySCeS arriving at 0 for the solution at that particular point (data not shown). Thus, when the logarithm for these points are taken, an undefined number results and the graphing software simply ignores them. The resulting undefined regions are, however, biologically implausible and it was therefore assumed that the data points that would have been generated would have been done so in a similar manner to the overall trend. Several methods of remodelling were attempted to resolve these undefined regions. However, while the undefined regions were eliminated, the ultrasensitive behaviour of the model was eliminated as well. Similarly, parameter values and concentrations that facilitated their removal were biologically implausible. The data sets used in the attempt to resolve the undefined regions are presented within Appendix B. Another alternative, however, may be that these “undefined” regions are actually areas where the model may exist in more than one steady state for the given input signal. The gap therefore represents a region where the system switches between steady-states. While solvers are available in PySCeS to explore these areas as potential multiple steady state switches, there was insufficient time to explore the possibility.

When populated with viable *in vitro* parameters, the realistic model still displayed an ultrasensitive, switch-like behaviour over a biologically plausible low mitogen concentration range (Fig. 3.4A – C). Over the range of mitogen concentration used, the sigmoidal activation pattern was absent in the growth-factor proximal cycles and only very mildly present in the medial cycles, the distal p38 and ATF2 cycles (Fig. 3.3A) responded with a clear sigmoidal pattern with p38 becoming completely active over a very small increase in mitogenic stimulation. This *in silico* ultrasensitive behaviour was comparable to *in vitro* responses of the p38 MAPK pathway (Waas et al., 2001).

Although ultrasensitivity remained within the model, other predictions of the model needed to be validated with biological data. To verify model output, the results of a time-course study of the activation of p38 MAPK under signaling conditions was compared to an *in vitro* data set of the activation of p38 MAPK (Fig. 3.5A) (Jeng and Watson, 2009).

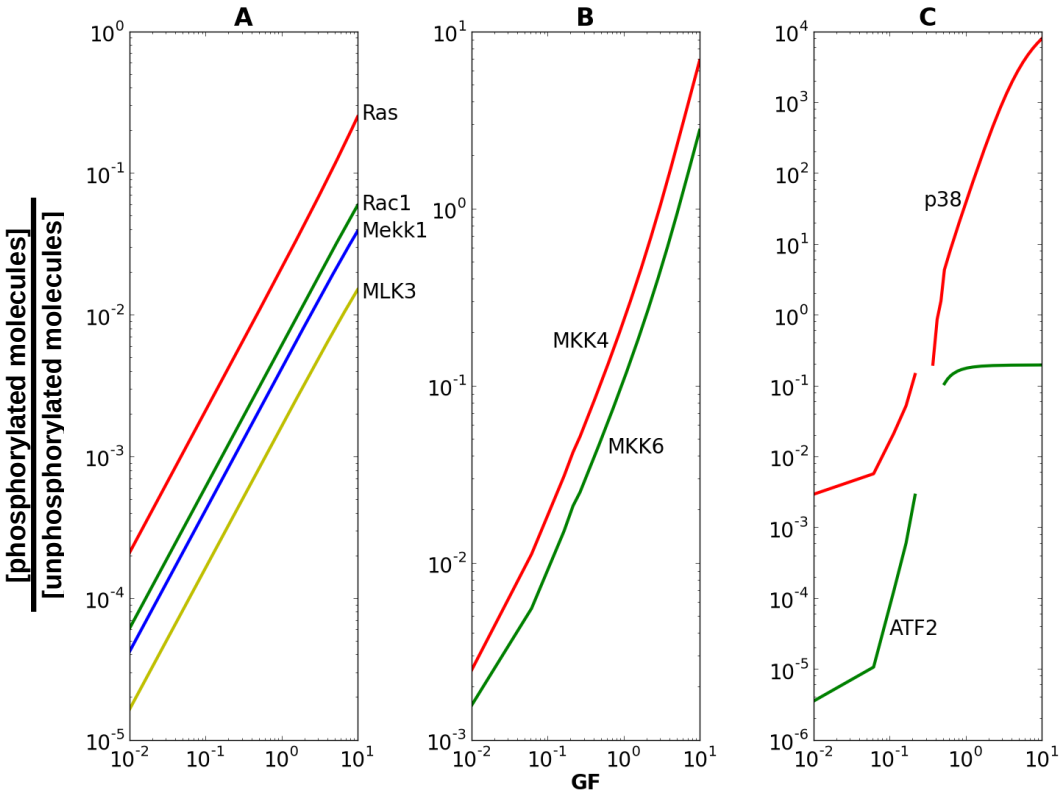

Figure 3.4: Experimental model displaying ultrasensitive behaviour. All plots are of respective phosphorylated molecules divided by unphosphorylated molecules. **A**: Growth factor proximal cycles. **B**: Medial cycles. **C**: Distal cycles.

The *in silico* model assumed that a small percentage of effectors are always active, even during periods of limited mitogenic stimuli. Under these conditions the model predicted that it would take approximately 400 – 600seconds or 10 minutes for p38 to become active. This prediction was validated by the *in vitro* biological data of Jeng and Watson (2009) who conducted a time-course study on the activation of p38 MAPK in murine pituitary cancer cells. This was accomplished using phosphorylation-state-specific antibodies against p38 where Western blot analysis was performed using an alkaline phosphatase conjugated secondary antibody. Upon stimulation by tetradecanoylphorbol acetate, a positive activator of p38 MAPK, it took approximately 15 minutes for levels of p38 to reach maximum activation. Further verification of the model could be accomplished through comparing the predicted ratios of phosphorylated to unphosphorylated molecules with those that have been experimentally determined. However, no information on the phosphorylation ratios of p38 MAPK was found. Therefore the model will require further *in vitro* experimentation before it is validated fully.

4.3.3 Limitations of the p38 MAPK model

There were three major limitations of the p38 model. Firstly, while p38 is capable of reaching near total phosphorylation, nearly all of its upstream effectors displayed very low levels of phosphorylation and the MAP2Ks and did not display a robust ultrasensitive response to stimulus as would be expected of a MAPK pathway (Huang and Ferrell, 1996). The graphs demonstrating a lack of an ultrasensitive response are given in Appendix B. Secondly, there was an inability of ATF2 to become active to appreciable levels (even given the near total activation of its immediate effector) as would be expected from available *in vitro* data (Huang et al., 2008). Although active ATF2 levels do rise over the 16 minute time frame, it would be difficult to assess the inhibition of p38 using ATF2 as a marker. Lastly, the computational model was stiff at the lower levels of the cascade, resulting in a number of undefined regions in both p38 MAPK and ATF2 when scanning their activation versus input.

Given the lack of ATF2 activation, the computational model was modified to lower the efficacy of the dephosphorylation of ATF2 by including a nuclear concentration of its phosphatase PP2A (Hatakeyama et al., 2003; Camps et al., 2000), that is several orders of magnitude less abundant than its cytosolic component, as ATF2 is a transcription factor that is active in the nucleus (Liu et al., 2006). Although the quantity of PP2A effective against ATF2p was substantially reduced the same catalytic efficacies outlined for PP2A in Table 3.1 were used.

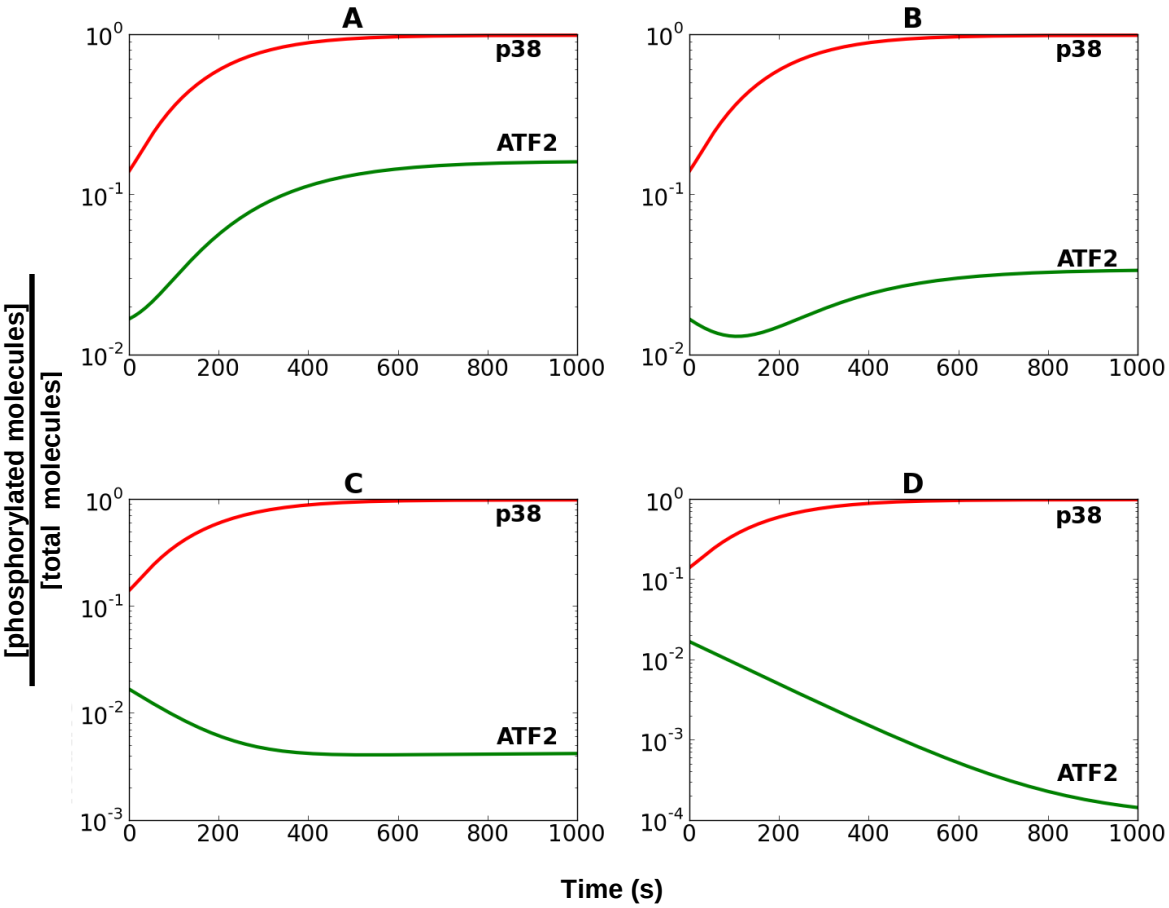

Figure 3.5: Experimental model of p38β inhibition via SB203580 and its effect on ATF2. The model was modified to include the concentrations of SB203580 as indicated by the following panels: **A**: 0 μM SB203580. **B**: 0.1 μM SB203580. **C**: 1 μM SB203580. **D**: 40 μM SB203580. Relative concentrations are represented as the ratio of phosphorylated molecules to the pool of phosphorylated and unphosphorylated molecules.

4.3.4 The effect of SB203580 on the p38 MAPK model

The inclusion of SB203580 into the model did not affect the activation of p38. This is expected both computationally, as SB203580 does not affect any of its upstream activators, as well as biologically, since SB203580 is known to not significantly affect the capacity of p38 to become active (Gum et al., 1998; Lisnock et al., 1998; Cuenda et al., 1995). The levels of ATF2 are however affected by SB203580. At a concentration of 0.1 μM SB203580 (Fig. 3.5B), ATF2 activity is substantially reduced. When the SB203580 concentration is increased to 1 μM and 40 μM (Fig. 3.5C, D respectively), activation of ATF2 has effectively ceased. These predictions are validated both by the

wet-lab results of Section 2.3.4 and published literature (Jones et al., 2005; Kang et al., 2005; Gum et al., 1998; Cuenda et al., 1995).

4.3.5 Comparison of the p38 MAPK model to other published models

As the p38 model was capable of generating biologically plausible data, it was compared with two other validated ERK models from the literature: the Huang (1996) and Kholodenko (2000) models. Both models have demonstrated ultrasensitive behaviour as well as the capacity to mimic *in vitro* behaviour. A comparative analysis of the responsiveness of the various models was undertaken to determine if the p38 MAPK model displayed similar attributes to models within the literature (Fig. 3.6). Each model was scanned against its respective first activator or the first activation reaction parameter. This was growth factor (GF) and the phosphorylation efficiency of MAP3K (r1b_k2 and J0_V1) for the p38 model (Fig. 3.3A), Huang (1996) model (Fig. 1.5), and Kholodenko (2000) model (Fig. 1.6) respectively.

While the Kholodenko (2000) and p38 model were ultrasensitive over the same small range of input (Fig. 3.6C, A respectively), the Huang (1996) model (Fig. 3.6B) was ultrasensitive over a range greater than both the other models. The p38 MAPK and Kholodenko models showed an increasing capacity for input signal to propagate through the cascade, while the Huang model displayed a sharply decreasing sensitivity to upstream signalling (Fig. 3.6D), eventually culminating a response of only 0.005 indicative of a signal that was almost ineffective at the lower tiers of the cascade. The Kholodenko model, however, showed an increase in signal responsiveness for lower tiers of the signalling cascade. Although the primary effector was only tentatively propagated, the lowest tier had a responsiveness of over 1; indicative of an overall amplification of signal effect.

The p38 model, however, showed the most substantial increase in amplification when compared to the Huang and Kholodenko models (Fig. 3.6D). The first three tiers had a response coefficient of almost 1, indicating that signal strength is, at least, being maintained. The MAP2Ks started to demonstrate amplification in signal with response coefficients slightly under 2, while p38 MAPK and its target ATF2 showed the most

substantive response coefficients of very nearly 4, indicative of a change in signal strength resulting in a relative quadrupling of output down the signalling cascade.

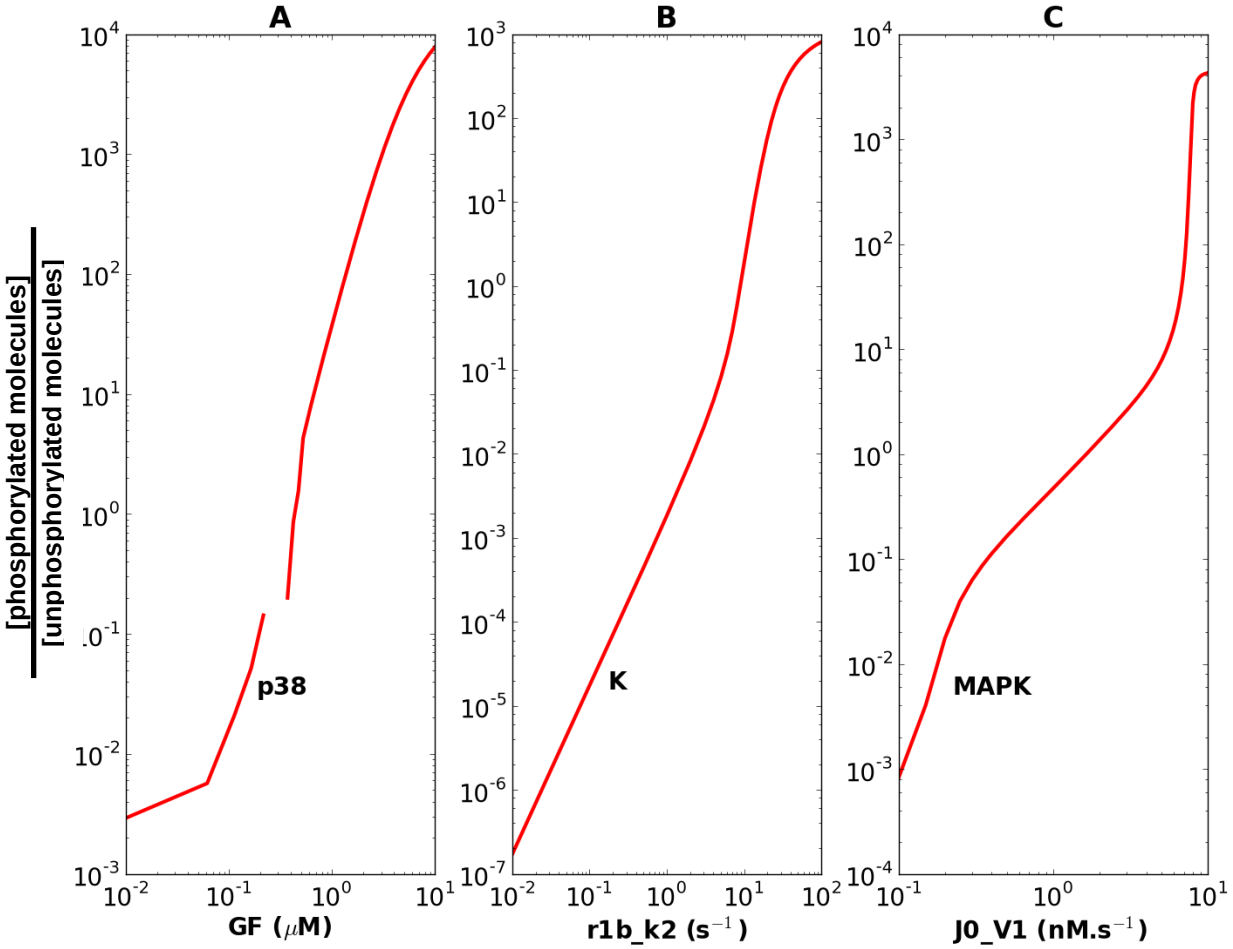

D

Substrate	p38 Model	Huang	Kholodenko
Input	0.998356		
MAP4K	0.993749		
MAP3K	0.993842	0.454842	0.030936
MAP2K	1.889075	0.151739	0.139954
MAPK	3.997191	0.00518	1.081234
MAPK Target	3.990573		

Figure 3.6: Ultrasensitivity* and response analysis** of the experimental model and published models. **A**: p38 model. **B**: Huang (1996) model. **C**: Kholodenko (2000) model. **D**: Table of response coefficients. * - The relative concentrations are given as the ratio of phosphorylated to unphosphorylated molecules. ** - As the Huang and Kholodenko models do not have effectors analogous to Input, MAP4K or MAPK Target, no response coefficients of these effectors were determined.

4.4 Discussion

An important property of many signal transduction pathways is the capacity to switch between states in response to changes in input. This is accomplished in a number of ways, such as having enzyme cooperativity or an ultrasensitive response (Kholodenko, 2000). An important aspect of any signal transduction model, therefore, is the capacity to mimic such behaviours. To this end, core structural models were necessary to evaluate whether these responses are intrinsic to pathway structure, or whether such activity arises out of specific enzymatic interactions.

Two core models were constructed and evaluated against a core model from the literature (Hornberg et al., 2005). The “monocore” model assumed that each dual-phosphorylation event occurred sufficiently fast so as to be simultaneous, and the “dualcore” model assumed that each phosphorylation event occurred sequentially. While both the “monocore” and the Hornberg (2005) models displayed ultrasensitive behaviours due to their structure, the “dualcore” model displayed a more apparent capacity to generate switch-like behaviour over similar variances in input (Fig. 3.2). This behaviour was even more pronounced in the branched “realcore” model, with very steep sigmoidal activation curves being present, as would be expected from a branching-converging pathway structure (Kholodenko et al., 1997).

An interesting note is that all the core models displayed better responsiveness to signal than the Hornberg (2005) model. While the “monocore” and “dualcore” models dropped in signal responsiveness down the cascade, the “realcore” model displayed an increasing efficacy for signal propagation (Table 3.2). This particular behaviour suggests that a branching/re-converging pathway structure, as seen in many signalling cascades, imparts better sensitivity to upstream signals than might a simple linear cascade. This also suggests that other MAPK modelling approaches may have underestimated the signal response generated in models that do not have these branches.

The p38 model generated an ultrasensitive response at the p38 MAPK level, even over small changes in input signal. The characteristic sigmoidal curve was not apparent in the earlier tiers of the cascade but became apparent at the p38 and ATF2 tiers of the cascade. This lack of uppermost ultrasensitivity did not, however, affect the capacity of

p38 to activate under constant signalling conditions. This stands in contrast to the data of Whitehurst *et al*. (2004) who indicated that in human cervical cancer HeLa cells the MAPK ERK was not activated via ultrasensitivity, instead displaying a graded response to input. However, this graded response may indicate that the uppermost levels of a MAPK pathway need not be ultrasensitive while leaving the lower levels of the pathway to be activated in an ultrasensitive manner. Since ultrasensitivity is present within other higher animals (Kholodenko, 2000; Huang and Ferrell, 1996), the lack of ultrasensitivity in humans may not necessarily also be present in the murine p38 MAPK cascade (which has been modeled in this chapter). Similarly, it may be an ERK-specific lack of ultrasensitivity in mammals, leaving the potential ultrasensitivity of p38 MAPK untouched. A prudent validation of the model, therefore, would be to study murine p38 MAPK *in vitro* and to check for an ultrasensitive response (or the lack thereof).

The model predicted that it would take approximately sixteen minutes to activate from a relatively inactive state, which is in agreement with the work of Jeng and Watson (2009), wherein it also took murine p38 approximately 16 minutes to activate *in vitro*. The p38 model also displayed an ability to inhibit the activation of ATF2 though SB203580 in a manner that was borne out both by the results of Section 2.3.3 and previously published data (Jones et al., 2005; Kang et al., 2005; Gum et al., 1998; Cuenda et al., 1995).

The final validation of the p38 model in this chapter was the comparison between it and two other peer-reviewed models known for generating biologically relevant data: the Huang (1996) model, and the Kholodenko (2000) model. All three models produced ultrasensitive profiles for the final MAPK, although the branched p38 model and feedback-inclusive Kholodenko models displayed both more prominent ultrasensitive profiles, and a greater responsiveness to signal input. With the p38 model significantly amplifying downstream targets. This data suggests that a more responsive model would be one that included both the branched nature of the MAPK pathway as well as feedback between the various effectors.

The main aim of this chapter was to produce a model that accurately reflects the p38 MAPK cascade. This was mostly accomplished with the resulting final model demonstrating several key characteristics: a.) a structure similar to the p38 MAPK

pathway governed by mitogens (Zarubin and Han, 2005), b.) an ultrasensitive switch-like behaviour present due to mitogenic stimulus (Huang and Ferrell, 1996), and c.) an overall responsiveness of the pathway amplifying target responses from signal induction (Kholodenko et al., 1997).

Three major limitations were still evident within the p38 model presented; these were irresolvable given the limited timeframe and scope of this dissertation. Firstly, the uppermost tiers of the cascade failed to activate correctly and did not display ultrasensitive profiles expected (Huang and Ferrell, 1996). Whilst this was unexpected, there is no readily available *in vitro* data on the levels of activation of these tiers. Secondly, in spite of the very high response to signal input and the high levels of p38 activation, ATF2 failed to activate to expected levels (Huang et al., 2008). Thirdly, the model itself was stiff, resulting in a number of undefined areas where the model was unable to supply data. These problems are most likely due to the oversimplification of parameters as each effector interacted with its targets in an identical manner. This simplification was necessary for the construction of the model as several parameters were not known. A detailed investigation and utilization of the kinetics of the effectors in relation to the different activation states of their targets should result in a more complete model that is capable of predicting activation levels correctly. Additionally, the model still requires further validation. Data is currently unavailable on most of the predictions the model makes, such as the ratios of phosphorylated to unphosphorylated molecules.

In summary, a model of p38 MAPK activation in relation to mitogenic stimulus was constructed. This model demonstrated ultrasensitive behaviour, was significantly responsive to its inputs, and was capable of generating data that may be biologically viable and relevant. This model may thus be used as a tool for further exploration of biological phenomena and may be included as an input to other models on the behaviour of the cell cycle in response to p38.

Chapter Four – Discussion

4.1 Summary of results

There were two aims to this dissertation, both of which are interrelated. The *in vitro* experimentation sought to analyse more thoroughly the cell cycle of the murine myoblast C_2C_{12} cell line by identifying the length of S-phase re-entry from G_0 quiescence and determining the position of the restriction point within G_1. It was determined that the cell takes 7 to 9 hours to re-enter S-phase, consistent with literature data (Tintignac et al., 2000). The restriction point was determined to be 6 to 7 hours post synchronous G_0. Although the determination of the position of the R-point is novel in the C_2C_{12} cell line, it is consistent with literature data from other lines, and what is currently known about the R-point in general (Zetterberg and Larsson, 1985; Campisi et al., 1982a; Pardee, 1974).

The *in silico* work sought to create a *de novo* model of the p38 MAPK cascade stimulated by mitogens. Through a number of core models of tiered cascades and the p38 model itself, it was determined that ultrasensitivity is inherent within the structure of the cascade. Moreover, the ultrasensitivity and responsiveness of the pathway to stimulus increased when dual phosphorylation of effectors occurred as a two-step, rather than a one-step, mechanism which was also reinforced by a branching/converging structure. The realistic model still managed to show evidence of ultrasensitivity, while also showing a far superior response to stimulus than the core models. The output of the realistic p38 model was in line with other published MAPK models (Kholodenko, 2000; Huang and Ferrell, 1996), as well as the data generated *in vitro* of section 2.3.4.

4.2 Future prospects

While the model showed some capacity for the prediction and replication of data, there were a number of instances whereupon it could be improved. It is unsuitable at present to act as a standalone model, but may either be improved to the point where it may do so, or be combined with other models to provide a more complete model than either alone.

4.2.1 Model improvements

The most significant improvement that could be made to the model would be the inclusion of better rate constants for all effectors. Due to the lack of available information at the time of construction of the model, a number of assumptions were made to fill in the missing information. It was assumed that effectors interact with and catalyse all their substrates with the same efficacy at the same rate, which is, of course, a biological implausibility (Klipp et al., 2009; Voet and Voet, 2004). Thus any change to a more accurate k_{cat} and/or K_M for any of the effectors will result in a more biologically feasible model.

As there is evidence that feedback is present within MAPK cascades (Vera et al., 2010; Kholodenko, 2000; Ferrell and Machleder, 1998), another method to produce a more biologically accurate and plausible model of the p38 pathway would be to include feedback within the model. Even within the p38 MAPK cascade itself, there is negative feedback present at a number of different levels, from mRNA inhibition, to Ras inhibition (Ambrosino et al., 2003; Chen et al., 2000; Ben-Levy et al., 1998). While it would therefore be prudent to model such interactions, care must also be taken as very little kinetic data is currently available for these specific interactions.

4.2.2 *In vitro* experiments

A model can only truly be considered valid when verified against *in vitro* data, and when its predictions are accurate. While some of the predictions of the model are borne out by the literature, more experimental *in vitro* work would be able to validate the p38 MAPK model. One significant experiment would be to determine if mammalian p38 MAPK is ultrasensitive *in situ*. The model predicts that this should occur, even if only at the p38 level itself, while other *in vitro* evidence suggests that the ERK MAPK cascade in mammalian cells is not ultrasensitive (Whitehurst et al., 2004). Should p38 *in situ* not be ultrasensitive, this will require the model being changed appropriately. However, if p38 is ultrasensitive *in situ*, then this will provide an interesting counterpoint to the lack of ultrasensitivity found in the ERK cascade.

Further validation of the p38 model could be accomplished through the *in vitro* measurement of the phosphorylated concentrations of the various effectors in the cascade. The model predicts certain phosphorylation ratios based on mitogenic input, but little work, even in the literature, has been done *in vitro* to determine them. Most assays found in the literature usually focus only on specific phosphorylation states in very context-dependent circumstances, such as under the effects of specific chemicals. Assays, then, on the concentrations of the unphosphorylated, monophosphorylated and biphosphorylated fractions of the effectors at various mitogen concentrations will provide good evidence, either for or against, for the validity of the p38 model.

The data generated by the core and realistic models of the complete p38 pathway suggest that a branching / re-converging structure may impart more sensitivity upon a pathway. This novel finding may be investigated *in silico by* computational models, or through *in vitro* inhibition of various branches of a pathway.It would thus be possible not only to elucidate how the flux through such a pathway redistributes itself, but also if such a structure truly does impart better sensitivity.

4.2.3 Model expansion

Two models immediately present themselves as having the potential for being merged with the p38 model: the Sundaramurthy (2009) model, which already has p38 within it, and the Novák (2004) model, which contains an easy point-of-entry for the p38 model and its effects on the cell cycle.

The Sundaramurthy (2009) model (Fig. 1.8) is a network that models the interactions between the main MAPK families, including p38. However, in this network, p38 is explicitly modelled as being a stress-activated MAPK with TAB and TAK being its upstream activators. While p38 is activated by stressors, it is also activated by mitogens and so a more complete model would be one where both occur. By merging the p38 and Sundaramurthy models it would be possible to make predictions to the MAPK network when stimulated by both mitogens and stressors.

The Novák (2004) model describes the cell cycle, with a relatively high number of effectors being present, both in an attempt to provide a model of the system and to

provide a computational model of the restriction point. In a simplification step, the entire entry into the cell cycle, from growth factor to the transcription factor of cyclin D, was black-boxed into early- and delayed-response genes (Fig. 4.1). Due to the nature of investigation of the paper, little attention was paid to cell cycle entry. This, coupled with the autocatalytic nature of the delayed-response genes, caused these effectors to be almost invariant in response to changes in growth factor concentration (data not shown). While the model is capable of replicating the Zetterberg and Larsson (1985) cyclohexamide experiments, it is currently poorly suited to investigating the effects of mitogenic stimulation on the cell cycle. By replacing the early- and delayed-response genes with the p38 model, a more complete model of the cell cycle would be constructed that should be capable of understanding the origin of the restriction point from multiple sources.

4.3 Conclusion

Both of the main aims of the dissertation, clarification of the C_2C_{12} cell cycle and the modelling of the p38 MAPK pathway, were achieved. Several limitations are, however, present within the model of the p38 MAPK cascade and the predictions of the model have not been entirely validated. Further *in vitro* work and corrections within the model will to validate its output. In conclusion, the C_2C_{12} restriction point was found to be between hours 6 and 7 in synchronous dividing cells, and a *de novo* model of the p38 MAPK pathway was constructed that replicates some *in vitro* data and may be suitable for inclusion in other MAPK and cell cycle models.

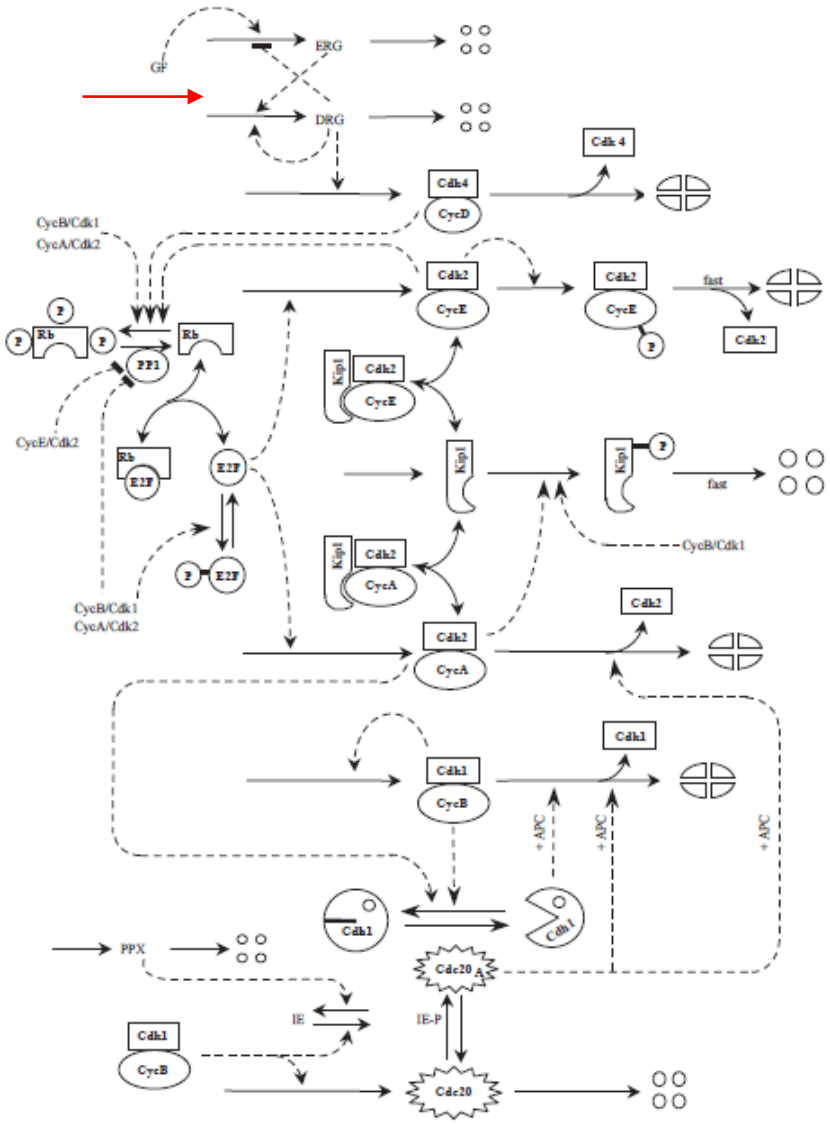

Figure 4.1: The Novák (2004) model of the cell cycle. The area that would be replaced, the early- and delayed-response genes (ERG and DRG respectively), is indicated by the red arrow.

Appendix A

In order to generate the flow cytometry data, a Beckman Coulter Epics flow cytometer was employed. The generation of the cell cycle phase peaks was done with two different settings for the whole-cell (Table A1) and isolated nuclei (Table A2). This was necessary as the nuclei are much smaller than whole cells and so require more amplification in order to detect them.

Table A1: Whole cell flow cytometry settings

Detector	Voltage	Gain
FS	388	2
SS	0	1
FL3	574	1
Aux	0	1

FS – Forward scatter; SS – Side scatter; FL3 – PI excitation lazer; Aux – Auxillary (Peak height divided by peak width)

Table A2: Isolated Nuclei flow cytometry settings

Detector	Voltage	Gain
FS	412	2
SS	83	20
FL3	710-825	1
Aux	115	1

FS – Forward scatter; SS – Side scatter; FL3 – PI excitation lazer; Aux – Auxillary (Peak height divided by peak width)

Before running samples through the flow cytometer, the prepared solutions were pipetted thoroughly to prevent doublet formation. Doublets will be detected by the cytometer as a single particle event with their fluorescence intensities combined. This potentially means that a G_0/G_1 doublet will be detected as a single G_2/M cell. This erroneous data, as well as cellular debris, were gated out (Figure A1A) of the analytical sample (Figure A1C).

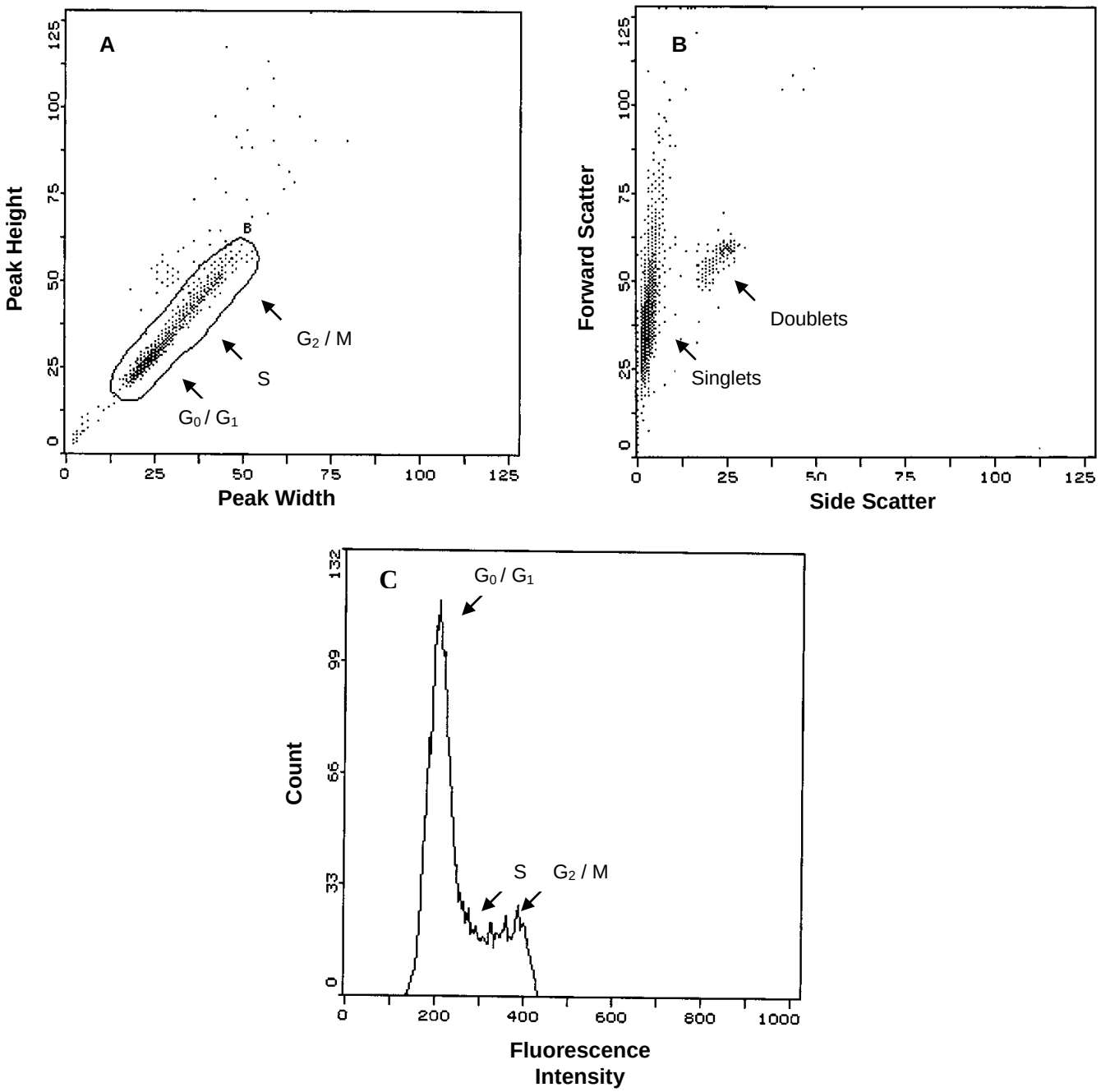

Figure A1: Flow cytometric data generation. Much data is automatically generated and graphed by the flow cytometer upon data acquisition. This data must be sorted to produce appropriate output. As the propidium iodide emission is detected, a scattergram is generated relating to fluorescence peak height and width/area (**A**). The population of interest emerges (the enclosed region of A) showing the G_0/G_1, S and G_2/M populations. Events outside this region are either doublets or debris. Comparing particle complexity (forward scatter) versus size (side scatter) gives a good indication of the presence of doublets (**B**). By only analysing the data present in the gated region B, a histogram of the population's current division of the cell cycle can be generated without potentially confounding doublets erroneously elevating the $S/G_2/M$ percentage of the population.

Appendix B

During the graph generation of the earlier constructions of the realistic p38 model, there were regions present where no information was generated, and where at certain points the predicted concentration would suddenly spike (Fig. B1). In an attempt to remove these regions, the concentrations of the main upstream effectors of p38, Mekk1 and MLK3, were modulated (Fig. B2). It was found that by changing the concentrations of Mekk1 and MLK3 to 2 μM and 1 μM respectively that all of the spikes in p38 were removed, although the data deficient regions remained. The concentrations and catalytic constants of p38's first upstream effectors (Ras and Rac1) were then modulated in an attempt to remove the data deficient regions (Fig. B3). While this was successful, the concentrations used in this modulation were ultimately biologically implausible, and the ultrasensitivity of p38 was abolished (Fig. B4). As such, these modifications were not used.

The models used in the generation of data are both in Appendix C and on the accompanying disk marked Appendix D. All of the scripts, software and modules used in the construction of the model, and for the generation of *in silico* data are available on the accompanying disk marked Appendix D.

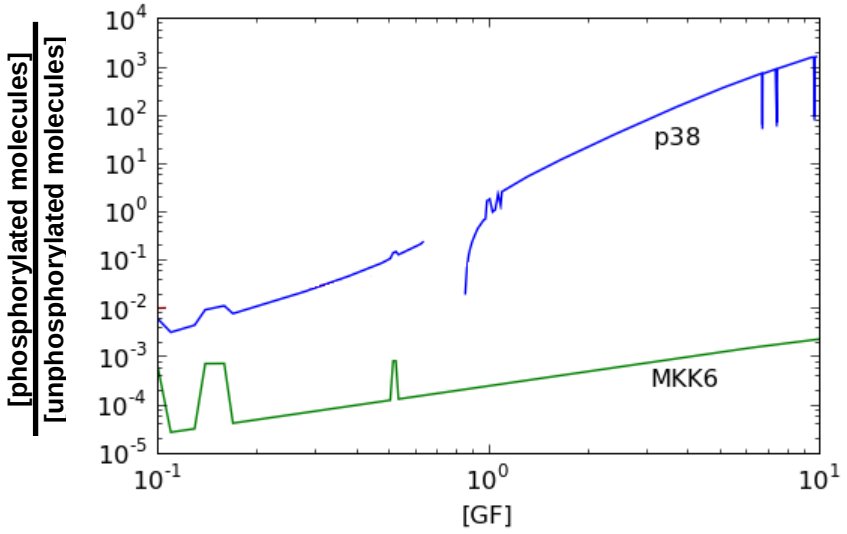

Figure B1: Spikes and gaps in generated data. An attempt to resolve these issues was done by modulating upstream effectors.

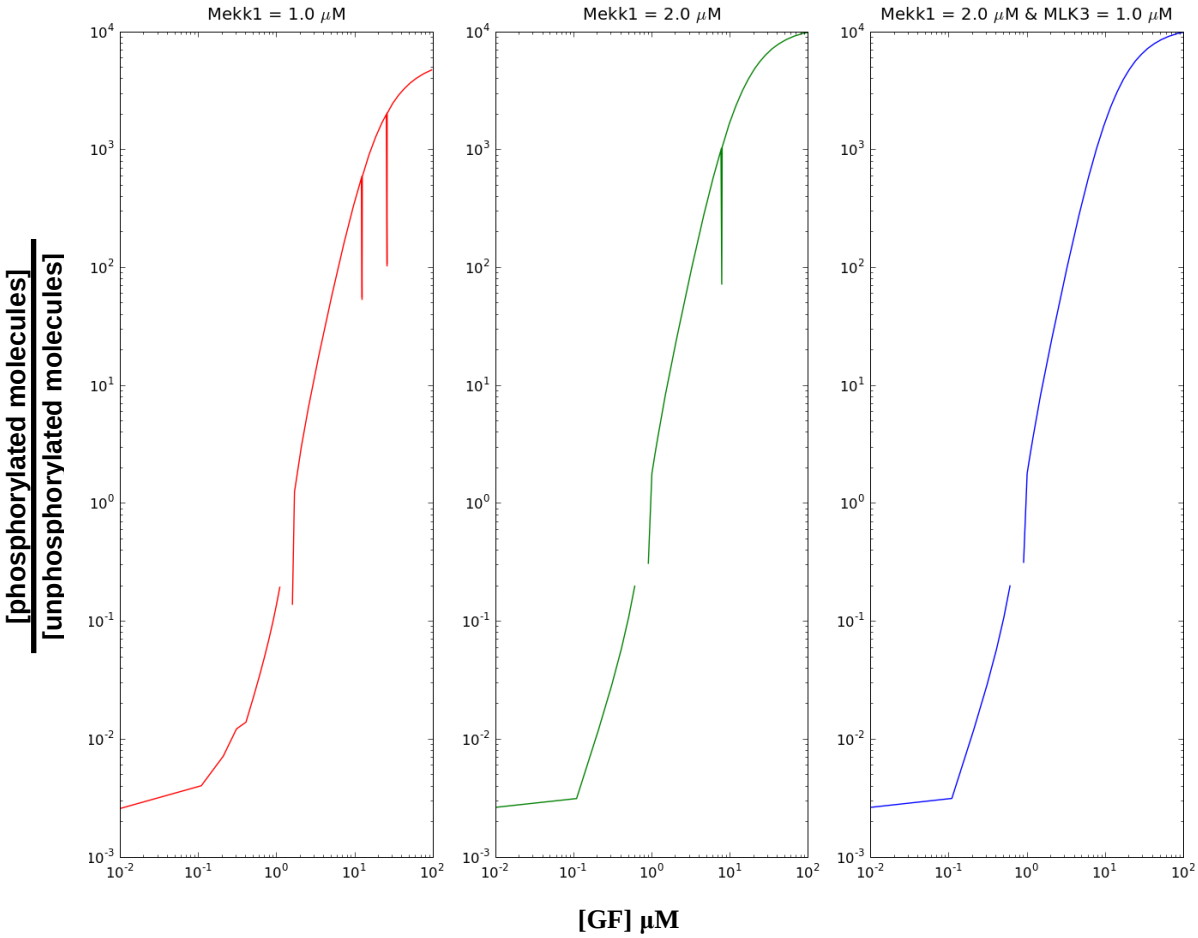

Figure B2: Modulation of Mekk1 and MLK3 concentrations in an attempt to remove spurious spikes and data deficient regions. The data presented is of the ratio of phosphorylated to unphosphorylated p38.

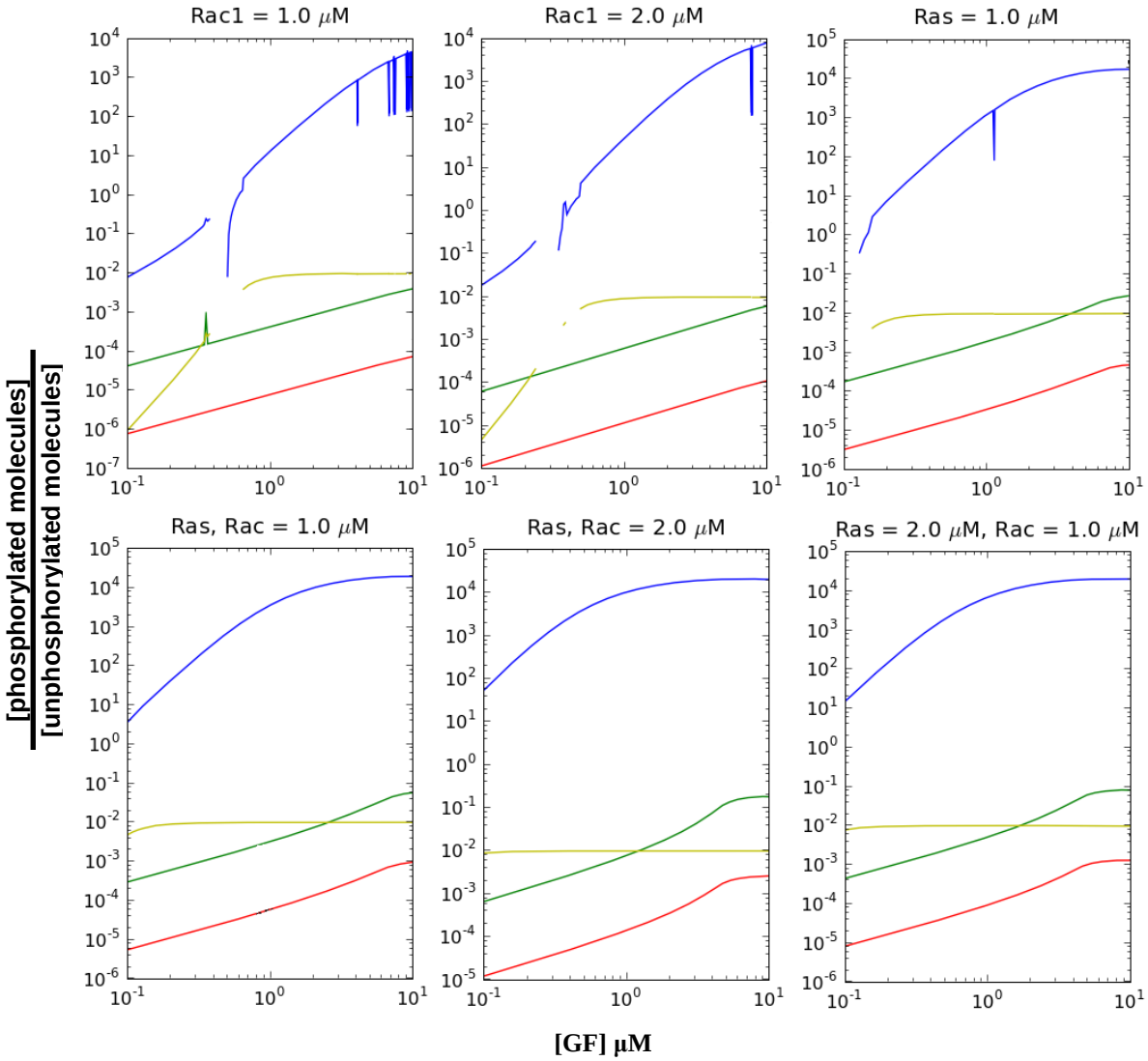

Figure B3: An attempt to resolve both spikes and data deficient regions present within the model by modulating Ras and Rac1 concentrations. While the 1 μM Ras and Rac1 concentration were sufficient to remove both the spikes and data deficient regions, this concentration is very high and not plausible on a cellular level. The data presented is of the ratios of phosphorylated to unphosphorylated molecules

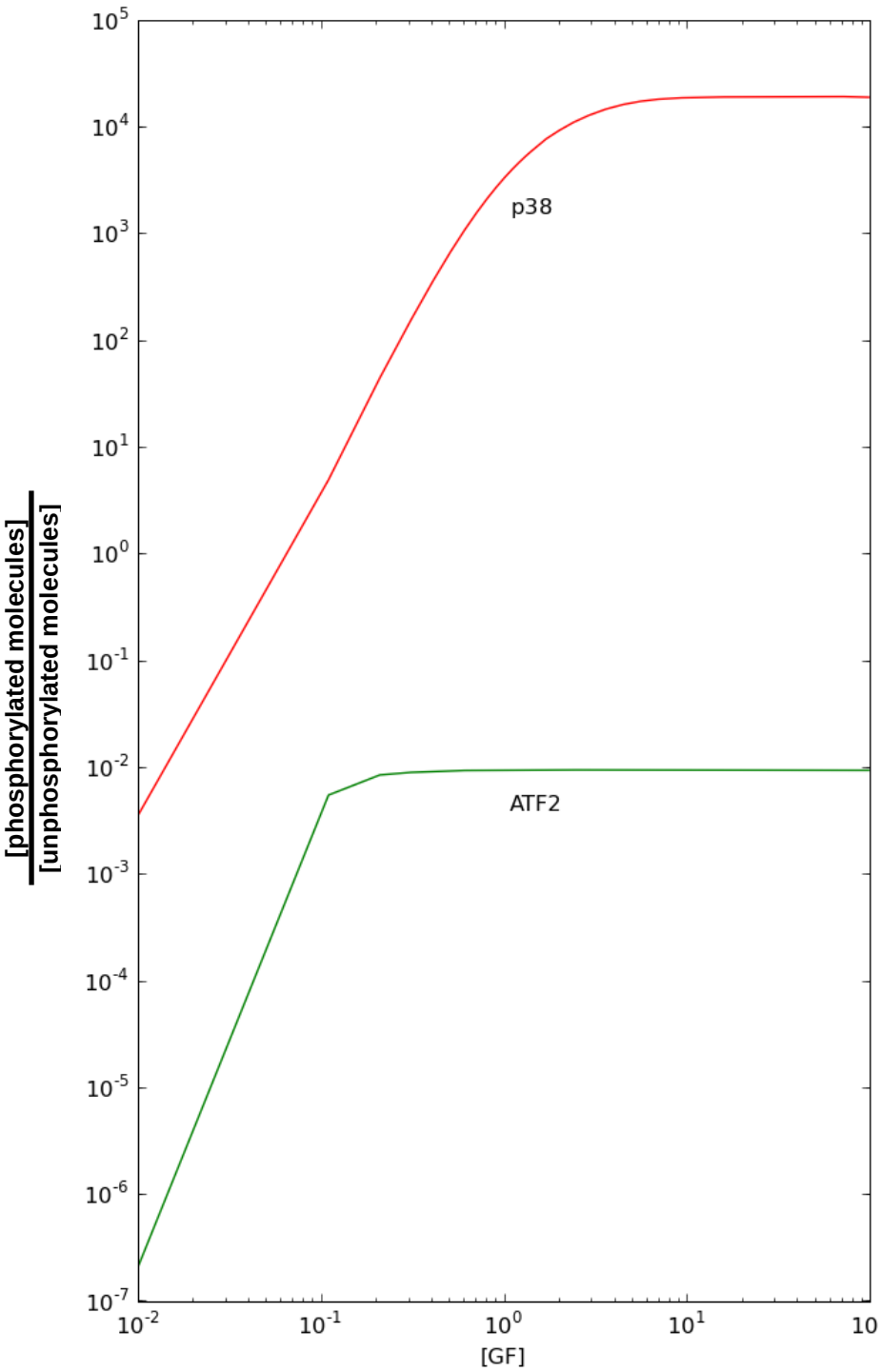

Figure B4: Lack of ultrasensitivity of p38 and ATF2. When all the changes, biologically plausible or not, were implemented in the model, all of the data deficient regions and spikes were abolished. However, the ultrasensitive response of p38 was abolished as well. Data is presented as a ratio of phosphorylated to unphosphorylated molecules.

Appendix C

The following presented below are the PySCeS model scripts used in the generation of *in silico* data. This text may be copied and pasted into a separate document and saved with the file extension ".psc" and be used without modification with PySCeS. The model scripts of the Hornberg, Huang, and Kholodenko models are included on the accompanying disk marked Appendix D.

##Monocore model

##Core model for demonstrating the principle of ultrasensitivity with one-step biphosphorylation

R1:

A = Ap

(K1 * I * A) / (Km1 + A)

R2:

Ap = A

K2 * Ap

R3:

B = Bpp

(K3 * Ap * B) / (Km3 + B)

R4:

Bpp = B

K4 * Bpp

R5:

C = Cpp

(K5 * Bpp * C) / (Km5 + C)

R6:

Cpp = C

K6 * Cpp

R7:

O = Op

(K7 * Cpp * O) / (Km7 + O)

R8:

Op = O

K8 * Op

#Km

Km1 = 0.01

Km3 = 0.01

Km5 = 0.01

Km7 = 0.01

#Kcat

K1 = 1.0

K2 = 1.0

K3 = 1.0

K4 = 1.0

K5 = 1.0

K6 = 1.0

K7 = 1.0

K8 = 1.0

#Concentrations

I = 1.0

A = 0.9

Ap = 0.1

B = 0.9

Bpp = 0.05

C = 0.9

Cpp = 0.05

O = 0.9

Op = 0.1

##Dualcore model

##Core model for demonstrating the principle of ultrasensitivity with two-step biphosphorylation

R1:

A = Ap

(K1 * I * A) / (Km1 + A)

R2:

Ap = A

K2 * Ap

R3:

B = Bp

(K3 * Ap * B) / (Km3 + B)

R4:

Bp = Bpp

(K4 * Ap * Bp) / (Km4 + Bp)

R5:

Bp = B

K5 * Bp

R6:

Bpp = Bp

K6 * Bpp

R7:

C = Cp

(K7 * Bpp * C) / (Km7 + C)

R8:

Cp = Cpp

(K8 * Bpp * Cp) / (Km8 + Cp)

R9:

Cp = C

K9 * Cp

R10:

Cpp = Cp

K10 * Cpp

R11:

O = Op

(K11 * Cpp * O) / (Km11 + O)

R12:

Op = O

K12 * Op

#Km

Km1 = 0.01

Km3 = 0.01

Km4 = 0.01

Km7 = 0.01

Km8 = 0.01

Km11 = 0.01

#Kcat

K1 = 1.0

K2 = 1.0

K3 = 1.0

K4 = 1.0

K5 = 1.0

K6 = 1.0

K7 = 1.0

K8 = 1.0

K9 = 1.0

K10 = 1.0

K11 = 1.0

K12 = 1.0

#Concentrations

I = 1.0

A = 0.9

Ap = 0.1

B = 0.9

Bp = 0.05

Bpp = 0.05

C = 0.9

Cp = 0.05

Cpp = 0.05

O = 0.9

Op = 0.1

Realcore Model

All Kcat set to 1

All Km set to 0.01

All concentrations range between 0 and 1

R1:

RasGDP = RasGTP

(K1 * GF * RasGDP) / (Km1 + RasGDP)

R2:

RasGTP = RasGDP

(K2 * RasGTP) / (Km2 + RasGTP)

R3:

Rac1GDP = Rac1GTP

(K3 * Rac1GDP * RasGTP) / (Km3 + Rac1GDP)

R4:

Rac1GTP = Rac1GDP

(K4 * Rac1GTP) / (Km4 + Rac1GTP)

R5:

Mekk1 = Mekk1p

(K5 * Mekk1 * Rac1GTP) / (Km5 + Mekk1)

R6:

Mekk1p = Mekk1

(KA * Mekk1p * PP2A) / (KmA + Mekk1p)

R7:

MLK3 = MLK3p

(K7 * MLK3 * Rac1GTP) / (Km7 + MLK3)

R8:

MLK3p = MLK3

(KA * MLK3p * PP2A) / (KmA + MLK3p)

R9:

MKK4 = MKK4p

(K9 * MKK4 * MLK3p) / (Km9 + MKK4)

R10:

MKK4 = MKK4p

(K10 * MKK4 * Mekk1p) / (Km10 + MKK4)

R11:

MKK4p = MKK4

(KC * MKK4p * PP2C) / (KmC + MKK4p)

R12:

MKK4p = MKK4pp

(K12 * MKK4p * MLK3p) / (Km12 + MKK4p)

R13:

MKK4p = MKK4pp

(K13 * MKK4p * Mekk1p) / (Km13 + MKK4p)

R14:

MKK4pp = MKK4p

(KC * MKK4pp * PP2C) / (KmC + MKK4pp)

R19:

MKK6 = MKK6p

(K19 * MKK6 * MLK3p) / (Km19 + MKK6)

R20:

MKK6p = MKK6

(KC * MKK6p * PP2C) / (KmC + MKK6p)

R21:

MKK6p = MKK6pp

(K21 * MKK6p * MLK3p) / (Km21 + MKK6p)

R22:

MKK6pp = MKK6p

(KC * MKK6pp * PP2C) / (KmC + MKK6pp)

R23:

p38b = p38bp

(K23 * p38b * MKK4pp) / (Km23 + p38b)

R25:

p38b = p38bp

(K25 * p38b * MKK6pp) / (Km25 + p38b)

R26:

p38bp = p38b

(KM * p38bp * MKP1) / (KmM + p38bp)

R27:

p38bp = p38bpp

(K27 * p38bp * MKK4pp) / (Km27 + p38bp)

R29:

p38bp = p38bpp

(K29 * p38bp * MKK6pp) / (Km29 + p38bp)

R30:

p38bpp = p38bp

(KM * p38bpp * MKP1) / (KmM + p38bpp)

R31:

ATF2 = ATF2p

(K31 * ATF2 * p38bpp) / ((Km31 + ATF2) * (KmATP * (1 + (SB / Ki)) + ATP))

R32:

ATF2p = ATF2

(KA * ATF2p * PP2A) / (KmA + ATF2p)

#Constants

Ki = 1.0

#Kcat constants

K1 = 1.0

K2 = 1.0

K3 = 1.0

K4 = 1.0

K5 = 1.0

KA = 1.0

K7 = 1.0

K9 = 1.0

K10 = 1.0

KC = 1.0

K12 = 1.0

K13 = 1.0

K19 = 1.0

K21 = 1.0

K23 = 1.0

K25 = 1.0

KM = 1.0

K27 = 1.0

K29 = 1.0

K31 = 1.0

#Km constants

Km1 = 0.01

Km2 = 0.01

Km3 = 0.01

Km4 = 0.01

Km5 = 0.01

KmA = 0.01

Km7 = 0.01

Km9 = 0.01

Km10 = 0.01

KmC = 0.01

Km12 = 0.01

Km13 = 0.01

Km19 = 0.01

Km21 = 0.01

Km23 = 0.01

Km25 = 0.01

KmM = 0.01

Km27 = 0.01

Km29 = 0.01

Km31 = 0.01

KmATP = 0.01

#Static species

GF = 1.0

SB = 0.0

ATP = 1.0

MKP1 = 1.0

PP2A = 1.0

PP2C = 1.0

#Variable species

RasGDP = 0.9

RasGTP = 0.1

Rac1GDP = 0.9

Rac1GTP = 0.1

Mekk1 = 0.9

Mekk1p = 0.1

MLK3 = 0.9

MLK3p = 0.1

MKK4 = 0.9

MKK4p = 0.05

MKK4pp = 0.05

MKK6 = 0.9

MKK6p = 0.05

MKK6pp = 0.05

p38b = 0.9

p38bp = 0.05

p38bpp = 0.05

ATF2 = 0.9

ATF2p = 0.1

Realistic p38 model

Parameter Standardization:

K per second

Km micromolar

Concentrations in micromolar

R1:

RasGDP = RasGTP

(K1 * RasGDP) / (Km1 + RasGDP)

R2:

RasGTP = RasGDP

(K2 * RasGTP) / (Km2 + RasGTP)

R3:

Rac1GDP = Rac1GTP

(K3 * Rac1GDP * RasGTP) / (Km3 + Rac1GDP)

R4:

Rac1GTP = Rac1GDP

(K4 * Rac1GTP) / (Km4 + Rac1GTP)

R5:

Mekk1 = Mekk1p

(K5 * Mekk1 * Rac1GTP) / (Km5 + Mekk1)

R6:

Mekk1p = Mekk1

(KA * Mekk1p * PP2A) / (KmA + Mekk1p)

R7:

MLK3 = MLK3p

(K7 * MLK3 * Rac1GTP) / (Km7 + MLK3)

R8:

MLK3p = MLK3

(KA * MLK3p * PP2A) / (KmA + MLK3p)

R9:

MKK4 = MKK4p

(K9 * MKK4 * MLK3p) / (Km9 + MKK4)

R10:

MKK4 = MKK4p

(K10 * MKK4 * Mekk1p) / (Km10 + MKK4)

R11:

MKK4p = MKK4

(KC * MKK4p * PP2C) / (KmC + MKK4p)

R12:

MKK4p = MKK4pp

(K12 * MKK4p * MLK3p) / (Km12 + MKK4p)

R13:

MKK4p = MKK4pp

(K13 * MKK4p * Mekk1p) / (Km13 + MKK4p)

R14:

MKK4pp = MKK4p

(KC * MKK4pp * PP2C) / (KmC + MKK4pp)

R19:

MKK6 = MKK6p

(K19 * MKK6 * MLK3p) / (Km19 + MKK6)

R20:

MKK6p = MKK6

(KC * MKK6p * PP2C) / (KmC + MKK6p)

R21:

MKK6p = MKK6pp

(K21 * MKK6p * MLK3p) / (Km21 + MKK6p)

R22:

MKK6pp = MKK6p

(KC * MKK6pp * PP2C) / (KmC + MKK6pp)

R23:

p38b = p38bp

(K23 * p38b * MKK4pp) / (Km23 + p38b)

R25:

p38b = p38bp

(K25 * p38b * MKK6pp) / (Km25 + p38b)

R26:

p38bp = p38b

(KM * p38bp * MKP1) / (KmM + p38bp)

R27:

p38bp = p38bpp

(K27 * p38bp * MKK4pp) / (Km27 + p38bp)

R29:

p38bp = p38bpp

(K29 * p38bp * MKK6pp) / (Km29 + p38bp)

R30:

p38bpp = p38bp

(KM * p38bpp * MKP1) / (KmM + p38bpp)

R31:

ATF2 = ATF2p

(K31 * ATF2 * p38bpp) / ((Km31 + ATF2) * (KmATP * (1 + (SB / Ki)) + ATP))

R32:

ATF2p = ATF2

(KA2 * ATF2p * PP2An) / (KmA2 + ATF2p)

#Constants

Ki = 0.021

#Kcat constants

K1 = 0.38

K2 = 0.1

K3 = 0.151

K4 = 0.39

K5 = 2.025

KA = 6.0

KA2 = 0.1

K7 = 0.0055

K9 = 0.005

K10 = 0.025

KC = 0.23

K12 = 0.005

K13 = 0.025

K19 = 0.005

K21 = 0.005

K23 = 0.0883

K25 = 0.0022

KM = 0.0238

K27 = 0.0883

K29 = 0.0022

K31 = 0.18

#Km constants

Km1 = 1.9

Km2 = 0.11

Km3 = 1.98

Km4 = 18.7

Km5 = 10

KmA = 7.82

KmA2 = 7.82

Km7 = 29.7

Km9 = 0.31

Km10 = 15

KmC = 15

Km12 = 0.31

Km13 = 15

Km19 = 0.31

Km21 = 0.31

Km23 = 0.4

Km25 = 0.6

KmM = 0.067

Km27 = 0.4

Km29 = 0.6

Km31 = 1.6

KmATP = 23

#Static species

SB = 0.0

ATP = 3.0

MKP1 = 0.0032

PP2A = 0.16

PP2An = 0.016

PP2C = 0.01

#Variable species

RasGDP = 0.09

RasGTP = 0.01

Rac1GDP = 0.49

Rac1GTP = 0.01

Mekk1 = 0.67

Mekk1p = 0.01

MLK3 = 0.67

MLK3p = 0.01

MKK4 = 0.2

MKK4p = 0.05

MKK4pp = 0.05

MKK6 = 0.2

MKK6p = 0.05

MKK6pp = 0.05

p38b = 0.26

p38bp = 0.05

p38bpp = 0.05

ATF2 = 0.59

ATF2p = 0.01

References

Aguda, B. D. and Tang, Y. (1999). The kinetic origins of the restriction point in the mammalian cell cycle. *Cell Proliferation***32**, 321-35.

Alt, J. R., Cleveland, J. L., Hannink, M. and Diehl, J. A. (2000). Phosphorylation-dependent regulation of cyclin D1 nuclear export and cyclin D1-dependent cellular transformation. *Genes and Development***14**, 3102-14.

Ambrosino, C., Mace, G., Galban, S., Fritsch, C., Vintersten, K., Black, E., Gorospe, M. and Nebreda, A. R. (2003). Negative Feedback Regulation of MKK6 mRNA Stability by p38α Mitogen-Activated Protein Kinase. *Molecular and Cellular Biology***23**, 370 - 381.

Badger, A. M., Cook, M. N., Lark, M. W., Newman-Tarr, T. M., Swift, B. A., Nelson, A. H., Barone, F. C. and Kumar, S. (1998). SB 203580 Inhibits p38 Mitogen-Activated Protein Kinase, Nitric Oxide Production, and Inducible Nitric Oxide Synthase in Bovine Cartilage-Derived Chondrocytes. *Journal of Immunology***161**, 467 - 473.

Bartkova, J., Rezaei, N., Liontos, M., Karakaidos, P., Kletsas, D., Issaeva, N., Vassiliou, L. V., Kolettas, E., Niforou, K., Zoumpourlis, V. C. et al. (2006). Oncogene-induced senescence is part of the tumorigenesis barrier imposed by DNA damage checkpoints. *Nature***444**, 633-7.

Beier, F., Lee, R. J., Taylor, A. C., Pestell, R. G. and LuValle, P. (1999). Identification of the cyclin D1 gene as a target of activating transcription factor 2 in chondrocytes. *Proceedings of the National Academy of Sciences***96**, 1433 - 1438.

Ben-Levy, R., Hooper, S., Wilson, R., Paterson, H. F. and Marshall, C. J. (1998). Nuclear export of the stress-activated protein kinase p38 mediated by its substrate MAPKAP kinase-2. *Current Biology***8**, 1049-57.

Benezra, R., Davis, R. L., Lassar, A., Tapscott, S., Thayer, M., Lockshon, D. and Weintraub, H. (1990a). Id: a negative regulator of helix-loop-helix DNA binding proteins. Control of terminal myogenic differentiation. *Annals of the New York Academy of Sciences***599**, 1-11.

Benezra, R., Davis, R. L., Lockshon, D., Turner, D. L. and Weintraub, H. (1990b). The protein Id: a negative regulator of helix-loop-helix DNA binding proteins. *Cell***61**, 49-59.

Beyene, R., Howard, B. M. and Bookvar, J. A. (2009). Stem cell populated implanted trachea. *Neurosurgery***64**, N12 - 13.

Bhalla, U. S. and Iyengar, R. (1999). Emergent properties of networks of biological signaling pathways. *Science***283**, 381-7.

Binne, U. K., Classon, M. K., Dick, F. A., Wei, W., Rape, M., Kaelin, W. G., Jr., Naar, A. M. and Dyson, N. J. (2007). Retinoblastoma protein and anaphase-promoting complex physically interact and functionally cooperate during cell-cycle exit. *Nature Cell Biology***9**, 225-32.

Blagosklonny, M. V. and Pardee, A. B. (2002). The restriction point of the cell cycle. *Cell Cycle***1**, 103-10.

Blain, S. W., Montalvo, E. and Massague, J. (1997). Differential interaction of the cyclin-dependent kinase (Cdk) inhibitor p27Kip1 with cyclin A-Cdk2 and cyclin D2-Cdk4. *Journal of Biological Chemistry***272**, 25863-72.

Blau, H., Pavlath, G., Hardeman, E., Chiu, C., Silberstein, L., Webster, S., Miller, S. and Webster, C. (1985). Plasticity of the differentiated state. *Science***230**, 758 - 766.

Bray, D. (1995). Protein molecules as computational elements in living cells. *Nature***376**, 307-12.

Brightman, F. A. and Fell, D. A. (2000). Differential feedback regulation of the MAPK cascade underlies the quantitative differences in EGF and NGF signalling in PC12 cells. *FEBS Letters***482**, 169-74.

Buttitta, L. A. and Edgar, B. A. (2007). Mechanisms controlling cell cycle exit upon terminal differentiation. *Current Opinion in Cell Biology***19**, 697-704.

Calcabrini, A., Garcia-Martinez, J. M., Gonzalez, L., Tendero, M. J., Ortuno, M. T., Crateri, P., Lopez-Rivas, A., Arancia, G., Gonzalez-Porque, P. and Martin-Perez, J. (2006). Inhibition of proliferation and induction of apoptosis in human breast cancer cells by lauryl gallate. *Carcinogenesis***27**, 1699-712.

Campion, D. R. (1984). The muscle satellite cell: a review. *International Review of Cytology***87**, 225 - 251.

Campisi, J. (2005a). Aging, tumor suppression and cancer: high wire-act! *Mechanisms of Ageing and Development***126**, 51-8.

Campisi, J. (2005b). Suppressing cancer: the importance of being senescent. *Science***309**, 886-7.

Campisi, J., Medrano, E. E., Morreo, G. and Pardee, A. B. (1982a). Restriction point control of cell growth by a labile protein: Evidence for increased stability in transformed cells. *Proceedings of the National Academy of Sciences***79**, 436 - 440.

Campisi, J., Medrano, E. E., Morreo, G. and Pardee, A. B. (1982b). Restriction point control of cell growth by a labile protein: Evidence for increased stability in transformed cells. *Proc Natl Acad Sci U S A***79**, 436 - 440.

Campisi, J., Medrano, E. E., Morreo, G. and Pardee, A. B. (1982c). Restriction point control of cell growth by a labile protein: evidence for increased stability in transformed cells. *Proceedings of the National Academy of Sciences***79**, 436-40.

Camps, M., Chabert, C., Muda, M., Boschert, U., Gillieron, C. and Arkinstall, S. (1998). Induction of the mitogen-activated protein kinase phosphatase MKP3 by nerve growth factor in differentiating PC12. *FEBS Letters***425**, 271-6.

Camps, M., Nichols, A. and Arkinstall, S. (2000). Dual specificity phosphatases: a gene family for control of MAP kinase function. *FASEB Journal***14**, 6-16.

Cano, E. and Mahadevan, L. C. (1995). Parallel signal processing among mammalian MAPKs. *Trends in Biochemical Sciences***20**, 117-22.

Cardone, M. H., Salvesen, G. S., Widmann, C., Johnson, G. and Frisch, S. M. (1997). The regulation of anoikis: MEKK-1 activation requires cleavage by caspases. *Cell***90**, 315-23.

Caunt, C. J., Rivers, C. A., Conway-Campbell, B. L., Norman, M. R. and McArdle, C. A. (2008). Epidermal Growth Factor Receptor and Protein Kinase C Signaling to ERK2: Spatiotemporal Regulation of ERK2 by Dual Specificity Phosphatases. *Journal of Biological Chemistry***283**, 6241 - 6252.

Chance, B., Garfinkel, D., Higgins, J. and Hess, B. (1960). Metabolic Control Mechanisms V. A solution for the equations representing interaction between glycolysis and respiration in ascites tumor cells. *Journal of Biological Chemistry***235**, 2426 - 2439.

Charge, S. and Rudnicki, M. A. (2004). Cellular and molecular regulation of muscle regeneration. *Physiological Reviews***84**, 209 - 238.

Chen, G., Hitomi, M., Han, J. and Stacey, D. W. (2000). The p38 pathway provides negative feedback for Ras proliferative signaling. *Journal of Biological Chemistry***275**, 38973-80.

Chen, Y. R. and Tan, T. H. (2000). The c-Jun N-terminal kinase pathway and apoptotic signaling. *International Journal of Oncology***16**, 651 - 662.

Collins, C. (2006). Satellite cell self-renewal. *Current Opinion in Pharmacology***6**, 301 - 306.

Collins, C. A., Gnocchi, V. F., White, R. B., Boldrin, L., Perez-Ruiz, A., Relaix, F., Morgan, J. E. and Zammit, P. S. (2009). Integrated Functions of Pax3 and Pax7 in the Regulation of Proliferation, Cell Size and Myogenic Differentiation. *PLoS ONE***4**, e4475.

Constant, S. L., Dong, C., Yang, D. D., Wysk, M., Davis, R. J. and Flavell, R. A. (2000). JNK1 is required for T cell-mediated immunity against Leishmania major infection. *Journal of Immunology***165**, 2671-6.

Cook, S. J. and McCormick, F. (1996). Kinetic and biochemical correlation between sustained p44ERK1 (44 kDa extracellular signal-regulated kinase 1) activation and lysophosphatidic acid-stimulated DNA synthesis in Rat-1 cells. *Biochemical Journal***320 (Pt 1)**, 237-45.

Cossu, G. and Molinaro, M. (1987). Cell heterogeneity in the myogenic lineage. *Current Topics in Developmental Biology***23**, 185 - 208.

Crissman, H. A. and Steinkamp, J. A. (1982). Rapid, one step staining procedures for analysis of cellular DNA and protein by single and dual laser flow cytometry. *Cytometry***3**, 84 - 90.

Csikász-Nagy, A., Battogtokh, D., Chen, K. C., Novák, B. and Tyson, J. J. (2006). Analysis of a Generic Model of Eukaryotic Cell-Cycle Regulation. *Biophysical Journal***90**, 4361 - 4379.

Cuenda, A., Rouse, J., Doza, Y. N., Meier, R., Cohen, P., Gallagher, T. F., Young, P. R. and Lee, J. C. (1995). SB 203580 is a specific inhibitor of a MAP kinase homologue which is stimulated by cellular stresses and interleukin-1. *FEBS Letters***364**, 229-33.

Das, J., Ho, M., Zikherman, J., Govern, C., Yang, M., Weiss, A., Chakraborty, A. K. and Roose, J. P. (2009). Digital signaling and hysteresis characterize ras activation in lymphoid cells. *Cell***136**, 337-51.

Davies, S. P., Reddy, H., Caivano, M. and Cohen, P. (2000). Specificity and mechanism of action of some commonly used protein kinase inhibitors. *Biochemical Journal***351**, 95-105.

Davis, R. (2000). Signal Transduction by the JNK Group of MAP Kinases. *Cell***103**, 239 - 252.

Denhardt, D. T. (1996). Signal-transducing protein phosphorylation cascades mediated by Ras/Rho proteins in the mammalian cell: the potential for multiplex signalling. *Biochemical Journal***318 (Pt 3)**, 729-47.

Denu, J. M. and Dixon, J. E. (1995). A catalytic mechanism for the dual-specific phosphatases. *Proceedings of the National Academy of Sciences***92**, 5910 - 5914.

Derijard, B., Hibi, M., Wu, I., Barrett, T., Su, B., Deng, T., Karin, M. and Davis, R. J. (1994). JNK1: a protein kinase stimulated by UV light and Ha-Ras that binds and phosphorylates the c-Jun activation domain. *Cell***76**, 1025 - 1037.

Dhawan, J. and Rando, T. (2005). Stem cells in postnatal myogenesis: molecular mechanisms of satellite cell quiescence, activation and replenishment. *Trends in Cell Biology***15**, 666 - 673.

Donati, C., Meacci, E., Nuti, F., Becciolini, L., M., F. and Bruni, P. (2005). Sphingosine 1-phosphate regulates myogenic differentiation: a major role for S1P2 receptor. *FASEB Journal***19**.

Dong, C., Yang, D. D., Tournier, C., Whitmarsh, A. J., Xu, J., Davis, R. J. and Flavell, R. A. (2000). JNK is required for effector T-cell function but not for T-cell activation. *Nature***405**, 91-4.

Dudley, D. T., Pang, L., Decker, S. J., Bridges, A. J. and Saltiel, A. R. (1995). A synthetic inhibitor of the mitogen-activated protein kinase cascade. *Proceedings of the National Academy of Sciences***92**, 7686-9.

Ekholm, S. V. and Reed, S. I. (2000). Regulation of G(1) cyclin-dependent kinases in the mammalian cell cycle. *Current Opinion in Cell Biology***12**, 676-84.

Ekholm, S. V., Zickert, P., Reed, S. I. and Zetterberg, A. (2001). Accumulation of cyclin E is not a prerequisite for passage through the restriction point. *Molecular and Cellular Biology***21**, 3256-65.

Evangelisti, C., Tazzari, P., Riccio, M., Fiume, R., Hozumi, Y., Fala, F., Goto, K., Manzoli, L., Cocco, L. and Martelli, A. (2007). Nuclear diacylglycerol kinase-ζ is a negative regulator of cell cycle progression in C2C12 mouse myoblasts. *FASEB Journal***12**, 3297 - 3307.

Evans, M. J. and Kaufman, M. H. (1981). Establishment in culture of pluripotent cells from mouse embryos. *Nature***292**, 154 - 156.

Eyers, P. A., van den IJssel, P., Quinlan, R. A., Goedert, M. and Cohen, P. (1999). Use of a drug-resistant mutant of stress-activated protein kinase 2a/p38 to validate the in vivo specificity of SB 203580. *FEBS Letters***451**, 191 - 196.

Ferrell, J. E., Jr. (1996). Tripping the switch fantastic: how a protein kinase cascade can convert graded inputs into switch-like outputs. *Trends in Biochemical Sciences***21**, 460-6.

Ferrell, J. E., Jr. and Machleder, E. M. (1998). The Biochemical Basis of an All-or-None Cell Fate Switch in Xenopus Oocytes. *Science***280**, 895 - 898.

Fjeld, C. C. and Denu, J. M. (1999). Kinetic analysis of human serine/threonine protein phosphatase 2Calpha. *Journal of Biological Chemistry***274**, 20336-43.

Frantz, B., Klatt, T., Pang, M., Parsons, J., Rolando, A., Williams, H., Tocci, M. J., O'Keefe, S. J. and O'Neill, E. A. (1998). The activation state of p38 mitogen-activated protein kinase determines the efficiency of ATP competition for pyridinylimidazole inhibitor binding. *Biochemistry***37**, 13846-53.

Freshney, N. W., Rawlinson, L., Guesdon, F., Jones, E., Cowley, S., Hsuan, J. and Saklatvala, J. (1994). Interleukin-1 activates a novel protein kinase cascade that results in the phosphorylation of Hsp27. *Cell***78**, 1039-49.

Frolov, M. V. and Dyson, N. J. (2004). Molecular mechanisms of E2F-dependent activation and pRB-mediated repression. *Journal of Cell Science***117**, 2173-81.

Fry, D. W., Kraker, A. J., McMichael, A., Ambroso, L. A., Nelson, J. M., Leopold, W. R., Connors, R. W. and Bridges, A. J. (1994). A specific inhibitor of the epidermal growth factor receptor tyrosine kinase. *Science***265**, 1093-5.

Fuchs, S. Y., Fried, V. A. and Ronai, Z. (1998). Stress-activated kinases regulate protein stability. *Oncogene***17**, 1483-90.

Fujita, H., Endo, A., Shimizu, K. and Nagamori, E. (2010). Evaluation of serum-free differentiation conditions for C2C12 myoblast cells assessed as to active tension generation capability. *Biotechnology and Bioengineering***107**, 894 - 901.

Fukada, S., Higuchi, S., Segawa, M., Koda, K., Yamamoto, Y., Tsujikawa, K., Kohama, Y., Uezumi, A., Imamura, M., Miyagoe-Suzuki, Y. et al. (2004). Purification and cell-surface marker characterization of quiescent satellite cells from murine skeletal muscle by a novel monoclonal antibody. *Experimental Cell Research***296**, 245 - 255.

Fung, T. K. and Poon, R. Y. (2005). A roller coaster ride with the mitotic cyclins. *Seminars in Cell and Developmental Biology***16**, 335-42.

Galabova-Kovacs, G., Kolbus, A., Matzen, D., Meissl, K., Piazzolla, D., Rubiolo, C., Steinitz, K. and Baccarini, M. (2006). ERK and beyond: Insights from B-Raf and Raf-1 conditional knockouts. *Cell Cycle***5**, 1514-18.

Geley, S., Kramer, E., Gieffers, C., Gannon, J., Peters, J. M. and Hunt, T. (2001). Anaphase-promoting complex/cyclosome-dependent proteolysis of human cyclin A starts at the beginning of mitosis and is not subject to the spindle assembly checkpoint. *Journal of Cell Biology***153**, 137-48.

Gilbert, D., Fuss, H., Gu, X., Orton, R., Robinson, S., Vyshemirsky, V., Kurth, M. J., Downes, C. S. and Dubitzky, W. (2006). Computational methodologies for modelling, analysis and simulation of signalling networks. *Briefings in Bioinformatics***7**, 339-53.

Gillespie, M. A., Le Grand, F., Scime, A., Kuang, S., von Maltzahn, J., Seale, V., Cuenda, A., Ranish, J. A. and Rudnicki, M. A. (2009). p38-γ-dependent gene silencing restricts entry into the myogenic differentiation program. *Journal of Cell Biology***187**, 991-1005.

Goldbeter, A. (1991). A minimal cascade model for the mitotic oscillator involving cyclin and cdc2 kinase. *Proceedings of the National Academy of Sciences***88**, 9107-11.

Goldbeter, A. and Koshland, D. E., Jr. (1981). An amplified sensitivity arising from covalent modification in biological systems. *Proceedings of the National Academy of Sciences***78**, 6840 - 6844.

Goldbeter, A. and Koshland, D. E., Jr. (1982). Sensitivity amplification in biochemical systems. *Quarterly Reviews of Biophysics***15**, 555 - 591.

Goldbeter, A. and Koshland, D. E., Jr. (1984). Ultrasensitivity in biochemical systems controlled by covalent modification. Interplay between zero-order and multistep effects. *Journal of Biological Chemistry***259**, 14441-7.

Goodell, M. A., Brose, K., Paradis, G., Conner, A. S. and Mulligan, R. C. (1996). Isolation and functional properties of murine hematopoietic stem cells that are replicating in vivo. *Journal of Experimental Medicine***183**, 1797 - 1806.

Graves, L. M., Guy, H. I., Kozlowski, P., Huang, M., Lazarowski, E., Pope, R. M., Collins, M. A., Dahlstrand, E. N., Earp, H. S., 3rd and Evans, D. R. (2000). Regulation of carbamoyl phosphate synthetase by MAP kinase. *Nature***403**, 328-32.

Gredinger, E., Gerber, A. N., Tamir, Y., Tapscott, S. and Bengal, E. (1998). Mitogen-activated Protein Kinase Pathway Is Involved in the Differentiation of Muscle Cells. *Journal of Biological Chemistry***273**, 10436 - 10444.

Guan, Z., Buckman, S. Y., Miller, B. W., Springer, L. D. and Morrison, A. R. (1998). Interleukin-1beta-induced cyclooxygenase-2 expression requires activation of both c-Jun NH2-terminal kinase and p38 MAPK signal pathways in rat renal mesangial cells. *Journal of Biological Chemistry***273**, 28670-6.

Gum, R. J., McLaughlin, M. M., Kumar, S., Wang, Z., Bower, M. J., Lee, J. C., Adams, J. L., Livi, G. P., Goldsmith, E. J. and Young, P. R. (1998). Acquisition of sensitivity of stress-activated protein kinases to the p38 inhibitor, SB 203580, by alteration of one or more amino acids within the ATP binding pocket. *Journal of Biological Chemistry***273**, 15605-10.

Gupta, S., Barrett, T., Whitmarsh, A. J., Cavanagh, J., Sluss, H. K., Derijard, B. and Davis, R. J. (1996). Selective interaction of JNK protein kinase isoforms with transcription factors. *EMBO Journal***15**, 2760-70.

Hagting, A., Karlsson, C., Clute, P., Jackman, M. and Pines, J. (1998). MPF localization is controlled by nuclear export. *EMBO Journal***17**, 4127-38.

Hansen, T. E., Puntervoll, P., Seternes, O. M. and Jorgensen, J. B. (2008). Atlantic salmon possess three mitogen activated protein kinase kinase 6 paralogs responding differently to stress. *FEBS Journal***275**, 4887-902.

Hara, K., Tydeman, P. and Kirschner, M. (1980). A cytoplasmic clock with the same period as the division cycle in Xenopus eggs. *Proceedings of the National Academy of Sciences***77**, 462-6.

Harvey, E. (1940). A comparison of the development of nucleate and non-nucleate eggs of Arabica punctulata. *Biolocial Bulletin***79**, 166 - 187.

Hatakeyama, M., Kimura, S., Naka, T., Kawasaki, T., Yumoto, N., Ichikawa, M., Kim, J. H., Saito, K., Saeki, M., Shirouzu, M. et al. (2003). A computational model on the modulation of mitogen-activated protein kinase (MAPK) and Akt pathways in heregulin-induced ErbB signalling. *Biochemical Journal***373**, 451-63.

Hatano, N., Mori, Y., Oh-hora, M., Kosugi, A., Fujikawa, T., Nakai, N., Niwa, H., Miyazaki, J., Hamaoka, T. and Ogata, M. (2003). Essential role for ERK2 mitogen-activated protein kinase in placental development. *Genes to Cells***8**, 847-56.

Heinrich, R., Neel, B. G. and Rapoport, T. A. (2002). Mathematical models of protein kinase signal transduction. *Molecular Cell***9**, 957-70.

Her, J., Wu, J., Rall, T. B., Sturgill, T. W. and Weber, M. J. (1991). Sequence of pp42/MAP kinase, a serine/threonine kinae regulated by tyrosine phosphorylation. *Nucleic Acids Research***19**, 3743.

Herrick, J. and Sclavi, B. (2007). Ribonucleotide reductase and the regulation of DNA replication: an old story and an ancient heritage. *Molecular Microbiology***63**, 22-34.

Hipp, J. and Atala, A. (2004). Tissue engineering, stem cells, cloning and parthenogenesis: new paradigms for therapy. *Journal of Experimental and Clinical Assisted Reproduction***1**, 3.

Hlaing, M., Shen, X., Dazin, P. and Bernstein, H. S. (2002). The Hypertropic Response in C2C12 Myoblasts Recruits G1 Cell Cycle Machinery. *Journal of Biological Chemistry***277**, 23794 - 23799.

Hornberg, J. J., Bruggeman, F. J., Binder, B., Geest, C. R., Marjolein Bij de Vaate, A. J., Lankelma, J., Heinrich, R. and Westerhoff, H. V. (2005). Principles behind the multifarious control of signal transduction. *FEBS Journal***272**, 244 - 258.

Huang, C. and Ferrell, J. E., Jr. (1996). Ultrasensitivity in the mitogen-activated protein kinase cascade. *Proceedings of the National Academy of Sciences***93**, 10078 - 10083.

Huang, S., Jiang, Y., Li, Z., Nishida, E., Mathias, P., Lin, S., Ulevitch, R. J., Nemerow, G. R. and Han, J. (1997). Apoptosis signaling pathway in T cells is composed of ICE/Ced-3 family proteases and MAP kinase kinase 6b. *Immunity***6**, 739-49.

Huang, Y., Minigh, J., Miles, S. and Niles, R. M. (2008). Retinoic acid decreases ATF-2 phosphorylation and sensitizes melanoma cells to taxol-mediated growth inhibition. *Journal of Molecular Signaling***3**, 3.

Ichijo, H., Nishida, E., Irie, K., ten Dijke, P., Saitoh, M., Moriguchi, T., Takagi, M., Matsumoto, K., Miyazono, K. and Gotoh, Y. (1997). Induction of apoptosis by ASK1, a mammalian MAPKKK that activates SAPK/JNK and p38 signaling pathways. *Science***275**, 90-4.

Jeng, Y. and Watson, C. S. (2009). Proliferative and anti-proliferative effects of dietary levels of phytoestrogens in rat pituitary GH3/B6/F10 cells - the involvement of rapidly activated kinases and caspases. *BMC Cancer***9**, 334.

Jia, Y., Quinn, C. M., Bump, N. J., Clark, K. M., Clabbers, A., Hardman, J., Gagnon, A., Kamens, J., Tomlinson, M. J., Wishart, N. et al. (2005). Purification and kinetic characterization of recombinant human mitogen-activated protein kinase kinase kinase COT and the complexes with its cellular partner NF-kappa B1 p105. *Archives of Biochemistry and Biophysics***441**, 64-74.

Jiang, Y., Chen, C., Li, Z., Guo, W., Gegner, J. A., Lin, S. and Han, J. (1996). Characterization of the structure and function of a new mitogen-activated protein kinase (p38beta). *Journal of Biological Chemistry***271**, 17920-6.

Jiang, Y., Gram, H., Zhao, M., New, L., Gu, J., Feng, L., Di Padova, F., Ulevitch, R. J. and Han, J. (1997a). Characterization of the structure and function of the fourth member of p38 group mitogen-activated protein kinases, p38delta. *Journal of Biological Chemistry***272**, 30122-8.

Jiang, Y., Li, Z., Schwarz, E. M., Lin, A., Guan, K., Ulevitch, R. J. and Han, J. (1997b). Structure-function studies of p38 mitogen-activated protein kinase. Loop 12 influences substrate specificity and autophosphorylation, but not upstream kinase selection. *Journal of Biological Chemistry***272**, 11096-102.

Jones, N. C., Tyner, K. J., Nibarger, L., Stanley, H. M., Cornelison, D. D., Fedorov, Y. V. and Olwin, B. B. (2005). The p38alpha/beta MAPK functions as a molecular switch to activate the quiescent satellite cell. *Journal of Cell Biology***169**, 105-16.

Kahn, D. and Westerhoff, H. V. (1991). Control theory of regulatory cascades. *Journal of Theoretical Biology***153**, 255 - 285.

Kaizu, K., Ghosh, S., Matsuoka, Y., Moriya, H., Shimizu-Yoshida, Y. and Kitano, H. (2010). A comprehensive molecular interaction map of the budding yeast cell cycle. *Molecular Systems Biology***6**, 415.

Kallunki, T., Su, B., Tsigelny, I., Sluss, H. K., Derijard, B., Moore, G., Davis, R. and Karin, M. (1994). JNK2 contains a specificity-determining region responsible for efficient c-Jun binding and phosphorylation. *Genes and Development***8**, 2996-3007.

Kang, S., Jung, M., Kim, C. and Shin, D. (2005). Inactivation of p38 kinase delays the onset of senescence in rabbit articular chondrocytes. *Mechanisms of Ageing and Development***126**, 591 - 597.

Kant, S., Schumacher, S., Singh, M. K., Kispert, A., Kotlyarov, A. and Gaestel, M. (2006). Characterization of the Atypical MAPK ERK4 and Its Activation of the MAPK-activated Protein Kinase MK5. *Journal of Biological Chemistry***281**, 35511 - 35519.

Kholodenko, B. N. (2000). Negative feedback and ultrasensitivity can bring about oscillations in the mitogen-activated protein kinase cascades. *European Journal of Biochemistry***267**, 1583-8.

Kholodenko, B. N., Hoek, J. B., Westerhoff, H. V. and Brown, G. C. (1997). Quantification of information transfer via cellular signal transduction pathways. *FEBS Letters***414**, 430 - 434.

Kitzmann, M., Carnac, G., Vandromme, M., Primig, M., Lamb, N. and Fernandez, A. (1998). The Muscle Regulatory Factors MyoD and Myf-5 Undergo Distinct Cell Cycle-specific Expression in Muscle Cells. *Journal of Cell Biology***142**, 1477 - 1459.

Klemke, R. L., Cai, S., Giannini, A. L., Gallagher, P. J., de Lanerolle, P. and Cheresh, D. A. (1997). Regulation of cell motility by mitogen-activated protein kinase. *Journal of Cell Biology***137**, 481-92.

Klipp, E., Liebermeister, W., Wierling, C., Kowald, A., Lehrach, H. and Herwig, R. (2009). Systems Biology : A textbook. Weinheim: Wiley-VCH.

Knebel, A., Morrice, N. and Cohen, P. (2001). A novel method to identify protein kinase substrates: eEF2 kinase is phosphorylated and inhibited by SAPK4/p38delta. *EMBO Journal***20**, 4360-4369.

Koepp, D. M., Harper, J. W. and Elledge, S. J. (1999). How the cyclin became a cyclin: regulated proteolysis in the cell cycle. *Cell***97**, 431-4.

Koh, G. Y., Klug, M. G., Soonpaa, M. H. and Field, L. J. (1993). Differentiation and long-term survival of C2C12 myoblast grafts in heart. *Journal of Clinical Investigation***92**, 1548 - 1554.

Kohn, K. W. (1999). Molecular interaction map of the mammalian cell cycle control and DNA repair systems. *Molecular Biology of the Cell***10**, 2703-34.

Kolch, W., Calder, M. and Gilbert, D. (2005). When kinases meet mathematics: the systems biology of MAPK signalling. *FEBS Letters***579**, 1891 - 1895.

Korenjak, M., Taylor-Harding, B., Binne, U. K., Satterlee, J. S., Stevaux, O., Aasland, R., White-Cooper, H., Dyson, N. and Brehm, A. (2004). Native E2F/RBF complexes contain Myb-interacting proteins and repress transcription of developmentally controlled E2F target genes. *Cell***119**, 181-93.

Kummer, J. L., Rao, P. K. and Heidenreich, K. A. (1997). Apoptosis Induced by Withdrawal of Trophic Factors Is Mediated by p38 Mitogen-activated Protein Kinase. *Journal of Biological Chemistry***272**, 20490 - 20494.

Kyriakis, J. M. and Avruch, J. (1990). Insulin, epidermal growth factor and fibroblast growth factor elicit distinct patterns of protein tyrosine phosphorylation in BC3H1 cells. *Biochimica et Biophysica Acta***1054**, 73-82.

Lassar, A. B. and Münsterberg, A. E. (1996). The role of positive and negative signals in somite patterning. *Current Opinion in Neurobiology***6**, 57 - 63.

Lassar, A. B., Skapek, S. X. and Novitch, B. (1994). Regulatory mechanisms that coordinate skeletal muscle differentiation and cell cycle withdrawal. *Current Opinion in Cell Biology***6**, 788.

Lavoie, J. N., L'Allemain, G., Brunet, A., Muller, R. and Pouyssegur, J. (1996). Cyclin D1 expression is regulated positively by the p42/p44MAPK and negatively by the p38/HOGMAPK pathway. *Journal of Biological Chemistry***271**, 20608-16.

Lechner, C., Zahalka, M. A., Giot, J. F., Moller, N. P. and Ullrich, A. (1996). ERK6, a mitogen-activated protein kinase involved in C2C12 myoblast differentiation. *Proceedings of the National Academy of Sciences***93**, 4355-9.

Legewie, S., Blüthgen, N., Schäfer, R. and Herzel, H. (2005). Ultrasensitization: Switch-Like Regulation of Cellular Signaling by Transcriptional Induction. *Public Library of Science Computational Biology***1**, e54.

Li, Z., Jiang, Y., Ulevitch, R. J. and Han, J. (1996). The primary structure of p38 gamma: a new member of p38 group of MAP kinases. *Biochemical and Biophysical Research Communications***228**, 334-40.

Lim, S., Pnueli, L., Tan, J. H., Naor, Z., Rajagopal, G. and Melamed, P. (2009). Negative Feedback Governs Gonadotrope Frequency-Decoding of Gonadotropin Releasing Hormone Pulse-Frequency. *PLoS ONE***4**, e7244.

Lisnock, J., Griffin, P., Calaycay, J., Frantz, B., Parsons, J., O'Keefe, S. J. and LoGrasso, P. (2000). Activation of JNK3 alpha 1 requires both MKK4 and MKK7: kinetic characterization of in vitro phosphorylated JNK3 alpha 1. *Biochemistry***39**, 3141-8.

Lisnock, J., Tebben, A., Frantz, B., O'Neill, E. A., Croft, G., O'Keefe, S. J., Li, B., Hacker, C., de Laszlo, S., Smith, A. et al. (1998). Molecular basis for p38 protein kinase inhibitor specificity. *Biochemistry***37**, 16573-81.

Litovchick, L., Sadasivam, S., Florens, L., Zhu, X., Swanson, S. K., Velmurugan, S., Chen, R., Washburn, M. P., Liu, X. S. and DeCaprio, J. A. (2007). Evolutionarily conserved multisubunit RBL2/p130 and E2F4 protein complex represses human cell cycle-dependent genes in quiescence. *Molecular Cell***26**, 539-51.

Liu, H., Deng, X., Shyu, J., Li, J. J., Taparowsky, E. J. and Hu, C. (2006). Mutual regulation of c-Jun and ATF2 by transcriptional activation and subcellular localization. *EMBO Journal***25**, 1058 - 1069.

Liu, J., Minemoto, Y. and Lin, A. (2004). c-Jun N-terminal protein kinase 1 (JNK1), but not JNK2, is essential for tumor necrosis factor alpha-induced c-Jun kinase activation and apoptosis. *Molecular and Cellular Biology***24**, 10844-56.

Lloyd, A. C. (2006). Distinct functions for ERKs? *Journal of Biology***5**, 13.

Lowe, S. W. and Sherr, C. J. (2003). Tumor suppression by Ink4a-Arf: progress and puzzles. *Current Opinion in Genetics and Development***13**, 77-83.

Mahtani, K. R., Brook, M., Dean, J. L., Sully, G., Saklatvala, J. and Clark, A. R. (2001). Mitogen-activated protein kinase p38 controls the expression and posttranslational modification of tristetraprolin, a regulator of tumor necrosis factor alpha mRNA stability. *Molecular and Cellular Biology***21**, 6461-9.

Martin, G. R. (1981). Isolation of a pluripotent cell line from early mouse embryos cultured in medium conditioned by teratocarcinoma stem cells. *Proceedings of the National Academy of Sciences***78**, 7634 - 7638.

Martinsson, H., Starborg, M., Erlandsson, F. and Zetterberg, A. (2005). Single cell analysis of G1 check points - The relationship between the restriction point and phosphorylation of pRb. *Experimental Cell Research***305**, 383 - 391.

Mauro, A. (1961). Satellite cell of skeletal muscle fibers. *Journal of Biophysical and Biochemical Cytology***9**, 493 - 495.

McGovern, S. L., Caselli, E., Grigorieff, N. and Shoichet, B. K. (2002). A common mechanism underlying promiscuous inhibitors from virtual and high-throughput screening. *Journal of Medicinal Chemistry***45**, 1712-22.

Meloche, S., Pages, G. and Pouyssegur, J. (1992a). Functional expression and growth factor activation of an epitope-tagged p44 mitogen-activated protein kinase, p44mapk. *Molecular Biology of the Cell***3**, 63-71.

Meloche, S., Seuwen, K., Pages, G. and Pouyssegur, J. (1992b). Biphasic and synergistic activation of p44mapk (ERK1) by growth factors: correlation between late phase activation and mitogenicity. *Molecular Endocrinology***6**, 845-54.

Mercer, S. E., Ewton, D. Z., Deng, X., Lim, S., Mazur, T. R. and Friedman, E. (2005). Mirk/Dyrk1B Mediates Survival during the Differentiation of C2C12 Myoblasts. *Journal of Biological Chemistry***280**, 25788 - 25801.

Molinari, M. (2000). Cell cycle checkpoints and their inactivation in human cancer. *Cell Proliferation***33**, 261-74.

Monick, M. M., Mallampalli, R. K., Bradford, M., McCoy, D., Gross, T. J., Flaherty, D. M., Powers, L. S., Cameron, K., Kelly, S., Merrill Jr., A. H. et al. (2004). Cooperative Prosurvival Activity by ERK and Akt in Human Alveolar Macrophages is Dependent on High Levels of Acid Ceramidase Activity. *Journal of Immunology***173**, 123 - 135.

Mor, A. and Philips, M. R. (2006). Compartmentalized Ras/MAPK signaling. *Annual Review of Immunology***24**, 771-800.

Moriguchi, T., Kuroyanagi, N., Yamaguchi, K., Gotoh, Y., Irie, K., Kano, T., Shirakabe, K., Muro, Y., Shibuya, H., Matsumoto, K. et al. (1996). A novel kinase cascade mediated by mitogen-activated protein kinase kinase 6 and MKK3. *Journal of Biological Chemistry***271**, 13675-9.

Muda, M., Boschert, U., Dickinson, R., Martinou, J. C., Martinou, I., Camps, M., Schlegel, W. and Arkinstall, S. (1996a). MKP-3, a novel cytosolic protein-tyrosine phosphatase that exemplifies a new class of mitogen-activated protein kinase phosphatase. *Journal of Biological Chemistry***271**, 4319-26.

Muda, M., Theodosiou, A., Rodrigues, N., Boschert, U., Camps, M., Gillieron, C., Davies, K., Ashworth, A. and Arkinstall, S. (1996b). The dual specificity

phosphatases M3/6 and MKP-3 are highly selective for inactivation of distinct mitogen-activated protein kinases. *Journal of Biological Chemistry***271**, 27205-8.

Müller, C., Alunni-Fabbroni, M., Kowenz-Leutz, E., Mo, X., Tommasino, M. and Leutz, A. (1999). Separation of C/EBPα-mediated proliferation arrest and differentiation pathways. *Proceedings of the National Academy of Sciences***96**, 7276 - 7281.

Münsterberg, A. E., Kitajewski, J., Bumcrot, D. A., McMahon, A. P. and Lassar, A. B. (1995). Combinatorial signaling by Sonic hedgehog and Wnt family members induces myogenic bHLH gene expression in the somite. *Genes & Development***9**, 2911 - 2922.

Murphy, L. O., Smith, S., Chen, R. H., Fingar, D. C. and Blenis, J. (2002). Molecular interpretation of ERK signal duration by immediate early gene products. *Nature Cell Biology***4**, 556-64.

Musti, A. M., Treier, M. and Bohmann, D. (1997). Reduced ubiquitin-dependent degradation of c-Jun after phosphorylation by MAP kinases. *Science***275**, 400-2.

Nagata, Y., Kobayashi, H., Umeda, M., Ohta, N., Kawashima, S., Zammit, P. S. and Matsuda, R. (2005). Sphingomyelin Levels in the Plasma Membrane Correlate with the Activation State of Muscle Satellite Cells. *Journal of Histochemistry & Cytochemistry***54**, 375 - 384.

Narita, M. and Lowe, S. W. (2005). Senescence comes of age. *Nature Medicine***11**, 920-2.

Neganova, I. and Lako, M. (2008). G1 to S phase cell cycle transition in somatic and embryonic stem cells. *Journal of Anatomy***213**, 30-44.

Nemoto, S., Sheng, Z. and Lin, A. (1998). Opposing effects of Jun kinase and p38 mitogen-activated protein kinases on cardiomyocyte hypertrophy. *Molecular and Cellular Biology***18**, 3518-26.

New, L., Li, Y., Ge, B., Zhong, H., Mansbridge, J., Liu, K. and Han, J. (2001). SB203580 promote EGF-stimulated early morphological differentiation in PC12 cell through activating ERK pathway. *Journal of Cellular Biochemistry***83**, 585 - 596.

Nishimoto, S. and Nishida, E. (2006). MAPK signalling: ERK5 versus ERK1/2. *EMBO Reports***7**, 782 - 786.

Novák, B. and Tyson, J. J. (2004). A model for restriction point control of the mammalian cell cycle. *Journal of Theoretical Biology***230**, 563-79.

Novák, B., Tyson, J. J., Gyorffy, B. and Csikasz-Nagy, A. (2007). Irreversible cell-cycle transitions are due to systems-level feedback. *Nature Cell Biology***9**, 724-8.

Nurse, P. (1990). Universal control mechanism regulating onset of M-phase. *Nature***344**, 503-8.

Olivier, B. G., Rohwer, J. M. and Hofmeyr, J. S. (2005). Modelling cellular systems with PySCeS. *Bioinformatics***21**, 560 - 561.

Olsen, E. (1992). Interplay between proliferation and differentiation within the myogenic lineage. *Developmental Biology***154**, 261 - 272.

Oottamasathien, S., Wang, Y., Williams, K., Franco, O. E., Wills, M. L., Thomas, J. C., Saba, K., Sharif-Afshar, A., Makari, J. H., Bhowmick, N. A. et al. (2007). Directed differentiation of embryonic stem cells into bladder tissue. *Developmental Biology***304**, 556.

Pajalunga, D., Mazzola, A., Salzano, A. M., Biferi, M. G., De Luca, G. and Crescenzi, M. (2007). Critical requirement for cell cycle inhibitors in sustaining nonproliferative states. *Journal of Cell Biology***176**, 807-18.

Pardee, A. B. (1974). A restriction point for control of normal animal cell proliferation. *Proceedings of the National Academy of Sciences***71**, 1286-90.

Pazolli, E. and Stewart, S. A. (2008). Senescence: the good the bad and the dysfunctional. *Current Opinion in Genetics and Development***18**, 42 - 47.

Petersen, B. E. and Terada, N. (2001). Stem Cells: A Journey into a New Frontier. *Journal of the American Society of Nephrology***12**, 1773 - 1780.

Pimienta, G. and Pascual, J. (2007). Canonical and alternative MAPK signaling. *Cell Cycle***6**, 2628-32.

Pines, J. and Hunter, T. (1991). Human cyclins A and B1 are differentially located in the cell and undergo cell cycle-dependent nuclear transport. *Journal of Cell Biology***115**, 1-17.

Planas-Silva, M. D. and Weinberg, R. A. (1997). The restriction point and control of cell proliferation. *Current Opinion in Cell Biology***9**, 768-72.

Preston, S. L., Alison, M. R., Forbes, S. J., Direkze, N. C., Poulsom, R. and Wright, N. A. (2003). The new stem cell biology: something for everyone. *Journal of Clinical Pathology***56**, 86 - 96.

Raingeaud, J., Gupta, S., Rogers, J. S., Dickens, M., Han, J., Ulevitch, R. J. and Davis, R. J. (1995). Pro-inflammatory cytokines and environmental stress cause p38 mitogen-activated protein kinase activation by dual phosphorylation on tyrosine and threonine. *Journal of Biological Chemistry***270**, 7420-6.

Raman, M., Earnest, S., Zhang, K., Zhao, Y. and Cobb, M. H. (2007). TAO kinases mediate activation of p38 in response to DNA damage. *EMBO Journal***26**, 2005 - 2014.

Recio, J. A. and Merlino, G. (2002). Hepatocyte growth factor/scatter factor activates proliferation in melanoma cells through p38 MAPK, ATF-2 and cyclin D1. *Oncogene***21**, 1000-8.

Rossi, F., Charlton, C. A. and Blau, H. (1997). Monitoring protein-protein interactions in intact eukaryotic cells by β-galactosidase complementation. *Proceedings of the National Academy of Sciences***94**, 8405 - 8410.

Rouse, J., Cohen, P., Trigon, S., Morange, M., Alonso-Llamazares, A., Zamanillo, D., Hunt, T. and Nebreda, A. R. (1994). A novel kinase cascade triggered by stress and heat shock that stimulates MAPKAP kinase-2 and phosphorylation of the small heat shock proteins. *Cell***78**, 1027-37.

Roux, P. and Blenis, J. (2004). ERK and p38 MAPK-Activated Protein Kinases: a Family of Protein Kinases with Diverse Biological Functions. *Microbiology and Molecular Biology Reviews***68**, 320 - 344.

Rust, M. J., Markson, J. S., Lane, W. S., Fisher, D. S. and O'Shea, E. K. (2007). Ordered phosphorylation governs oscillation of a three-protein circadian clock. *Science***318**, 809-12.

Sabapathy, K., Hochedlinger, K., Nam, S. Y., Bauer, A., Karin, M. and Wagner, E. F. (2004). Distinct roles for JNK1 and JNK2 in regulating JNK activity and c-Jun-dependent cell proliferation. *Molecular Cell***15**, 713-25.

Sabapathy, K. and Wagner, E. F. (2004). JNK2: a negative regulator of cellular proliferation. *Cell Cycle***3**, 1520-3.

Sasagawa, S., Ozaki, Y., Fuijita, K. and Kuroda, S. (2005). Prediction and validation of the distinct dynamics of transient and sustained ERK activation. *Nature Cell Biology***7**, 365 - 372.

Schreiber, M., Kolbus, A., Piu, F., Szabowski, A., Mohle-Steinlein, U., Tian, J. M., Karin, M., Angel, P. and Wagner, E. F. (1999). Control of cell cycle progression by c-Jun is p53 dependent. *Genes & Development***13**, 607 - 619.

Schubbert, S., Shannon, K. and Bollag, G. (2007). Hyperactive Ras in developmental disorders and cancer. *Nature Reviews Cancer***7**, 295 - 308.

Schutte, B., Reynders, M. M., Bosman, F. T. and Blijham, G. H. (1985). Flow cytometric determination of DNA ploidy level in nuclei isolated from paraffin-embedded tissue. *Cytometry***6**, 26-30.

Shalom-Barak, T., Quach, J. and Lotz, M. (1998). Interleukin-17-induced gene expression in articular chondrocytes is associated with activation of mitogen-activated protein kinases and NF-kappaB. *Journal of Biological Chemistry***273**, 27467-73.

Shapiro, L., Heidenreich, K. A., Meintzer, M. K. and Dinarello, C. A. (1998). Role of p38 mitogen-activated protein kinase in HIV type 1 production in vitro. *Proceedings of the National Academy of Sciences***95**, 7422-6.

Sherr, C. J. (1995a). D-type cyclins. *Trends in Biochemical Sciences***20**, 187-90.

Sherr, C. J. (1995b). Mammalian G1 cyclins and cell cycle progression. *Proceedings of the Association of American Physicians***107**, 181-6.

Sherr, C. J. and Roberts, J. M. (1999). CDK inhibitors: positive and negative regulators of G1-phase progression. *Genes and Development***13**, 1501-12.

Siegel, M. R. and Sisler, H. D. (1964). Site of action of cycloheximide in cells of saccharomyces pastorianus. *Biochimica et Biophysica Acta***87**, 83 - 89.

Sigrist, S., Jacobs, H., Stratmann, R. and Lehner, C. F. (1995). Exit from mitosis is regulated by Drosophila fizzy and the sequential destruction of cyclins A, B and B3. *EMBO Journal***14**, 4827-38.

Siminovitch, L., McCulloch, E. and Till, J. (1963). The distribution of colony-forming cells among spleen colonies. *Journal of Cellular and Comparative Biology***62**, 327 - 336.

Snoep, J. L. (2005). The Silicon Cell initiative: working towards a detailed kinetic description at the cellular level. *Current Opinion in Biotechnology***16**, 336 - 343.

Snoep, J. L., Bruggeman, F. J., Olivier, B. G. and Westerhoff, H. V. (2006). Towards building the silicon cell: A modular approach. *Biosystems***83**, 207 - 216.

Snustad, D. P., Simmons, M. J. and Jenkins, J. B. (1997). Principles of Genetics: John Wiley & Sons, Incorporated.

Squires, M. S., Nixon, P. M. and Cook, S. J. (2002). Cell-cycle arrest by PD184352 requires inhibition of extracellular signal-regulated kinases (ERK) 1/2 but not ERK5/BMK1. *Biochemical Journal***366**, 673-80.

Srividhya, J. and Gopinathan, M. S. (2006). A simple time delay model for eukaryotic cell cycle. *Journal of Theoretical Biology***241**, 617 - 627.

Stacey, D. W. (2003). Cyclin D1 serves as a cell cycle regulatory switch in actively proliferating cells. *Current Opinion in Cell Biology***15**, 158-63.

Stefanovsky, V. Y., Langlois, F., Bazett-Jones, D., Pelletier, G. and Moss, T. (2006). ERK modulates DNA bending and enhancesome structure by phosphorylating HMG1-boxes 1 and 2 of the RNA polymerase I transcription factor UBF. *Biochemistry***45**, 3626-34.

Stein, B., Yang, M. X., Young, D. B., Janknecht, R., Hunter, T., Murray, B. W. and Barbosa, M. S. (1997). p38-2, a Novel Mitogen-activated Protein Kinase with Distinct Properties. *Journal of Biological Chemistry***272**, 19509 - 19517.

Stöcklein, W. and Piepersberg, W. (1980). Binding of Cycloheximide to Ribosomes from Wild-Type and Mutant Strains of Saccharomyces cerevisiae. *Antimicrobial Agents and Chemotherapy***18**, 863 - 867.

Stokoe, D., Engel, K., Campbell, D. G., Cohen, P. and Gaestel, M. (1992). Identification of MAPKAP kinase 2 as a major enzyme responsible for the phosphorylation of the small mammalian heat shock proteins. *FEBS Letters***313**, 307-13.

Subramanian, M. and Shaha, C. (2007). Up-Regulation of Bcl-2 through ERK Phosphorylation Is Associated with Human Macrophage Survival in an Estrogen Microenvironment. *Journal of Immunology***179**, 2330 - 2338.

Sun, H., Charles, C. H., Lau, L. F. and Tonks, N. K. (1993). MKP-1 (3CH134), an immediate early gene product, is a dual specificity phosphatase that dephosphorylates MAP kinase in vivo. *Cell***75**, 487-93.

Sun, L., Trausch-Azar, J. S., Muglia, L. J. and Schwartz, A. L. (2008). Glucocortoids differentially regulate degradation of MyoD and Id1 by N-terminal ubiquitination to promote muscle protein catabolism. *Proceedings of the National Academy of Sciences***105**, 3339 - 3344.

Sundaramurthy, P., Gakkhar, S. and Sowdhamini, R. (2009). Analysis of the impact of ERK5, JNK, and P38 kinase cascades on each other: A systems approach. *Bioinformation***3**, 244-9.

Takeda, D. Y. and Dutta, A. (2005). DNA replication and progression through S phase. *Oncogene***24**, 2827 - 2843.

Takekawa, M., Posas, F. and Saito, H. (1997). A human homolog of the yeast Ssk2/Ssk22 MAP kinase kinase kinases, MTK1, mediates stress-induced activation of the p38 and JNK pathways. *EMBO Journal***16**, 4973-82.

Tan, Y., Rouse, J., Zhang, A., Cariati, S., Cohen, P. and Comb, M. J. (1996). FGF and stress regulate CREB and ATF-1 via a pathway involving p38 MAP kinase and MAPKAP kinase-2. *EMBO Journal***15**, 4629-42.

Tan, Y. C., Wu, H., Wang, W. N., Zheng, Y. and Wang, Z. X. (2002). Characterization of the interactions between the small GTPase RhoA and its guanine nucleotide exchange factors. *Analytical Biochemistry***310**, 156-62.

Tang, D., Wu, D., Hirao, A., Lahti, J. M., Liu, L., Mazza, B., Kidd, V. J., Mak, T. W. and Ingram, A. J. (2002). ERK activation mediates cell cycle arrest and apoptosis after DNA damage independently of p53. *Journal of Biological Chemistry***277**, 12710-7.

Tapscott, S. (2005). The circuitry of a master switch: Myod and the regulation of skeletal muscle gene transcription. *Development***132**, 2685 - 2695.

Teramoto, H., Coso, O. A., Miyata, H., Igishi, T., Miki, T. and Gutkind, J. S. (1996). Signaling from the Small GTP-binding Proteins Rac1 and Cdc42 to the c-Jun N-

terminal Kinase/Stress-activated Protein Kinase Pathway. *Journal of Biological Chemistry***271**, 27225 - 27228.

Thomson, J. A., Itskovitz, A., Eldor, J., Shapiro, S. S., Waknitz, M. A., Swiergiel, J. J., Marshall, V. S. and Jones, J. M. (1998). Embryonic stem cell lines derived from human blastocysts. *Science***282**, 1145 - 1147.

Tintignac, L. A., Leibovitch, M. P., Kitzmann, M., Fernandez, A., Ducommun, B., Meijer, L. and Leibovitch, S. A. (2000). Cyclin E-Cdk2 Phosphorylation Promotes Late G1-Phase Degradation of MyoD in Muscle Cells. *Experimental Cell Research***259**, 300 - 307.

Tong, L., Pav, S., White, D. M., Rogers, S., Crane, K. M., Cywin, C. L., Brown, M. L. and Pargellis, C. A. (1997). A highly specific inhibitor of human p38 MAP kinase binds in the ATP pocket. *Nature Structural Biology***4**, 311-6.

Tournier, C., Hess, P., Yang, D. D., Xu, J., Turner, T. K., Nimnual, A., Bar-Sagi, D., Jones, S. N., Flavell, R. A. and Davis, R. J. (2000). Requirement of JNK for stress-induced activation of the cytochrome c-mediated death pathway. *Science***288**, 870-4.

Trakatellis, A. C., Montjar, M. and Axelrod, A. E. (1965). Effect of Cycloheximide on Polysomes and Protein Synthesis in the Mouse Liver. *Biochemistry***4**, 2065 - 2071.

Turing, A. (1952). The mathematical basis of morphogenesis. *Philosophical Transactions of the Royal Society B: Biological Sciences***237**, 37 - 47.

Tyson, J. J. (1991). Modeling the cell division cycle: cdc2 and cyclin interactions. *Proceedings of the National Academy of Sciences***88**, 7328-32.

Tyson, J. J., Chen, K. C. and Novák, B. (2003). Sniffers, buzzers, toggles and blinkers: dynamics of regulatory and signaling pathways in the cell. *Current Opinion in Cell Biology***15**, 221-31.

Tyson, J. J. and Novák, B. (2001). Regulation of the Eukaryotic Cell Cycle: Molecular Antagonism, Hysteresis, and Irreversible Transitions. *Journal of Theoretical Biology***210**, 249 - 263.

Van den Heever, M. (2006). Synchronisation of C2C12 satellite cells. In *Department of Physiological Sciences*, vol. Bachelor of Science (Honours). Stellenbosch: University of Stellenbosch.

van den Heuvel, S. (2005). Cell-cycle Regulation. *WormBook***21**, 1 - 16.

Vandromme, M., Carnac, G., Gauthier-Rouviere, C., Fesquet, D., Lamb, N. and Fernandez, A. (1994). Nuclear import of the myogenic factor MyoD requires cAMP-dependent protein kinase activity but not the direct phosphorylation of MyoD. *Journal of Cell Science***107**, 613 - 620.

Vera, J., Rath, O., Balsa-Canto, E., Banga, J., Kolch, W. and Wolkenhauer, O. (2010). Investigating dynamics of inhibitory and feedback loops in ERK signalling using power-law models. *Molecular BioSystems***6**, 2174 - 2191.

Vindeløv, L. L., Christensen, I. J., Jensen, G. and Nissen, N. I. (1983a). Limits of detection of nuclear DNA abnormalities by flow cytometric DNA analysis. Results obtained by a set of methods for sample-storage, staining and internal standardization. *Cytometry***3**, 332-9.

Vindeløv, L. L., Christensen, I. J. and Nissen, N. I. (1983b). A detergent-trypsin method for the preparation of nuclei for flow cytometric DNA analysis. *Cytometry***3**, 323-7.

Vlach, J., Hennecke, S. and Amati, B. (1997). Phosphorylation-dependent degradation of the cyclin-dependent kinase inhibitor p27. *EMBO Journal***16**, 5334-44.

Voet, D. and Voet, J. G. (2004). Biochemistry: John Wiley & Sons, Inc.

Voit, E., Neves, A. R. and Santos, H. (2006). The intricate side of systems biology. *Proceedings of the National Academy of Sciences***103**, 9452 - 9457.

Waas, W. F., Lo, H. and Dalby, K. N. (2001). The Kinetic Mechanism of the Dual Phosphorylation of the ATF2 Transcription Factor by p38 Mitogen-activated Protein (MAP) Kinase α. *Journal of Biological Chemistry***276**, 5676 - 5684.

Walsh, K. and Perlman, H. (1997). Cell cycle exit upon myogenic differentiation. *Current Opinion in Genetics and Development***7**, 597-602.

Walsh, S., Margolis, S. and Kornbluth, S. (2003). Phosphorylation of the Cyclin B1 Cytoplasmic Retention Sequence by Mitogen-Activated Protein Kinase and Plx. *Molecular Cancer Research***1**, 280 - 289.

Waskiewicz, A. J., Johnson, J. C., Penn, B., Mahalingam, M., Kimball, S. R. and Cooper, J. A. (1999). Phosphorylation of the cap-binding protein eukaryotic translation initiation factor 4E by protein kinase Mnk1 in vivo. *Molecular and Cellular Biology***19**, 1871-80.

Weston, A. D., Sampaio, A. V., Ridgeway, A. G. and Underhill, T. M. (2003). Inhibition of p38 MAPK signaling promotes late stages of myogenesis. *Journal of Cell Science***116**, 2885 - 2893.

Whitehurst, A., Cobb, M. H. and White, M. A. (2004). Stimulus-Coupled Spatial Restriction of Extracellular Signal-Related Kinase 1/2 Activity Contributes to the Specificity of Signal-Response Pathways. *Molecular and Cellular Biology***24**, 10145 - 10150.

Wilson, K. P., Fitzgibbon, M. J., Caron, P. R., Griffith, J. P., Chen, W., McCaffrey, P. G., Chambers, S. P. and Su, M. S. (1996). Crystal structure of p38 mitogen-activated protein kinase. *Journal of Biological Chemistry***271**, 27696-700.

Wisdom, R., Johnson, R. S. and Moore, C. (1999). c-Jun regulates cell cycle progression and apoptosis by distinct mechanisms. *EMBO Journal***18**, 188-97.

Wu, H., Naya, F. J., McKinsey, T. A., Mercer, B., Shelton, J. M., Chin, E. R., Simard, A. R., Michel, R. N., Bassel-Duby, R., Olson, E. N. et al. (2000a). MEF2 responds to multiple calcium-regulated signals in the control of skeletal muscle fiber type. *EMBO Journal***19**, 1963-73.

Wu, Z., Woodring, P. J., Bhakta, K. S., Tamura, K., Wen, F., Feramisco, J. R., Karin, M., Wang, J. Y. and Puri, P. L. (2000b). p38 and Extracellular Signal-Regulated Kinases Regulate the Myogenic Program at Multiple Steps. *Molecular and Cellular Biology***20**, 3951 - 3964.

Xia, Z., Dickens, M., Raingeaud, J., Davis, R. J. and Greenberg, M. E. (1995). Opposing effects of ERK and JNK-p38 MAP kinases on apoptosis. *Science***270**, 1326-31.

Yaffe, D. and Saxel, O. (1977). A myogenic line with altered serum requirements for differentiation. *Differentiation***7**, 159 - 166.

Yamaji, A., Sekizawa, Y., Emoto, K., Sakuraba, H., Inoue, K., Kobayashi, H. and Umeda, M. (1998). Lysenin, a novel sphingomyelin-specific binding protein. *Journal of Biological Chemistry***273**, 5300 - 5306.

Yamamoto, T., Ebisuya, M., Ashida, F., Okamoto, K., Yonehara, S. and Nishida, E. (2006). Continuous ERK activation downregulates antiproliferative genes throughout G1 phase to allow cell-cycle progression. *Current Biology***16**, 1171-82.

Yang, D. D., Kuan, C. Y., Whitmarsh, A. J., Rincon, M., Zheng, T. S., Davis, R. J., Rakic, P. and Flavell, R. A. (1997). Absence of excitotoxicity-induced apoptosis in the hippocampus of mice lacking the Jnk3 gene. *Nature***389**, 865-70.

Yang, L., Han, Z., Robb MacLellan, W., Weiss, J. N. and Qu, Z. (2006). Linking cell division to cell growth in a spatiotemporal model of the cell cycle. *Journal of Theoretical Biology***241**, 120-33.

Yang, S. H., Whitmarsh, A. J., Davis, R. J. and Sharrocks, A. D. (1998a). Differential targeting of MAP kinases to the ETS-domain transcription factor Elk-1. *EMBO Journal***17**, 1740-9.

Yang, S. H., Yates, P. R., Whitmarsh, A. J., Davis, R. J. and Sharrocks, A. D. (1998b). The Elk-1 ETS-domain transcription factor contains a mitogen-activated protein kinase targeting motif. *Molecular and Cellular Biology***18**, 710-20.

Zarubin, T. and Han, J. (2005). Activation and signaling of the p38 MAP kinase pathway. *Cell Research***15**, 11-8.

Zetser, A., Gredinger, E. and Bengal, E. (1999). p38 mitogen-activated protein kinase pathway promotes skeletal muscle differentiation. Participation of the Mef2c transcription factor. *Journal of Biological Chemistry***274**, 5193-200.

Zetterberg, A. and Larsson, O. (1985). Kinetic analysis of regulatory events in G1 leading to proliferation or quiescence of Swiss 3T3 cells. *Proceedings of the National Academy of Sciences***82**, 5365-9.

Zetterberg, A., Larsson, O. and Wiman, K. G. (1995). What is the restriction point? *Current Opinion in Cell Biology***7**, 835-42.

Zhang, B., Chernoff, J. and Zheng, Y. (1998). Interaction of Rac1 with GTPase-activating proteins and putative effectors. A comparison with Cdc42 and RhoA. *Journal of Biological Chemistry***273**, 8776-82.

Zhang, W. and Liu, H. T. (2002). MAPK signal pathways in the regulation of cell proliferation in mammalian cells. *Cell Research***12**, 9-18.

Zhao, M., New, L., Kravchenko, V. V., Kato, Y., Gram, H., di Padova, F., Olson, E. N., Ulevitch, R. J. and Han, J. (1999). Regulation of the MEF2 family of transcription factors by p38. *Molecular and Cellular Biology***19**, 21-30.

Zhu, W., Giangrande, P. H. and Nevins, J. R. (2004). E2Fs link the control of G1/S and G2/M transcription. *EMBO Journal***23**, 4615-26.